Wefer, G., Berger, W.H., Richter, C., et al., 1998
Proceedings of the Ocean Drilling Program, Initial Reports, Vol. 175

12. SITE 1084[1]

Shipboard Scientific Party[2]

HOLE 1084A

Position: 25°30.8345′S, 13°1.6668′E

Start hole: 0310 hr, 21 September 1997

End hole: 0315 hr, 24 September 1997

Time on hole: 72.08 hr

Seafloor (drill pipe measurement from rig floor, mbrf): 2003.5

Total depth (drill pipe measurement from rig floor, mbrf): 2608.5

Distance between rig floor and sea level (m): 11.6

Water depth (drill pipe measurement from sea level, m): 1991.9

Penetration (mbsf): 605

Coring totals:
Type: APC
Number: 17
Cored: 149.50 m
Recovered: 156.80 m (104.88%)

Type: XCB
Number: 48
Cored: 455.50 m
Recovered: 354.76 m (77.88%)

Lithology:
Subunit IA: foraminifer- and diatom-bearing nannofossil clay and foraminifer-bearing diatom-rich clayey nannofossil ooze
Subunit IB: nannofossil-rich diatomaceous clay, clayey nannofossil ooze, and diatom-bearing clay
Subunit IC: nannofossil-rich diatomaceous clay and nannofossil diatomaceous clay
Unit II: clay-rich nannofossil diatom ooze, diatomaceous nannofossil ooze, and clay-rich nannofossil ooze
Unit III: clay, nannofossil clay, and diatom-bearing nannofossil clay
Unit IV: clayey nannofossil ooze, diatom-bearing clayey nannofossil ooze, and diatom-rich clayey nannofossil ooze

HOLE 1084B

Position: 25°30.8206′S, 13°1.6665′E

Start hole: 0315 hr, 24 September 1997

End hole: 1750 hr, 24 September 1997

Time on hole: 14.58 hr

Seafloor (drill pipe measurement from rig floor, mbrf): 2004.4

Total depth (drill pipe measurement from rig floor, mbrf): 2187.2

Distance between rig floor and sea level (m): 11.6

Water depth (drill pipe measurement from sea level, m): 1992.8

Penetration (mbsf): 182.8

Coring totals:
Type: 20
Number: 20
Cored: 182.80 m
Recovered: 186.60 m (102.08%)

Lithology:
Subunit IA: foraminifer- and diatom-bearing nannofossil clay and foraminifer-bearing diatom-rich clayey nannofossil ooze
Subunit IB: nannofossil-rich diatomaceous clay, clayey nannofossil ooze, and diatom-bearing clay

HOLE 1084C

Position: 25°30.8037′S, 13°1.6670′E

Start hole: 1750 hr, 24 September 1997

End hole: 1230 hr, 25 September 1997

Time on hole: 18.67 hr

Seafloor (drill pipe measurement from rig floor, mbrf): 2003.4

Total depth (drill pipe measurement from rig floor, mbrf): 2211

Distance between rig floor and sea level (m): 11.6

Water depth (drill pipe measurement from sea level, m): 1991.8

Penetration (mbsf): 207.6

Coring totals:
Type: APC
Number: 22
Cored: 207.60 m
Recovered: 217.82 m (104.92%)

Lithology:
Subunit IA: foraminifer- and diatom-bearing nannofossil clay, and foraminifer-bearing diatom-rich clayey nannofossil ooze
Subunit IB: nannofossil-rich diatomaceous clay, clayey nannofossil ooze, and diatom-bearing clay

Principal results: One of the main objectives of drilling at Site 1084 was to document the northward migration of the Benguela Current system from the Miocene to the Quaternary, as well as the shoreward and seaward migrations of the upwelling center. Filaments of cold, nutrient-rich waters from the coastal upwelling area extend well offshore and mix with low-productivity oceanic water, forming a zone of intermediate productivity at Site 1084. This site is expected to provide a high-resolution record because of high sedimentation rates. The close vicinity to the Lüderitz upwelling cell should result in well-expressed organic carbon (C_{org}), diatom, and coccolith cycles via cyclic productivity intensity. In addition, this site is closest to the area with elevated primary production and should have the best representation of coastal upwelling signals. A close tie-in between pelagic and terrigenous sedimentation is expected within the slope record.

---

[1] Wefer, G., Berger, W.H., Richter, C., et al., 1998. *Proc. ODP, Init. Repts.,* 175: College Station, TX (Ocean Drilling Program).

[2] Shipboard Scientific Party is given in the list preceding the Table of Contents.

Three holes were cored with the advanced hydraulic piston corer/extended core barrel (APC/XCB) at Site 1084 to a maximum depth of 605.0 meters below seafloor (mbsf), which recovered an apparently continuous hemipelagic sedimentary section spanning the Holocene to lower Pliocene (0–4.7 Ma). Hole 1084A was cored with the APC to 149.5 mbsf and was extended with the XCB to a depth of 605.0 mbsf. Hole 1084A was logged with a full suite of sensors (seismostratigraphic suite, lithoporosity suite, Formation MicroScanner [FMS] suite, and the geological high-sensitivity magnetic tool [GHMT]) from 601 to 90 mbsf. At Hole 1084B, 20 cores were taken with the APC to 182.8 mbsf. Hole 1081C was cored with the APC to 202.0 mbsf. Detailed comparisons between the magnetic susceptibility and the gamma-ray attenuation porosity evaluator (GRAPE) density records generated on the multisensor track (MST) and the color reflectance measured with the Minolta spectrophotometer demonstrated complete recovery of the sedimentary sequence down to 175 meters composite depth (mcd).

Sediments form four lithostratigraphic units defined by the changes in the major lithology between clay and ooze. The uppermost lithology is composed of moderately bioturbated, intercalated intervals of clays that contain varying abundances of diatoms, nannofossils, foraminifers, and radiolarians. Three subunits are distinguished based on microfossil type and abundance. The section continues downward with ~100 m of clay-rich nannofossil diatom ooze, diatomaceous nannofossil ooze, and clay-rich nannofossil ooze. The following 50-m-thick unit is composed of clay with varying amounts of nannofossils and diatoms, underlain by a unit consisting predominantly of clayey nannofossil ooze.

Several decimeter-thick intervals of dark, organic-rich clay layers are present between 120 and 410 mbsf. Compared with the under- and overlying sediment layers, these horizons are characterized by lower carbonate contents averaging just <10 wt% and higher organic carbon ranging between 8 and 18 wt%. The detrital component of the sediments consists of clay with rare silt-sized, angular and subangular mono- and polycrystalline quartz grains. Subangular feldspar grains are present in trace amounts. Authigenic minerals include framboidal pyrite and dolomite rhombs in rare or trace amounts. The dark horizons generally contain slightly higher abundances of pyrite and exhibit significant compositional variations in the relative abundances of diatoms, foraminifers, and nannofossils. The biogenic component of the dark layers is commonly dominated by diatom resting spores.

Sedimentation rates range from 100 to 270 m/m.y., with the highest values located within the last 1 m.y. A second episode of high sedimentation rate (170 m/m.y.) is associated with an upper Pliocene diatom-rich interval.

An integrated biostratigraphic framework composed of both calcareous and siliceous microfossils was established, resulting in a well-constrained age model for Site 1084. Calcareous nannofossils are abundant within the top 280 mbsf and between 410 and 600 mbsf and provided 13 biohorizons, which were constrained within an average depth interval of 3 m. Planktonic foraminiferal zonation is difficult because of an absence of marker species and the dissolution of planktonic foraminifers, particularly in the lower Pleistocene to upper Pliocene sediments. It is difficult to determine whether the absence of marker species is caused by ecological conditions or by selective dissolution. Both cool- and warm-water faunas are present in the same assemblages downcore and may indicate an increased contribution from cooler Southern Ocean waters. The benthic foraminifers are abundant and well preserved, and abundances correlate well with the different lithostratigraphic units. Radiolarians are abundant and well preserved in almost all samples examined. Diatom preservation is moderate throughout Hole 1084A. In contrast to the other sites, diatom abundances, although highly variable, remain moderately high throughout the Pleistocene. In addition to the “background” diatom assemblage composed of a mixture of upwelling-indicator and oceanic species, we recorded many more cold-water markers characteristic of the Southern Oceans than were observed at Sites 1081, 1082, and 1083.

A complete magnetostratigraphy was determined at Site 1084 after alternating-field (AF) demagnetization at 20 mT. All chrons from the Brunhes (C1n) to the latter part of the Gilbert (~4.4 Ma) were identified. No short polarity-reversal event during the Brunhes Chron was detected, despite the high sedimentation rates.

Sediments from 1084 are notably rich in marine organic matter. Well-developed light–dark sediment color cycles, in which concentrations of calcium carbonate and organic carbon vary between 1 and 69 wt% and between 1.2 to 18 wt%, respectively, record fluctuations in the elevated marine production associated with the Benguela Current. Higher concentrations of organic carbon from 0 to 392 mbsf indicate that productivity was higher during the last 2 m.y. than earlier in the history of this upwelling system.

Interstitial water chemistry profiles at this organic carbon–rich site record some of the most extreme conditions of sediment diagenesis ever recovered in the history of Deep Sea Drilling Project (DSDP) and Ocean Drilling Program (ODP) drilling. Maximum values of alkalinity (172 mM) and ammonium (50 mM) are greater than those observed at any site, except ODP Site 688, within the Peruvian upwelling system. Sulfate is completely depleted within the uppermost 5 mbsf, which is much more rapidly than at any other Leg 175 site and speaks to the availability of oxidizable organic matter. These changes are accompanied by calcite dissolution and dolomite precipitation, as recorded in the calcium, magnesium, and strontium distributions.

Physical sediment properties were determined both by high-resolution MST core logging and index properties measurements. Magnetic susceptibility and GRAPE signals reveal pronounced cyclicities, which were used for high-quality stratigraphic correlation in conjunction with digital color data.

Hole 1084A was logged with a full suite of sensors to continuously characterize the sedimentary changes through depth and to provide data for core-log integration. Hole conditions above 170 mbsf are poor with a regular increase in the hole size. Nineteen dolomitic layers and 114 anomalous, probably organic-rich, dark layers were identified from logging data. Natural gamma-ray intensity can be used for detailed core-log correlations and for correlation with Site 1082 in the Walvis Basin.

Based on pore-water chemistry and C_{org} concentrations, Site 1084 records by far the highest productivity of the Leg 175 sites. This was to be expected because the site is close to the most active upwelling cell off southwest Africa, the Lüderitz Bay. The sediments recovered will allow high-resolution documentation of the variability of coastal upwelling of the last ~4.7 m.y.

BACKGROUND AND OBJECTIVES

Site 1084 documents the northward migration of the Benguela Current system from the Miocene to the Quaternary, as well as the shoreward and seaward migrations of the upwelling center. The upwelling area of the Benguela Coastal Current (BCC) is fed from the thermocline by South Atlantic Central Water, which originates at the Subtropical Convergence Zone by mixing and sinking of subtropical and subantarctic surface water (Lutjeharms and Valentine, 1987). Filaments of cold, nutrient-rich waters from the coastal upwelling area extends well offshore (as much as ~600 km offshore; Lutjeharms and Stockton, 1987; also see Fig. 1). Here, it mixes with low-productivity oceanic water and forms a zone of intermediate productivity.

Coastal upwelling within the Benguela Current system varies with the seasonal extremes of summer and winter (Shannon and Nelson, 1996). The seasonal pattern is used to divide the system into a northern Benguela Region (NBR) and a southern Benguela Region (SBR; Dingle, 1995). This is seen in the modern-day planktonic foraminiferal distributions (Giraudeau, 1993; Fig. 2) and has been demonstrated using benthic ostracoda (Dingle, 1995) and satellite imaging (Lutjeharms and Meeuwis, 1987). The boundary between the NBR and SBR (Lüderitz Boundary) is the site of maximum upwelling intensity at 26°–27°S, which has the coldest and the most persistent upwelling.

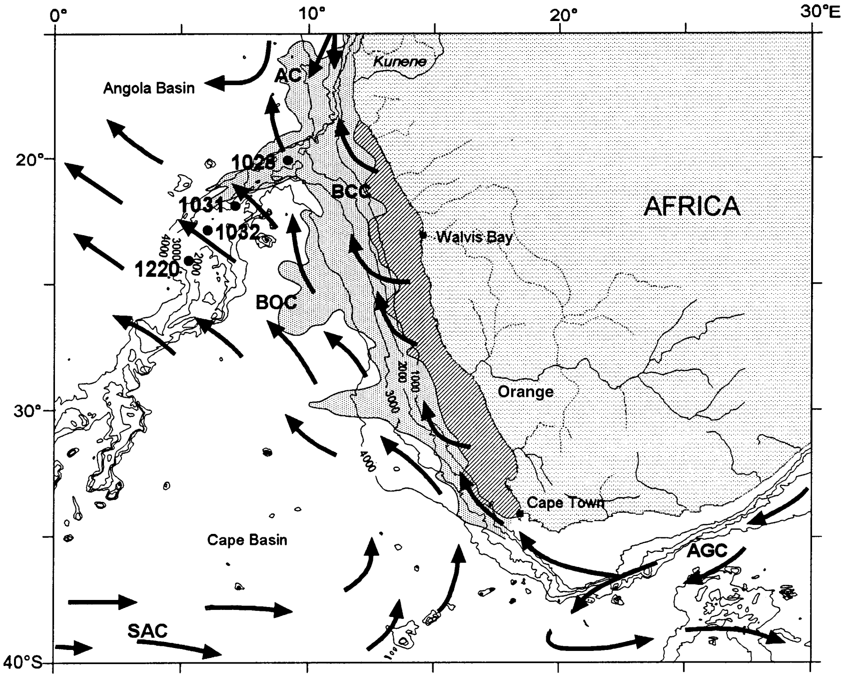

Figure 1. Major upwelling regions off South Africa, with the area of coastal upwelling (hatched pattern) and the extension of the upwelling filaments in the mixing zone between the Benguela Coastal Current (BCC) and the Benguela Oceanic Current (BOC; dark gray pattern), during Southern Hemisphere winter (August; from Wefer et al., 1996; modified after Lutjeharms and Stockton, 1987). AC = Angola Current; SAC = South Atlantic Current; AGC = Agulhas Current. Bold numbers = locations of Geosciences Bremen gravity cores.

Upwelling in the area north of the Lüderitz Boundary (at the location of Site 1084) is typified by year-round high productivity and enhanced accumulation of phytoplankton (Brown et al., 1991). Wind speeds are of medium intensity with a wide, oceanic, filamentous, mixing domain (Lutjeharms and Stockton, 1987). Surface sediments are rich in organics with a maximum in the inner-shelf belt of diatomaceous ooze (Bremner, 1983; Rogers and Bremner, 1991). The SBR has a highly seasonal upwelling regime, with its maximum in summer, and a restricted mixing domain (Lutjeharms and Meeuwis, 1987; Giraudeau and Rogers, 1994). Sites 1085 and 1086 are located within the SBR.

Site 1084 is expected to provide a high-resolution record because of high sedimentation rates. Its close vicinity to the Lüderitz upwelling cell should result in well-expressed organic carbon, diatom, and coccolith cycles via cyclic productivity intensity. In addition, this site is closest to the area with elevated primary production and should have the best representation of coastal upwelling signals. Rapid oceanographic changes in the Benguela upwelling system for the last 160,000 yr are indicated by fluctuating abundances of planktonic foraminifers (Little et al., 1997). The coincidence of increased upwelling intensity with the movement of the Angola-Benguela Front has been interpreted mainly by changes in strength and zonality of the trade-wind system. A close tie-in between pelagic and terrigenous sedimentation is expected to be present within the slope record. Previous work in this area has documented anaerobic, in part varved, sedimentation in the upper margin regions (for a summary, see Dingle et al., 1987; Summerhayes et al., 1995). Phosphatic deposits also are abundant (Calvert and Price, 1983).

OPERATIONS

Hole 1084A (Proposed Site NCB-2B)

The 294-nmi voyage to Site 1084 was accomplished at an average speed of 9.3 kt. The vessel approached the Global Positioning System coordinates of the site, and a beacon was deployed at 0310 hr on 21 September. Hole 1084A was spudded with the advanced APC at 0810 hr. The seafloor depth was estimated from the recovery of the first core at 1991.9 meters below sea level (mbsl). APC coring advanced without incident to 149.5 mbsf (Cores 175-1084A-1H through 17H; see Table 1; also see the expanded core summary table on CD-ROM, back pocket, this volume), which was considered refusal depth for piston coring. The recovery for the APC at Hole 1084A was 104.9%. Cores were oriented starting with Core 4H. Adara heat-flow measurements were taken at 60.0 mbsf (7H), 79.0 mbsf (9H), 117.0 mbsf (13H), and 136.0 mbsf (15H). Hole 1084A was extended with the XCB to 605.0 mbsf (175-1084A-65X), which was the depth objective for this site. The penetration with the XCB was 455.5 m, with 77.9% recovery. The total recovery at Hole 1084A was 84.6% of the cored interval.

Logging Operations in Hole 1084A

In preparation for logging, an aluminum go-devil was dropped to ensure the opening of the lockable float valve. After the hole was flushed with a high-viscosity mud treatment, the drill string was pulled back to 565.5 mbsf, where the top drive was set back. The drill string was then placed at the logging depth of 89.7 mbsf.

Hole 1084A was logged with a full suite of sensors. For each run, the pipe was set at 89.7 mbsf and pulled back to 59.0 mbsf during logging. The wireline logging heave compensator was started when the logging tools reached the mudline. Logging operations began at 0715 hr on 23 September. The first log was conducted with the seismostratigraphic suite (25.8 m long). This suite was made up of the spectral gamma-ray (NGT), long-spacing sonic (LSS), phasor dual-induction (DIT), and Lamont-Doherty high-resolution temperature (TLT) sondes. The tool string was deployed in the pipe at 0905 hr and logged the hole up from 601.0 mbsf. The tool string was recovered at 1330 hr. The second log was run with the lithoporosity suite (19.5 m long) and included the hostile environment gamma spectrometry (HNGS), accelerator porosity (APS), lithodensity (LDS), and TLT sondes. The tool string was deployed at 1425 hr and logged the hole up from 601.0 mbsf. The tool string was retrieved at 1900 hr. The third log was made with the FMS suite (12.10 m long) and included the NGT, general purpose inclinometer, and FMS sondes. This tool string was deployed at 2310 hr and logged the hole up from 604.5 mbsf. The tool string was recovered at 2245 hr. The fourth and last log was made with the magnetic susceptibility suite (11.8 m long) and

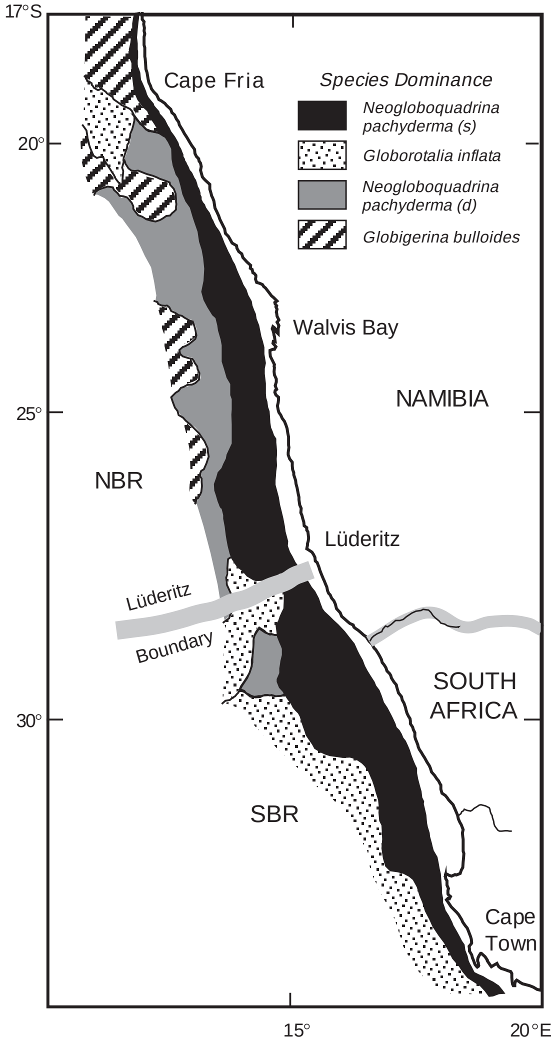

Figure 2. Recent distribution of planktonic foraminifers in the Benguela upwelling system. The Lüderitz Boundary represents the boundary between the northern and southern Benguela regions (NBR and SBR, respectively). From Giraudeau (1993).

included the NGT, magnetic susceptibility, and the nuclear resonance magnetometer sondes. The tool string was deployed in the pipe at 2310 hr and logged the hole up from 603.6 mbsf. It was retrieved at 0210 hr on 24 September. The logging equipment was rigged down by 0300 hr. The drill string was then pulled out of the hole, with the bit clearing the seafloor at 0315 hr on 24 September.

Hole 1084B

The vessel was offset 30 m to the north, and Hole 1084B was spudded with the APC at 0415 hr. The recovery of the first core established the seafloor depth at 1992.8 mbsl. APC coring advanced without incident to refusal at 182.8 mbsf (Cores 175-1084B-1H through 20H), with 102.1% recovery (Table 1). Cores were oriented starting with Core 4H. The bit cleared the seafloor at 1750 hr on 24 September, thereby ending operations at Hole 1084B.

Hole 1084C

The vessel was offset 30 m to the north, and Hole 1084C was spudded with the APC on 24 September. The recovery of the first core established the seafloor depth at 1991.8 mbsl. APC coring ad-

Table 1. Coring summary for Site 1084.

Core	Date (Sept 1997)	Time (UTC)	Interval (mbsf)	Length cored (m)	Length recovered (m)	Recovery (%)
175-1084A-						
1H	21	0820	0.0-3.0	3.0	2.98	99.3
2H	21	0900	3.0-12.5	9.5	9.87	103.9
3H	21	0930	12.5-22.0	9.5	10.06	105.9
4H	21	1005	22.0-31.5	9.5	9.99	105.2
5H	21	1100	31.5-41.0	9.5	10.28	108.2
6H	21	1130	41.0-50.5	9.5	10.13	106.6
7H	21	1225	50.5-60.0	9.5	10.25	107.9
8H	21	1305	60.0-69.5	9.5	10.12	106.5
9H	21	1355	69.5-79.0	9.5	10.15	106.8
10H	21	1435	79.0-88.5	9.5	10.11	106.4
11H	21	1515	88.5-98.0	9.5	10.29	108.3
12H	21	1555	98.0-107.5	9.5	10.40	109.5
13H	21	1650	107.5-117.0	9.5	10.32	108.6
14H	21	1730	117.0-126.5	9.5	10.12	106.5
15H	21	1825	126.5-136.0	9.5	10.18	107.2
16H	21	1915	136.0-145.5	9.5	7.17	75.5
17H	21	1955	145.5-149.5	4.0	4.38	109.5
18X	21	2210	149.5-152.5	3.0	0.15	5.0
19X	21	2250	152.5-162.2	9.7	6.01	62.0
20X	21	2330	162.2-171.8	9.6	5.68	59.2
21X	22	0005	171.8-181.5	9.7	8.58	88.5
22X	22	0035	181.5-191.2	9.7	1.32	13.6
23X	22	0105	191.2-200.8	9.6	4.31	44.9
24X	22	0140	200.8-210.4	9.6	6.23	64.9
25X	22	0220	210.4-220.1	9.7	9.35	96.4
26X	22	0255	220.1-229.7	9.6	2.56	26.7
27X	22	0320	229.7-239.3	9.6	6.14	64.0
28X	22	0355	239.3-248.9	9.6	9.37	97.6
29X	22	0430	248.9-258.5	9.6	5.62	58.5
30X	22	0505	258.5-268.2	9.7	7.44	76.7
31X	22	0540	268.2-277.8	9.6	3.59	37.4
32X	22	0615	277.8-287.4	9.6	5.43	56.6
33X	22	0645	287.4-297.0	9.6	7.34	76.5
34X	22	0715	297.0-306.6	9.6	7.42	77.3
35X	22	0745	306.6-316.3	9.7	6.64	68.5
36X	22	0815	316.3-325.9	9.6	6.52	67.9
37X	22	0850	325.9-335.6	9.7	9.68	99.8
38X	22	0920	335.6-345.2	9.6	9.29	96.8
39X	22	0950	345.2-354.8	9.6	9.15	95.3
40X	22	1020	354.8-364.4	9.6	9.56	99.6
41X	22	1050	364.4-374.1	9.7	9.60	99.0
42X	22	1120	374.1-383.7	9.6	8.39	87.4
43X	22	1150	383.7-393.3	9.6	9.97	103.9
44X	22	1235	393.3-402.9	9.6	9.94	103.5
45X	22	1315	402.9-412.6	9.7	9.96	102.7
46X	22	1420	412.6-422.2	9.6	9.62	100.2
47X	22	1500	422.2-431.9	9.7	6.94	71.5
48X	22	1620	431.9-441.6	9.7	7.77	80.1
49X	22	1700	441.6-451.2	9.6	9.42	98.1
50X	22	1740	451.2-460.8	9.6	9.49	98.9
51X	22	1815	460.8-470.0	9.2	9.13	99.2
52X	22	1855	470.0-479.7	9.7	7.88	81.2
53X	22	1935	479.7-489.4	9.7	6.08	62.7
54X	22	2015	489.4-499.1	9.7	7.33	75.6
55X	22	2050	499.1-508.7	9.6	4.49	46.8
56X	22	2130	508.7-518.3	9.6	5.13	53.4
57X	22	2210	518.3-528.0	9.7	8.89	91.6
58X	22	2250	528.0-537.7	9.7	7.24	74.6
59X	22	2330	537.7-547.3	9.6	6.43	67.0
60X	23	0010	547.3-557.0	9.7	8.23	84.8
61X	23	0055	557.0-566.6	9.6	7.99	83.2
62X	23	0135	566.6-576.2	9.6	10.02	104.4
63X	23	0220	576.2-585.9	9.7	9.54	98.4
64X	23	0305	585.9-595.5	9.6	8.71	90.7
65X	23	0355	595.5-605.0	9.5	9.19	96.7
Coring totals:				605	511.56	84.6
175-1084B-						
1H	24	0425	0.0-4.1	4.1	4.15	101.2
2H	24	0455	4.1-13.6	9.5	9.14	96.2
3H	24	0530	13.6-23.1	9.5	9.17	96.5
4H	24	0605	23.1-32.6	9.5	9.98	105.1
5H	24	0640	32.6-42.1	9.5	10.01	105.4
6H	24	0715	42.1-51.6	9.5	10.16	106.9
7H	24	0750	51.6-61.1	9.5	10.12	106.5
8H	24	0825	61.1-70.6	9.5	8.95	94.2
9H	24	0905	70.6-80.1	9.5	10.24	107.8
10H	24	0940	80.1-89.6	9.5	9.54	100.4
11H	24	1015	89.6-99.1	9.5	8.54	89.9
12H	24	1045	99.1-108.6	9.5	10.01	105.4
13H	24	1125	108.6-118.1	9.5	10.20	107.4
14H	24	1200	118.1-127.6	9.5	10.22	107.6
15H	24	1240	127.6-137.1	9.5	10.48	110.3
16H	24	1325	137.1-146.6	9.5	9.79	103.1
17H	24	1400	146.6-156.1	9.5	8.29	87.3
18H	24	1440	156.1-165.6	9.5	10.12	106.5
19H	24	1530	165.6-175.1	9.5	10.07	106.0

Table 1 (continued).

Core	Date (Sept 1997)	Time (UTC)	Interval (mbsf)	Length cored (m)	Length recovered (m)	Recovery (%)
20H	24	1605	175.1-182.8	7.7	7.42	96.4
Coring totals:				182.8	186.6	102.1
175-1084C-						
1H	24	1840	0.0-8.1	8.1	8.16	100.7
2H	24	1910	8.1-17.6	9.5	8.80	92.6
3H	24	1950	17.6-27.1	9.5	9.92	104.4
4H	24	2030	27.1-36.6	9.5	10.08	106.1
5H	24	2105	36.6-46.1	9.5	9.95	104.7
6H	24	2140	46.1-55.6	9.5	9.77	102.8
7H	24	2215	55.6-65.1	9.5	10.12	106.5
8H	24	2255	65.1-74.6	9.5	10.13	106.6
9H	24	2335	74.6-84.1	9.5	10.10	106.3
10H	25	0010	84.1-93.6	9.5	10.59	111.5
11H	25	0045	93.6-103.1	9.5	10.12	106.5
12H	25	0120	103.1-112.6	9.5	10.07	106.0
13H	25	0155	112.6-122.1	9.5	10.07	106.0
14H	25	0230	122.1-131.6	9.5	10.08	106.1
15H	25	0300	131.6-141.1	9.5	10.06	105.9
16H	25	0340	141.1-150.6	9.5	10.13	106.6
17H	25	0420	150.6-160.1	9.5	10.23	107.7
18H	25	0455	160.1-169.6	9.5	9.88	104.0
19H	25	0530	169.6-179.1	9.5	10.40	109.5
20H	25	0610	179.1-188.6	9.5	9.97	104.9
21H	25	0645	188.6-198.1	9.5	9.64	101.5
22H	25	0725	198.1-207.6	9.5	9.55	100.5
Coring totals:				207.6	217.82	104.9

Notes: UTC = Universal Time Coordinated. An expanded version of this coring summary table that includes lengths and depths of sections and comments on sampling is included on CD-ROM (back pocket, this volume).

vanced to 202.0 mbsf (Cores 175-1084C-1H through 22H), with 104.9% recovery (Table 1). Cores were oriented starting with Core 3H. The drill string was retrieved with the bit clearing the seafloor at 0835 hr and the plane of the rotary table at 1225 hr on 25 September, thereby ending operations at Site 1084.

SITE GEOPHYSICS

Introduction and Strategy

The distribution of drill sites along the southwest African continental margin was chosen to reconstruct the latitudinal evolution of the Benguela Current system in space and through time. The working area in the Northern Cape Basin (NCB) lies directly seaward of the currently most productive coastal upwelling cells in the area. Therefore, the drill sites are targeted to study the variability of the upwelling system and mechanisms of "leakage" of upwelling sediments into the hemipelagic realm and to analyze and date the onset and early stages of upwelling processes at this latitude.

Two drill sites, NCB-1 and NCB-2, had been originally proposed. These sites were derived from Line AM-1 of Austin and Uchupi (1982). Site NCB-1, in shallow water of 180 m depth, was not included in the final drilling plan because of the lack of Neogene sediments and the general problems of drilling in shelf areas.

The area was visited during *Sonne* Cruise SO 86 (Bleil et al., 1994), when multichannel seismic data complementary to Line AM-1 were collected (Fig. 3). After the survey of the shallow-water site, technical problems caused us to abandon the profile across the deeper site. During *Meteor* Cruise M34/1 (Bleil et al., 1996), three additional seismic lines totaling 321 km in length were acquired (Fig. 3) to understand the local tectonic and depositional framework and its relationship to the continental shelf. Together with the previously collected data, the area of the proposed site was now sufficiently studied to precisely locate the drill site.

Seismostratigraphy

Site 1084 is located in 1992 m water depth on seismic Line Geosciences Bremen (GeoB)/AWI 96-014 (common depth point [CDP] 2067; see Fig. 4) at the downslope rim of a depositional basin. The sedimentary structures are more complex than in the Walvis Basin, but the uppermost sedimentary sequence (between CDPs 1200 and 3700) of 500–800 ms two-way traveltime (TWT) thickness appears mostly undisturbed and unaffected by earlier mass movements.

Although the area is located more than 200 nmi south of the Walvis Basin, the general seismic and depositional patterns appear to be very similar. The upper seismic unit, which was not penetrated, is characterized by numerous high-amplitude reflectors. The thickness generally decreases seaward, except for at the center of the basin.

Upslope from Site 1084 (from CDP 2400 to 3200), a zone of high-amplitude reflectors is identified beneath 300 ms TWT, which also reveals a decrease in seismic frequency. This might be caused by gas charges or intensified dolomitization, and, consequently, the area was avoided for drilling. At ~700 ms TWT, a thin intercalated slump unit can be identified by diffractions and acoustic transparency.

Several locations have disturbed sediment structures beneath the upper unit (CDP 700–1000, 450 ms TWT; CDP 3200–3700, 800 ms TWT; and CDP 0–800, 800 ms TWT), which seem to have no impact on the integrity of the Neogene sediment cover.

Site 1084

Figure 5 shows a 10-km-long seismic section of Line GeoB/AWI 96-014 across Site 1084 at 1992 m water depth. The seismic pattern reflects hemipelagic deposition without major disturbances or faulting. Some indication for slumping was found at 700 ms TWT sub-bottom depth. Seismic amplitudes are generally high for the upper 700 ms TWT. Several reflectors appear diffuse and patchy, indicating either lateral inhomogeneities or interference.

Figure 6 shows a close-up of the seismic section, plotted against TWT, for a 1-km-long interval near the drill site. Seismic reflectors are compared with the sound velocity log (see "Downhole Logging" section, this chapter), which was also used to recalculate logging depth to TWT. Velocity peaks are associated either with dolomite layers or lithified intervals at depth or with intervals of high organic matter content (black layers; see "Lithostratigraphy" section, this chapter). Black layers are not associated with an increase in logging density, and, accordingly, the change in acoustic impedance is small. The interval of velocity anomalies from 240 to 340 ms TWT is not associated with a distinct increase in seismic energy, although between 200 and 390 ms TWT, amplitudes are generally higher than above. Another interval of lower seismic energy from 390 to 550 ms TWT goes parallel to a smooth velocity log. In the middle of lithologic Unit II, ~570 ms TWT (440 mbsf), an increase in the velocity gradient is associated with a higher variability, which may be related to a change from diatomaceous sediments to nannofossil ooze and clay. This directly affects the returned seismic energy, which shows a significant increase.

Most lithologic changes and variations have a stronger impact on the density in shallow sediments, and it cannot be expected to find their expression also in the velocity log. A decrease in logging sound velocity at 710 ms TWT sub-bottom depth might indicate undercompacted sediments. This decrease coincides well with the observation of a zone of low energy and diffraction, which was tentatively identified as a slump interval above and is confirmed by a disturbed unit with cross-bedding, as described in the "Lithostratigraphy" section (this chapter).

LITHOSTRATIGRAPHY

Description of Lithostratigraphic Units

Sediments from Site 1084 form four lithostratigraphic units defined by the changes in the major lithology between clay and ooze (see Figs. 7, 8). Unit I is composed of moderately bioturbated, intercalated intervals of olive (5Y 4/3), olive-gray (5Y 4/2), dark olive-gray (5Y 4/1), and black (5Y 2.5/1) clays, which contain varying

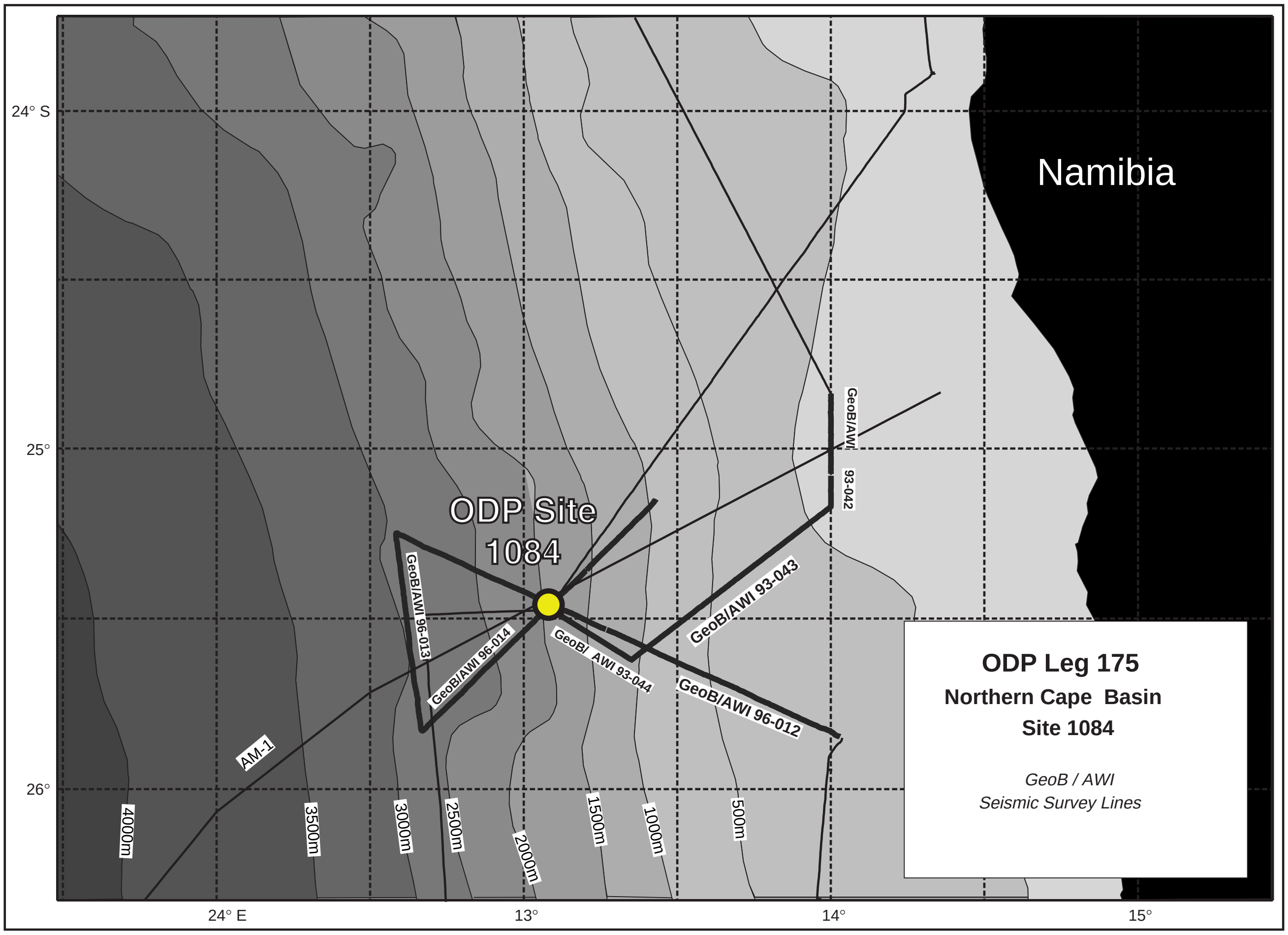

Figure 3. Map of seismic presite survey lines, proposed site locations, and ODP Leg 175 drill Site 1084 in the Northern Cape Basin. Bathymetry was derived from Gebco Digital Dataset on CD-ROM.

abundances of diatoms, nannofossils, foraminifers, and radiolarians. Three subunits are distinguished based on microfossil type and abundance. Unit II is composed of olive (5Y 4/3) clay-rich nannofossil diatom ooze that grades into olive (5Y 4/3) diatomaceous nannofossil ooze and clay-rich nannofossil ooze. Unit III comprises olive (5Y 4/3 and 5Y 5/3) and olive-gray (5Y 5/2) clay, nannofossil clay, and diatom-bearing nannofossil clay. Unit IV is composed of olive-gray (5Y 4/2) and dark olive-gray (5Y 3/2) clayey nannofossil ooze and diatom-rich clayey nannofossil ooze.

Unit I

Intervals: 175-1084A-1H-1, 0 cm, through 175-1084A-43H; 175-1084B-1H-1, 0 cm, to bottom of hole; 175-1084C-1H-1, 0 cm, to bottom of hole
Age: Holocene to late Pleistocene
Depth: 175-1084A: 0–393 mbsf; 175-1084B: 0–183 mbsf; 175-1084C: 0–208 mbsf

Subunit IA

Intervals: 175-1084A-1H-1, 0 cm, through 175-1084A-12H; 175-1084B-1H-1, 0 cm, through 175-1084B-12H; 175-1084C-1H-1, 0 cm, through 175-1084C-13H;
Age: Holocene to Pleistocene
Depth: 175-1084A: 0–107.5 mbsf; 175-1084B: 0–109 mbsf; 175-1084C: 0–122 mbsf

Subunit IA is composed of moderately bioturbated olive-gray (5Y 3/2 to 5Y 4/2), very dark grayish brown (5Y 3/3), and olive (5Y 4/3) foraminifer- and diatom-bearing nannofossil clay, and foraminifer-bearing diatom-rich clayey nannofossil ooze. The abundance of microfossils, particularly nannofossils, increases downcore through this subunit. Cores 175-1084A-7H through 11H contain intervals with nannofossil abundances high enough to define the major lithology as a nannofossil ooze. Sediments in Subunit IA have relatively high carbonate and organic carbon contents, which average 37 and 8.2 wt%, respectively (see "Organic Geochemistry" section, this chapter). The boundary between Subunits IA and IB is relatively sharp and occurs between Cores 175-1084A-12H and 13H, 175-1084B-12H and 13H, and 175-1084C-13H and 14H. The contact is marked by an increase in diatom abundance from diatom-bearing and sporadically diatom-rich to continuously diatomaceous clay and a decrease in nannofossil abundance from ooze to nannofossil-rich. Subunit IA contains several intervals of dark olive-brown (5Y 3/3) and black (5Y 2.5/1 and 2.5Y 2.5/1) sediment. These intervals range in thickness between 30 cm and 9 m and are composed of clay, diatom-rich clay, and nannofossil clay (intervals 175-1084A-3H-6, 0–90 cm, 4H-1, 90–98 cm, 5H-6, 0–70 cm, and 7H-4, 80 cm to 7H-5, 70 cm; 175-1084A-11H-5, 0 cm, to 11H-8, 150 cm; 175-1084A-12H-1, 0 cm, to 12H-3, 150 cm; and 175-1084A-12H-6, 0 cm, to 12H-7, 50 cm; see Table 2). In general, these horizons are characterized by lower carbonate contents, which average just below 10 wt%, and higher organic carbon, which range between 8 and 18 wt% (see "Organic Geochemistry"

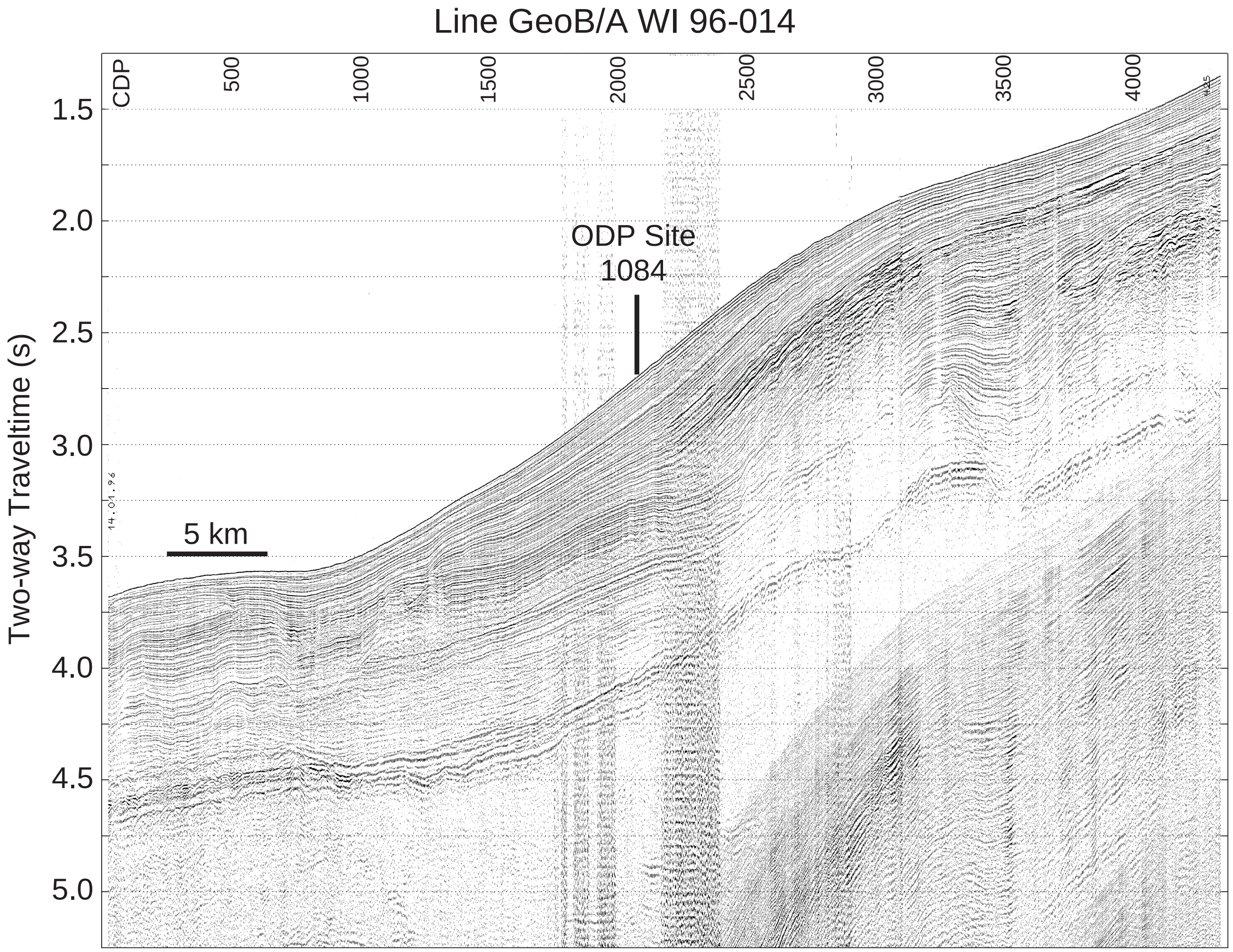

Figure 4. Seismic Line GeoB/AWI 96-014 with Site 1084. Vertical axis is given in TWT. CDP interval is 25 m for a shotpoint spacing of 25 m. Seismic data is 24-fold stacked and not migrated. Site 1081 is located at CDP 2067.

section, this chapter) when compared to the under- and overlying sediment layers.

Subunit IB

Intervals: 175-1084A-13H through 175-1084A-36H; 175-1084B-13H through the end of the core; 175-1084C-14H through the end of the core
Age: Pleistocene to late Pliocene
Depth: 175-1084A: 107.5–325.9 mbsf; 175-1084B: 109–183 mbsf; 175-1084C: 122–208 mbsf

The contact between Subunit IB and Subunit IA is defined by the increase in diatom abundance from frequent and common to abundant. Its boundary with Subunit IC is marked by a change from clays that are nannofossil-rich clay to those that are diatomaceous. This transition occurs between Cores 175-1084A-36X and 37X. Subunit IB is characterized by frequent and irregular variations in color and lithology over short depth intervals. A comparable variation in color and lithology is not observed in the other subunits. Lithologies frequently alternate between olive (5Y 4/3) nannofossil-rich diatomaceous clay (e.g., Sections 175-1084A-13H-1 through 13H-4), olive (5Y 4/3) clayey nannofossil ooze, and black (5Y 2.5/1) diatom-bearing clay (e.g., Sections 175-1084A-29X-1 through 29X-2). Intervals of these lithologies range in thickness from 3.5 to 8 m (see visual core descriptions, Section 4, this volume). Concentrations of calcium carbonate and organic carbon average 26 and 7.0 wt%, respectively. Dolomitized clay nodules are present in Core 175-1084A-18X. In Subunit IB, the dark olive-brown (5Y 3/3) and black (5Y 2.5/1 and 2.5Y 2.5/1) layers are composed of nannofossil-bearing diatomaceous clay, foraminifer-bearing diatom-rich nannofossil clay, diatom-rich clay, and nannofossil-bearing diatom-rich clay (intervals 175-1084A-14H-6, 130 cm, to 14H-7, 10 cm; 175-1084A-21X-6, 0–94 cm, 22X-1, 22X-CC, and 24X-4, 0 cm, to 24X-CC, 30 cm; 175-1084A-25X-3, 130 cm, to 25X-4, 70 cm; and 175-1084A-29X-1, 0 cm, to 29X-2, 150 cm). The "dark" horizons in Subunit IB are generally more carbonate rich compared with those found in Subunit IA.

Subunit IC

Interval: 175-1084A-36X through 175-1084A-43X
Age: late Pliocene
Depth: 175-1084A: 325.9–393.3 mbsf

Subunit IC contains moderately bioturbated, dark olive-gray (5Y 3/2) and olive (5Y 4/3) nannofossil-rich diatomaceous clay and nan-

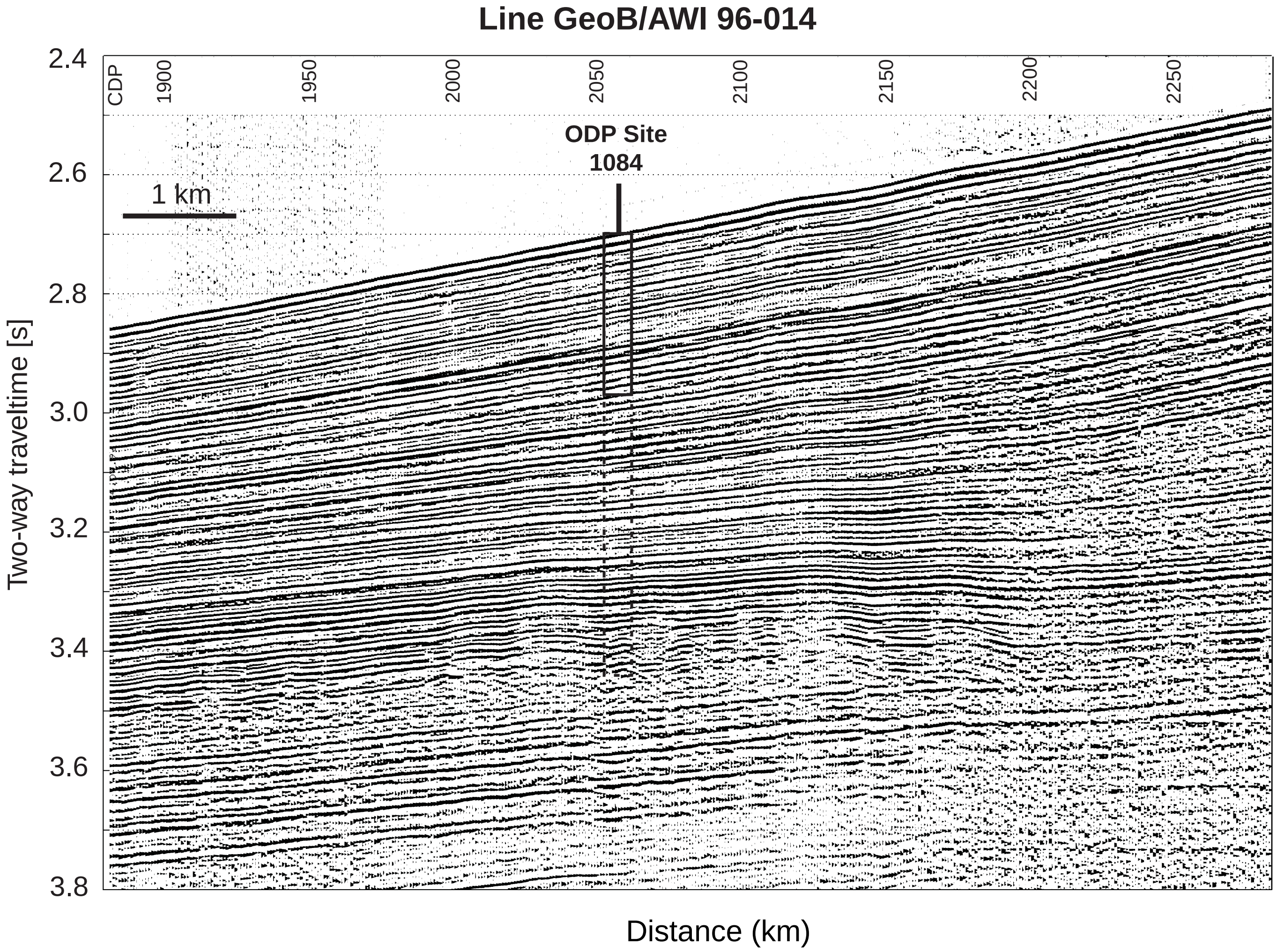

Figure 5. Seismic section of Line GeoB/AWI 96-014 at Site 1084. Vertical axis is given in TWT. CDP interval is 25 m for a shotpoint spacing of 25 m. Site 1084 is located at CDP 2067. The box indicates the approximate penetration of the borehole of 200 (APC) and 600 m (XCB), respectively.

nofossil diatomaceous clay. This subunit is characterized by carbonate and organic carbon contents that average 14 and 4.9 wt%, respectively (see “Organic Geochemistry” section, this chapter). Subunit IC is a transitional unit between Subunit IB and Unit II and is lithologically more homogeneous than Subunit IB. Its upper contact is characterized by a change from diatomaceous clay to diatom ooze. This transition occurs between Cores 175-1084A-36 and 37X and is gradual. The lithologic contact between Subunit IC and Unit II occurs between Cores 175-1084A-43X and 44X and marks a transition from diatomaceous clay to clay-rich diatomaceous nannofossil ooze. The absolute change in diatom abundance across this transition is smaller when compared with the change in diatom abundance observed between black and olive horizons within this subunit. This change is gradual and occurs between Cores 43X and 44X. Subunit IC contains only one interval (175-1084A-43X-4, 100–115 cm) of black (5Y 2.5/1) diatomaceous clay.

Unit II

Interval: 175-1084A-43X through 175-1084A-53X
Age: late Pliocene
Depth: 175-1084A: 393.3–498.4 mbsf

Unit II contains olive (5Y 4/3) clay-rich nannofossil diatom ooze that grades into olive (5Y 4/3) diatomaceous nannofossil ooze and clay-rich nannofossil ooze. This subunit is characterized by carbonate and organic carbon contents, which average 28 and 3 wt%, respectively (see “Organic Geochemistry” section, this chapter). The boundary between Units II and III is defined as the change in the major lithology from nannofossil and diatom ooze to nannofossil clay. This gradual transition occurs between Cores 175-1084A-53X and 54X. Unit II contains two intervals of black (5Y 2.5/1) nannofossil-bearing diatom ooze at 175-1084A-43X-3, 0–70 cm, 46X-3, 0–94 cm, and 51X, 85–105 cm.

Unit III

Interval: 175-1084A-54X through 175-1084A-59X
Age: late Pliocene
Depth: 175-1084A: 498.4–547.3 mbsf

Unit III contains moderately bioturbated olive (5Y 4/3 and 5Y 5/3), pale olive (5Y 6/3), and olive-gray (5Y 5/2) clay, nannofossil clay, and diatom-bearing nannofossil clay. The unit contains few dark olive-gray (5Y 3/2), 50- to 100-cm-thick clay and nannofossil-rich clay in-

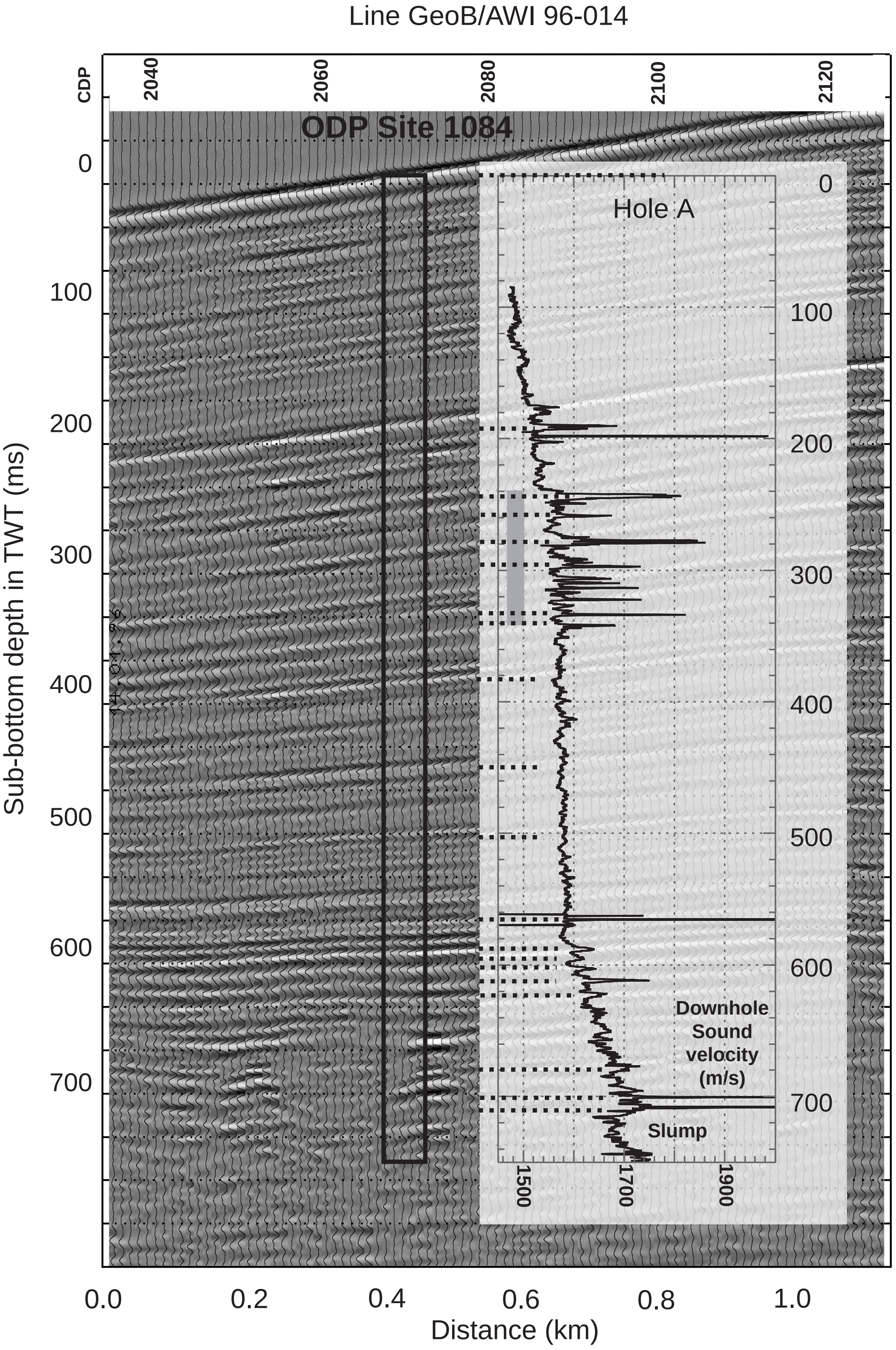

Figure 6. Close-up of Line GeoB/AWI 96-014 near Site 1084. Vertical axis is given in TWT. Amplitudes are grayscaled. For comparison the sound velocity profile from downhole logging is shown. Logging depth is transferred to TWT using the logging results. Selected reflectors can be correlated with local extremes in the velocity log (thick dashed lines), but density-controlled lithologic changes are not reflected in the logging data.

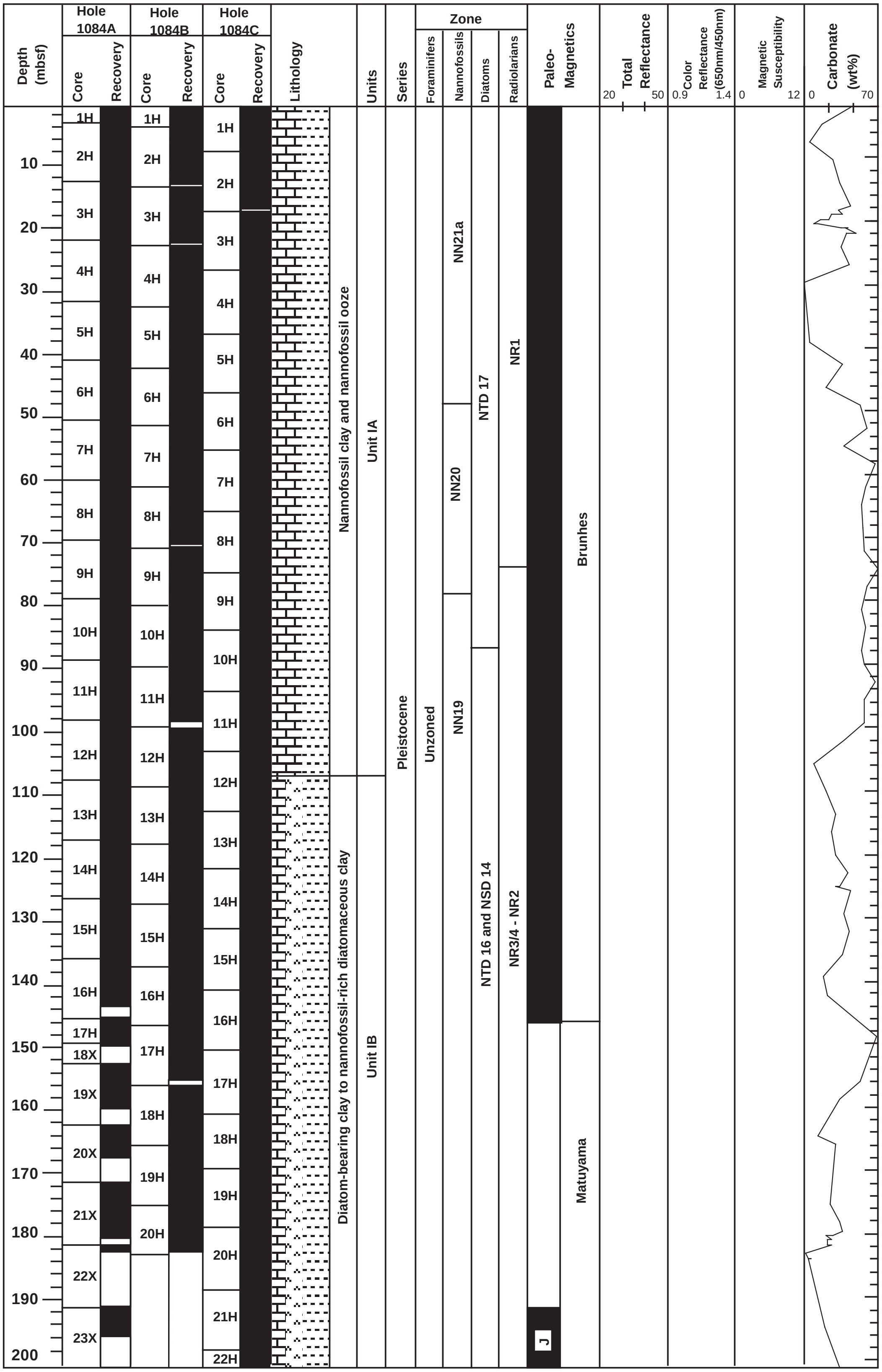

Figure 7. Composite stratigraphic section for Site 1084 showing core recovery in all holes, a simplified summary of lithology, age, total reflectance (400–700 nm), color reflectance (650 nm/450 nm), magnetic susceptibility, and calcium carbonate content. J = Jaramillo Subchron; O = Olduvai Subchron. (Continued next page.)

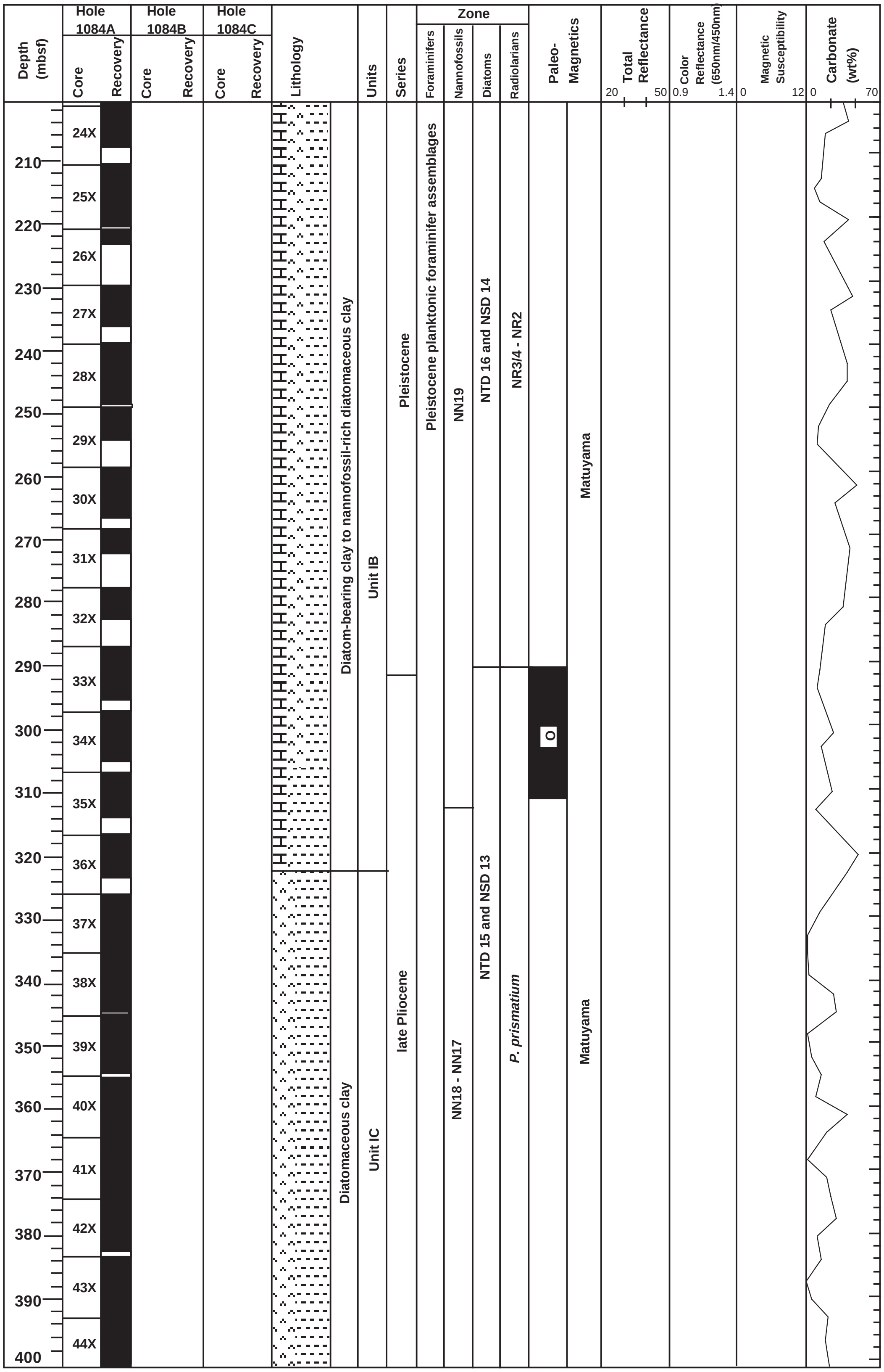

Figure 7 (continued).

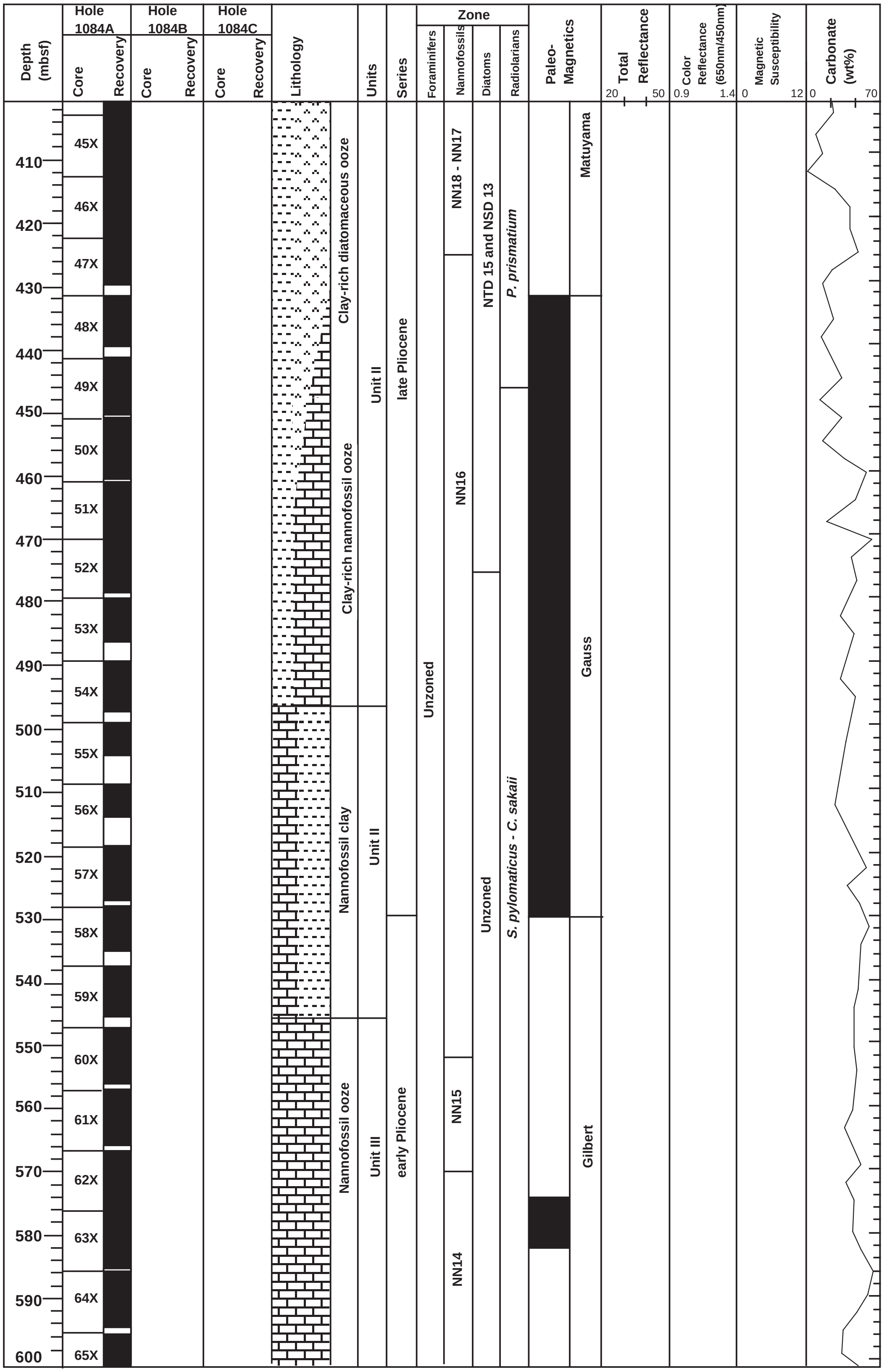

Figure 7 (continued).

tervals. These intervals occur irregularly throughout the unit. Unit III is characterized by carbonate and organic carbon contents that average 42 and 4 wt%, respectively (see "Organic Geochemistry" section, this chapter). The contact between Units III and IV is defined as the change in the major lithology from clay to nannofossil ooze. This boundary occurs between Cores 175-1084A-59X and 60X.

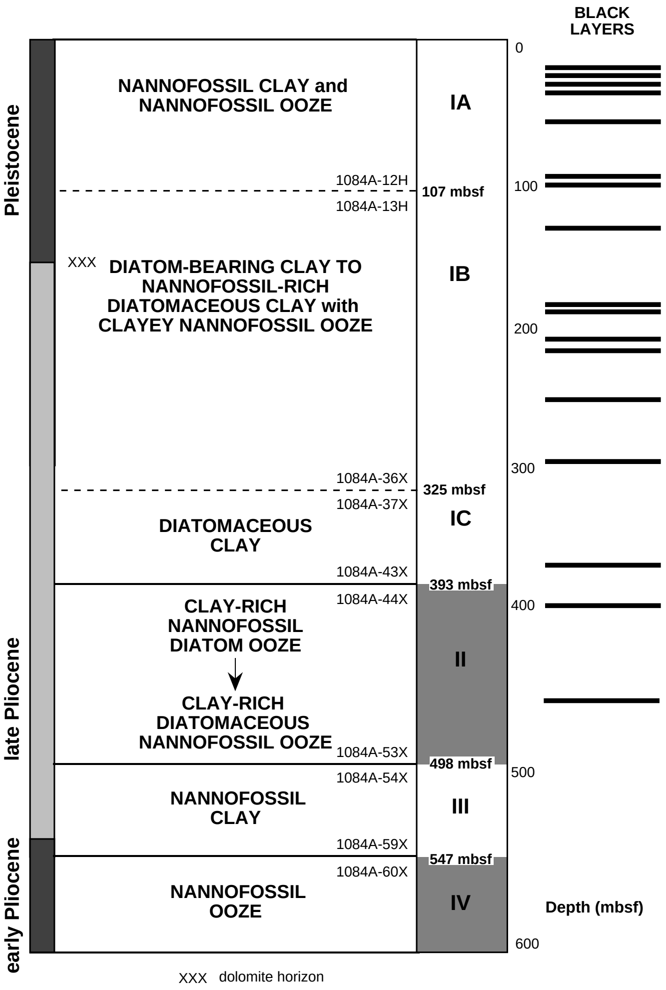

Figure 8. Description of the lithostratigraphic units at Site 1084 and the approximate occurrence of the organic-rich black layers.

Unit IV

Interval: 175-1084A-60X through 175-1084A-65X
Age: early Pliocene
Depth: 175-1084A: 547.3–604.7 mbsf

Unit IV is composed of moderately bioturbated olive-gray (5Y 4/2 and 5Y 5/2), pale olive (5Y 6/3) clayey nannofossil ooze, diatom-bearing clayey nannofossil ooze, and diatom-rich clayey nannofossil ooze. Dark olive-gray (5Y 3/2) intervals, 20 to 50 cm in thickness, of diatom-bearing clay-rich nannofossil ooze and diatom-bearing nannofossil clay are present throughout this unit. Unit IV is characterized by high carbonate and organic carbon contents, which average 46 and 3 wt%, respectively (see "Organic Geochemistry" section, this chapter). The contact between Units III and IV is defined as the change in the major lithology from clay to nannofossil ooze. This transition occurs between Cores 175-1084A-59X and 60X.

Synthesis of Smear-Slide Analyses

Smear-slide analyses indicate that the detrital component of the sediments in the four units consists of clay with rare silt-sized, angular and subangular mono- and polycrystalline quartz grains. Subangular feldspar grains are present in trace amounts. Authigenic minerals include framboidal pyrite and dolomite rhombs in rare or trace abundances. The dark horizons generally contain slightly higher abundances of pyrite. Silt-sized cryptocrystalline carbonate grains are generally rare to frequent in abundance and, at times, common. Subunit IA contains trace and rare amounts of quartz and pyrite throughout. Rare silt-sized, cryptocrystalline carbonate grains are found in Subunit IA in Core 175-1084A-7H. Subunit IB contains pyrite in increased abundance and trace amounts of silt-sized quartz grains, feldspar, and mica. In the lower part of Subunit IB, between Cores 175-1084A-25X and 36X, silt-sized cryptocrystalline carbonate grains are consistently present in rare or few abundance. Subunit IC and Unit II contain trace and rare amounts of silt-sized quartz and pyrite grains throughout. Unit III also contains silt-sized, subhedral pyrite grains. Unit IV contains rare pyrite and trace amounts of both silt-sized quartz and cryptocrystalline carbonate grains. Dark horizons exhibit significant compositional variations in the relative abundances of diatoms, foraminifers, and nannofossils (Table 2). Most of the dark layers in Subunit IA have lower abundances of nannofossils compared with Subunits IB and IC and Unit II. The biogenic component of the dark layers is commonly dominated by diatom resting spores. Resting spores are present only in trace abundances in the sediments under- and overlying the black layers.

Table 2. Lithologic summary of dark layers at Hole 1084A.

Core, section, interval (cm)	Depth (mbsf)	Clay	Pyrite	Diatoms	Foraminifers	Nannofossils	Organic debris	Sediment name	Lithostratigraphic units
175-1084A-									
3H-6, 50	20.5	A	R	F	R	C	R	Nannofossil- and diatom-bearing clay	Subunit IA
4H-1, 50	22.5	A	R	F	R	C	R	Diatom-bearing, nannofossil-rich clay	Subunit IA
5H-1, 100	32.5	A	F	C	T	T	A	Organic-rich clay	Subunit IA
5H-6, 80	39.7	A	F	C	B	B	A	Organic-rich clay	Subunit IA
7H-4, 120	55.73	A	R	F	R	C	F	Diatom-bearing, nannofossil-rich clay	Subunit IA
11H-6, 80	95.47	F	B	C	F	A	B	Diatom-rich nannofossil ooze	Subunit IA
12H-2, 80	99.06	A	R	R	B	C	C	Nannofossil clay	Subunit IA
14H-6, 144	126	A	F	A	B	B	B	Diatom-rich clay	Subunit IB
21X-6, 40	179.7	A	R	F-C	B	A	R	Foraminifer-bearing nannofossil clay	Subunit IB
22X-1, 40	181.9	A	R	C	T	F-C	R	Diatom-rich clay	Subunit IB
24X-5, 40	206.1	A	T	C	R-F	C	R	Clay	Subunit IB
29X-2, 80	251.2	A	T	F	B	B	C	Diatom-bearing clay	Subunit IB
33X-5, 70	294	A	R	C	R	C	F	Diatom-rich nannofossil clay	Subunit IB
43X-4, 113	389.3	A	T	A	B	T	R	Diatomaceous clay	Subunit IC
46X-3, 15	414.8	C	F	D	B	F	R	Nannofossil-bearing clayey diatom ooze	Unit II
51X-4, 100	466.3	A	R	F	B	R	T	Diatom-bearing clay	Unit II

Notes: D = dominant (>60%); A = abundant (30%–60%); C = common (10%–30%); F = few (5%–10%); R = rare(1%–5%); T = trace(<1%); and B = barren.

Spectrophotometry

Color data were measured for all the cores from Holes 1084A, 1084B, 1084C. At Site 1084, total reflectance values range from 20% to 58% (Fig. 9), which represent the alternating carbonate-rich and organic-rich black-colored sediment layers. The highest values in total reflectance were observed in Subunit IA and Unit II, which correspond to nannofossil ooze intervals (see "Description of the Lithostratigraphic Unit," this section). Low values of total reflectance correspond to the presence of black (5Y 2.5/1 and 2.5Y 2.5/1) clay horizons (Fig. 9; Table 2). The lowest values for total reflectance vary between 20% and 25% and were observed in Subunits IA and IB. These sediments have very low calcium carbonate (0–10 wt%) and high organic carbon concentrations (8–18 wt%; see "Organic Geochemistry" section, this chapter; also see Fig. 10). Numerous gaps in the total reflectance record caused by poor core recovery, especially within Subunit IB (between 150 and 300 mbsf), prevents the determination of the cyclicity of the black layers. The general trends in total reflectance can be correlated to the lithostratigraphic units and subunits at Hole 1082A (Fig. 3, "Site 1082" chapter, this volume) and display well-defined cycles that may be used for high-resolution stratigraphy—except within Subunit IB.

BIOSTRATIGRAPHY AND SEDIMENTATION RATES

Sediments recovered from Site 1084 represent a relatively continuous hemipelagic section spanning the last 4.7 m.y. Micropaleontological studies were carried out on core-catcher samples from Hole 1084A. Additional samples from within the cores were examined to improve the biostratigraphic resolution. An integrated biostratigraphic framework composed of both calcareous and siliceous microfossils was established (Fig. 11), resulting in a well-constrained age model for Site 1084. Sedimentation rates range from 10 to 27 cm/k.y. with highest values located within the last 1 m.y. A second episode of high sedimentation rate (17 cm/k.y.) is associated with an upper Pliocene diatom-rich interval. These sediments (at an approximate age interval of 2–3 Ma.) are rich in the pennate diatom *Thalassiothrix antarctica* and may represent mat deposits similar to the ones discovered in the eastern equatorial Pacific during Leg 138.

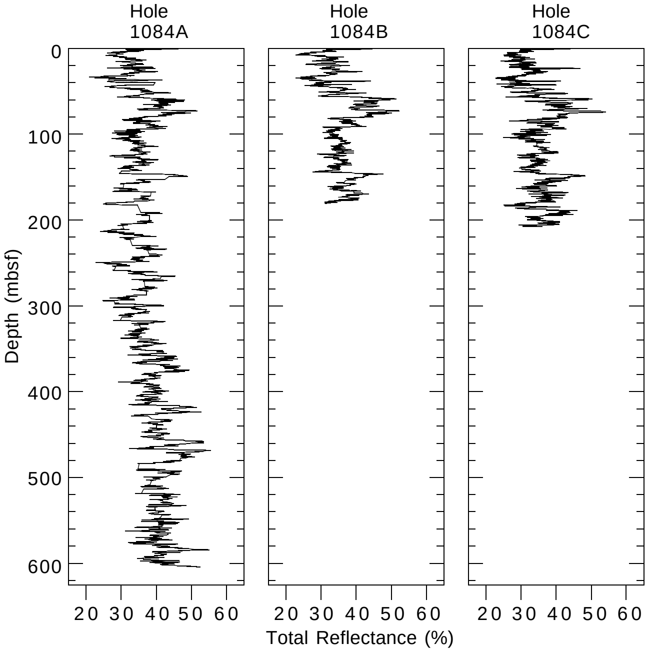

Figure 9. Downcore variation in the total reflectance at Holes 1084A, 1084B, and 1084C.

Calcareous Nannofossils

Calcareous nannofossils were studied in core-catcher samples from Hole 1084A. Additional samples from within the cores were examined close to datum events to improve the stratigraphic resolution. Overall abundance ranges from abundant to very abundant within the top 280 mbsf (Cores 175-1084A-1H through 32X) and the bottom 190 mbsf (Cores 46X through base) of Site 1084. Nannofossil abundance shows minima within Cores 175-1084A-33X through 45X, a sedimentary section composed of diatom-rich clays (lithostratigraphic Subunit IC; see "Lithostratigraphy" section, this chapter) grading downcore to diatom oozes (upper part of Unit II). Preservation within this diatom-rich interval is moderate to poor, but improves in the over- and underlying carbonate-rich sequences.

Calcareous nannofossils provided 13 biohorizons (Table 3). These datum events were constrained within an average depth interval of 3 mbsf. Within the sampling resolution, the sedimentation appears continuous throughout the entire section. Based on the youngest identified datum (last occurrence [LO] of *Gephyrocapsa caribbeanica* acme, 0.26 Ma), no sediments recovered from Site 1084 were younger than 0.09 Ma (i.e., Zone NN21b is missing from the top cores). Paleomagnetic evidence (see "Paleomagnetism" section, this chapter) suggests that Site 1084 terminated within the lower Pliocene sediment at 4.8 ± 0.2 Ma. The oldest identified biostratigraphic datum event (LO of *Amaurolithus tricorniculatus;* 4.5 Ma, mean depth = 570.7 mbsf) is offset from the C3n.1n paleomagnetic Chron by ~30 mbsf, an indication of reworking of the nannofossil assemblages

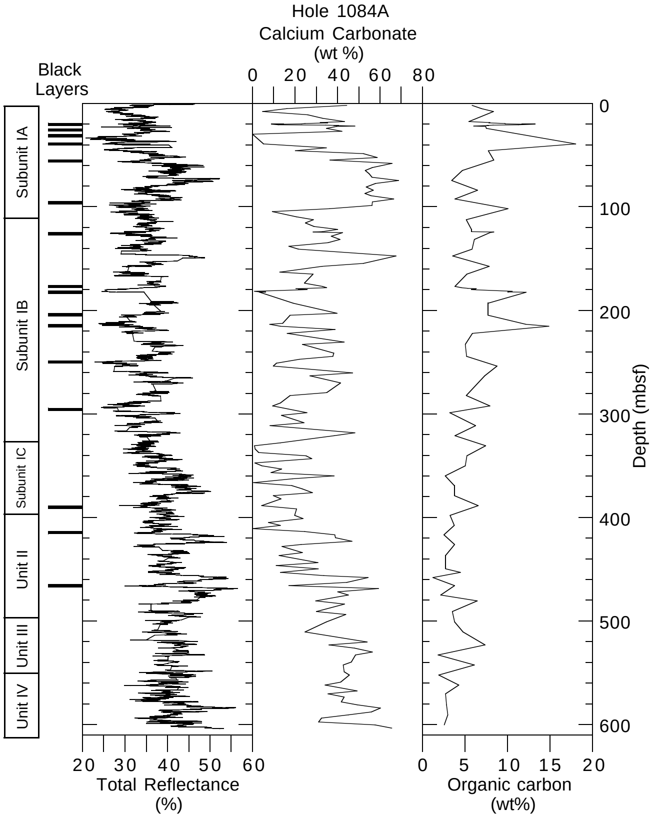

Figure 10. Downcore variation in the total reflectance, calcium carbonate content (in weight percent), and organic carbon content (in weight percent) at Hole 1084A. The position of the black layers and the lithostratigraphic units are also indicated.

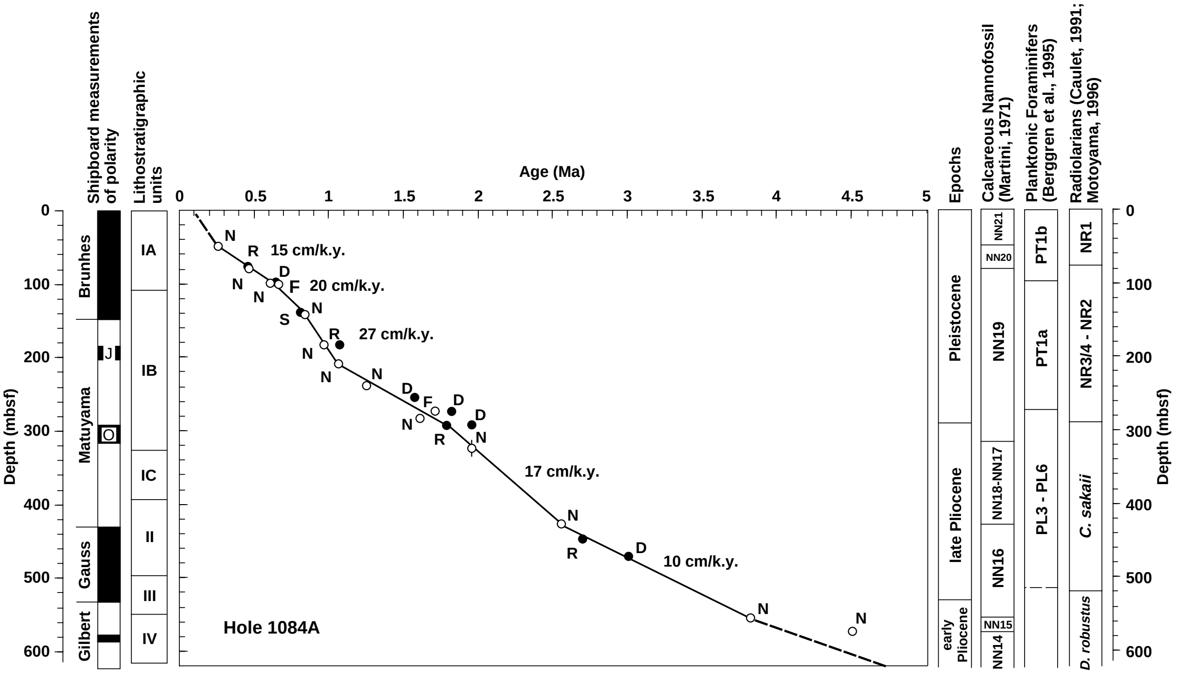

Figure 11. Age-depth plot and sedimentation rates estimated from calcareous microfossil (open circles; F = planktonic foraminifers and N = calcareous nannofossils) and siliceous microfossil (closed circles; D = diatoms, R = radiolarians, and S = silicoflagellates) datums at Hole 1084A.

Table 3. Microfossil datums at Hole 1084A.

Fossil group	Event	Age (Ma)	Zone (base) A	Zone (base) B	Core, section, interval (cm) Top	Core, section, interval (cm) Bottom	Depth (mbsf) Top	Depth (mbsf) Bottom	Depth (mbsf) Mean
					175-1084A-	175-1084A-			
N	FO *Emiliania huxleyi*	0.26	NN21a	CN15	6H-5, 110	6H-6, 110	47.90	49.40	48.65
N	LO *Gephyrocapsa caribbeanica* acme	0.26	NN21a	CN15	6H-5, 110	6H-6, 110	47.90	49.40	48.65
N	LO *Pseudoemiliania lacunosa*	0.46	NN20	CN14b	9H-5, 110	9H-CC	76.50	79.35	77.93
R	LO *Axoprunum angelinum*	0.46			8H-CC	9H-CC	70.02	79.55	74.79
N	LO Small *Gephyrocapsa* acme (Weaver, 1993)	0.60			11H-6, 100	11H-CC	95.67	98.69	97.18
D	LO *Nitzschia reinholdii*	0.69			10H-CC	11H-CC	89.03	98.69	93.86
S	LO *Bachmannocena quadrangula*	0.80			15H-CC	16H-CC	136.63	143.12	139.88
N	LO *Reticulofenestra asanoi*	0.83			16H-2, 130	16H-4, 140	138.80	141.90	140.35
N	LO Small *Gephyrocapsa* acme (Gartner, 1977)	0.96			21X-CC	22X-CC	180.33	182.33	181.33
N	FO *Reticulofenestra asanoi*	1.06			24X-5, 40	24X-CC	206.13	206.98	206.56
R	LO *Lamprocyrtis neoheteroporos*	1.07			21X-CC	22X-CC	180.33	182.33	181.33
N	LO *Helicosphaera sellii*	1.25			27X-2, 140	27X-4, 140	231.52	233.81	232.67
N	LO *Calcidiscus macintyrei*	1.67			32X-4, 40	32X-CC	282.14	283.18	282.66
D	LO *Proboscia barboi*	1.68			29X-CC	30X-CC	254.47	265.89	260.18
R	LO *Cycladophora pliocenica*	1.83			32X-CC	33X-CC	283.18	294.69	288.94
D	LO *Fragilariopsis doliolus*	1.88			30X-CC	31X-CC	265.89	271.74	268.82
N	LO *Discoaster brouweri*	1.95	NN19	CN13a	34X-CC	36X-CC	304.37	322.77	313.57
D	LO *Thalassiosira kolbei*	1.96			32X-CC	33X-CC	283.18	294.69	288.94
N	LO *Discoaster surculus*	2.55	NN17	CN12c	46X-CC	47X-CC	422.12	429.04	425.58
R	FO *Cycladophora davisiana*	2.70			48X-CC	49X-CC	439.49	450.97	445.23
D	FO *Rhizosolenia praebergonii*	3.12			51X-CC	52X-CC	469.88	477.83	473.86
N	LO *Reticulofenestra pseudoumbilicus*	3.82	NN16	CN12a	60X-4, 108	60X-4, 114	552.88	552.94	552.91
N	LO *Amaurolithus tricorniculatus*	4.50	NN15	CN11	61X-CC	62X-CC	564.94	576.57	570.76

Notes: Fossil group: N = calcareous nannofossils, R = radiolarians, D = diatoms, S = silicoflagellates. FO = first occurrence and LO = last occurrence. Zonal codes refer to the standard calcareous nannofossil zonations of (A) Martini (1971) and (B) Okada and Bukry (1980).

within the bottom part of the section. Despite the reworking of bottom assemblages, the sedimentation rate pattern suggests that Site 1084 terminated within Zone NN14.

Zone NN21

Subzone NN21b, which describes the last 0.09 m.y., was not recognized in the uppermost core of Site 1084. The 0.26 Ma datum event (Zone NN21/NN20 boundary) was identified at the mean depth of 48.6 mbsf between Samples 175-1084A-6H-5, 110 cm, and 6H-6, 110 cm.

Zone NN20

The LO of *Pseudoemiliania lacunosa*, which defined the Zone NN20/NN19 boundary, was constrained between Samples 175-1084A-9H-5, 110 cm, and 9H-CC (mean depth = 77.9 mbsf).

Zone NN19

In addition to the zonal boundary events, six biohorizons were identified within this interval. These include the top and bottom ranges of *Reticulofenestra asanoi*, a species whose LO and first occurrence

(FO) are close to the Brunhes/Matuyama boundary and the onset of the Jaramillo Chron, respectively. Sedimentation rates within Zone NN19 are the highest recorded throughout Site 1084, with a maximum of 27 cm/k.y. from 0.83 to 1.06 Ma. The LO of the Small *Gephyrocapsa* acme (Weaver, 1993), dated at 0.6 Ma (middle oxygen-isotopic Stage 15), was identified at the mean depth of 97.1 mbsf and can therefore be used to approximate the age of a major lithologic change within Hole 1084A (boundary between lithostratigraphic Subunits IA and IB; see "Lithostratigraphy" section, this chapter).

Zones NN18–NN17

The Zone NN19/NN18 boundary (1.95 Ma) was identified at the mean depth of 313.5 mbsf with the LO of *Discoaster brouweri* between Samples 175-1084A-34X-CC and 36X-CC. Because of poor preservation of the nannofossil assemblages as well as barren samples, the depth location of this zonal boundary event could not be constrained further. Zone NN17 was lumped with Zone NN18 because of the sparse occurrence of *D. pentaradiatus*, whose LO datum event defines the Zone NN18/NN17 boundary.

Zone NN16

The LO event of *Reticulofenestra pseudoumbilica,* one of the few non-*Discoaster* index species within the Neogene, was constrained within the interval bounded by Samples 175-1084A-60X-4, 108 cm, and 60X-4, 114 cm. This datum event defines the Zone NN16/NN15 boundary. The Zone NN17/NN16 boundary was identified at the mean depth of 425.5 mbsf (LO of *D. surculus* between Samples 46X-CC and 47X-CC).

Zone NN15

This short interval (0.68 m.y. in duration) was identified between 552.9 and 570.8 mbsf. The base of Zone NN15 is probably offset by ~30 mbsf because of possible reworking of the index species *Amaurolithus tricorniculatus*, whose LO event defines the Zone NN15/NN14 boundary.

Planktonic Foraminifers

The uppermost Sample (175-1084A-1H-CC) is dominated by *Globigerina bulloide*s and contains abundant *Globorotalia inflata* and *Neogloboquadrina pachyderma.* Other components of the assemblage include *Globigerina umbilicata, Globorotalia hirsuta, G. scitula, G. truncatulinoides,* and *N. dutertrei* (Table 4). The assemblages are generally dominated by *G. bulloide*s and *G. inflata* (Table 4). Sporadic occurrences of *Globigerinoides ruber* indicate an input of a warmer fauna (Cores 175-1084A-7H-CC, 8H-CC, 14H-CC, 15H-CC, 25X-CC, 26X-CC, 38X-CC, 40X-CC, 41X-CC, 44X-CC, 48X-CC, and 50X-CC). The presence of *G. ruber* correlates with intervals of higher color reflectance values that are interpreted as probable periods of interglacial sedimentation (see "Lithostratigraphy" section, this chapter).

It is difficult to determine whether the absence of marker species is caused by ecological conditions or by selective dissolution. For example, the dominance of *G. inflata* may be ecological and indicate oligotrophic waters (e.g., the assemblages identified in the Benguela Current system by Little et al., 1997). It may also be a preservation signal; dissolution-susceptible species such as *G. bulloides* and *G. margaritae,* although expected, are commonly absent from the assemblages. Both cool (e.g., *N. pachyderma* (sinistral) and warm (*H. siphonifera, G. ruber,* and *N. dutertrei*) water faunas are present in the same assemblages downcore and may indicate an increased contribution from cooler Southern Ocean waters. *N. pachyderma* (sinistral) is generally present during the interval where subantarctic diatoms are found (Cores 175-1084A-6H-CC and 11H-CC through 50X-CC).

G. truncatulinoides is present consistently in Samples 175-1084A-1H-CC through 17H-CC and in Sample 175-1084A-30X-CC. Samples 175-1084A-19X-CC through 29X-CC and 31X-CC through 37X-CC are severely affected by dissolution, and so the exact position of the Pliocene/Pleistocene boundary, which is defined on the FO of *G. truncatulinoides*, could not be determined. It falls between Samples 175-1084A-30X-CC and 38X-CC. The boundary between Zones Pt1b and Pt1a occurs at the LO of *G. tosaensis* (~0.65 Ma; Sample 175-1084A-12H-CC) and is placed at 100 mbsf. Pliocene Zones PL3–PL6 are undifferentiated because of the absence of index species.

The species *G. crassaformis viola* is restricted to the late Pliocene and earliest Pleistocene. It is present in the interval between Samples 175-1084A-28X-CC through 55X-CC. A single specimen of *G. margaritae,* which is restricted to the early Pliocene, is present in Sample 55X-CC. It is not present elsewhere in the core and may be reworked because an early Pliocene age is in disagreement with calcareous nannofossil age estimates. Calcareous nannofossils also show evidence for reworking. Although *G. margaritae* is a temperate species, it is quite susceptible to dissolution.

Benthic Foraminifers

Benthic foraminifers were studied in core-catcher samples from Hole 1084A. The overall abundance of benthic foraminifers at Hole 1084 is high with some exceptions: Samples 175-1084A-37X-CC (335.53 mbsf) and 49X-CC (450.97 mbsf) were barren of benthic foraminifers, and Samples 175-1084A-22X-CC (182.77 mbsf), 46X-CC (422.12 mbsf), and 52X-CC (477.83 mbsf) contained only traces or rare benthic foraminifers (Table 5). The preservation was good throughout Hole 1084A.

As at Site 1082 the benthic foraminiferal fauna studied at Hole 1084A correlates well with the different lithostratigraphic units recognized (see "Lithostratigraphy" section, this chapter). The benthic foraminiferal species dominating lithostratigraphic Subunit IA (nannofossil clay and nannofossil ooze) are *Bulimina aculeata, B. exilis*, and *Nonionella turgida* (Table 5; Fig. 12). The species *B. exilis* is present in high relative abundance throughout Hole 1084A, except for lithostratigraphic Unit IV, in which it is absent. The other two species are more or less restricted to lithostratigraphic Subunit IA.

Lithostratigraphic Subunit IB (diatom-bearing clay to nannofossil-rich diatomaceous clay with clayey nannofossil ooze) spans the uppermost upper Pliocene and lower Pleistocene sediments; it is dominated by *B. exilis* and *Uvigerina hispidocostata* (Table 5; Fig. 12). Several species are present in high abundances in a pulse-like manner in this interval; *Bolivina seminuda* (Sample 175-1084-13H-CC [117.72 mbsf], ~91%), *Bulimina aculeata* (24X-CC [206.98 mbsf], ~51%), *Stilostomella* spp. (25X-CC [219.65 mbsf], ~52%), *Epistominella exigua* (27X-CC [235.79 mbsf], ~20%), and *U. auberiana* (28X-CC [248.62 mbsf], ~21%; see Table 5; Fig. 12).

Lithostratigraphic Subunit IC (diatomaceous clay) is dominated by *Cibicidoides wuellerstorfi* and *Pullenia bulloides;* several other species are present, but in low relative abundances (Table 5; Fig. 12). Lithostratigraphic Unit II (clay-rich nannofossil diatom ooze to clay-rich diatomaceous nannofossil ooze) and Subunit IC are characterized by the common occurrence of diatom mats. The benthic foraminifer fauna is much the same as in lithostratigraphic Subunit IC, with the addition of overall high abundance of *Bulimina exilis* and *Oridorsalis umbonatus* and high abundance of *Astrononion novozealandicum* and *Melonis barleeanum* in the lower part (Table 5; Fig. 12).

Lithostratigraphic Unit III (nannofossil clay) spans the lowermost late Pliocene and is dominated by *B. exilis* together with *Epistominella exigua* and *Oridorsalis umbonatus* (Table 5; Fig. 12).

Table 4. Dominant and abundant planktonic foraminiferal species at Hole 1084A.

Core, section, interval	Depth (mbsf)	Overall abundance	Overall preservation	*Orbulina universa*	*Globigerina bulloides*	*Globorotalia inflata*	*Globorotalia crassaformis*	*Neogloboquadrina pachyderma* (dextral)	*Neogloboquadrina pachyderma* (sinistral)	*Globorotalia crassaformis* cf. *viola*	*Globorotalia crassaformis viola*	*Globorotalia crassaformis*	*Globorotalia margaritae*	*Globorotalia extremus*	*Globorotalia ruber*	*Globorotalia truncatulinoides*	*Globorotalia tosaensis*	*Globorotalia scitula*	*Globorotalia menardii*	*Neogloboquadrina dutertrei*
175-1084A-																				
1H-CC	2.9	5	5		D	A		A								P		P		P
2H-CC	12.8	5	5		A	A										P				
3H-CC	22.5	5	5			D		A												
4H-CC	31.9	5	5	A	A	A										P				
5H-CC	41.7	1	5		D			A												
6H-CC	51	4	4		A	A														P
7H-CC	60.7	5	5		A	A									P					
8H-CC	70	4	4		D	D		A							P	P				P
9H-CC	79.6	4	4		A	D										P				
10H-CC	89	4	4		A				P							P				
11H-CC	98.7	2	5			D														
12H-CC	108.4	1	4			D						P					P			
13H-CC	117.7	3	4			D			P	P		P				P	P			
14H-CC	127	4	3			D			P			P			P					
15H-CC	136.6	4	3		A	A						P			P	P	P			
16H-CC	143.1	2	1			D						P								
17H-CC	149.8	4	4		A	D			P							P	P			
19X-CC	158.5	1	1			A		D	P											
20X-CC	167.8	4	3		A				P			P					P	P		
21X-CC	180.3	1	1						P											
22X-CC	182.8	1	1																	
23X-CC	195.5	1	1									P								
24X-CC	207	2	4									P								
25X-CC	219.7	4	3							P		P			P					
26X-CC	222.6	1	1		A	A									P					
27X-CC	235.8	1	1							P		P								
28X-CC	248.6	2	4		A	A					P	P								
29X-CC	254.5	0	1																	
30X-CC	265.9	5	4		D	A						P				P				P
31X-CC	271.7	1	1																	
32X-CC	283.2	1	1																	
33X-CC	294.7	0	1																	
34X-CC	304.4	0	1																	
35X-CC	313.2	0	1																	
36X-CC	322.8	1	1																	
37X-CC	335.5	0	1																	
38X-CC	344.8	2	3						P		P	P			P					
39X-CC	354.3	0	1																	
40X-CC	364.3	3	4									P			P					
41X-CC	374	3	3		D	A				P		P			P					
42X-CC	382.4	0	1																	
43X-CC	393.6	0	1																	
44X-CC	403.2	3	4						P	P		P			P					
45X-CC	412.8	1	1																	
46X-CC	422.1	3	5								P	P						P		
47X-CC	429	0	1																	
48X-CC	439.5											P			P					
49X-CC	451	0	1																	
50X-CC	460.6	1	1								P				P					
51X-CC	469.9	3	3								P	P								P
52X-CC	477.8	3	3						P					P						
53X-CC	485.7	3	3						P					P						
54X-CC	496.7	3	2						P	P	P									
55X-CC	503.5	3	3		A		A				P	P	P							
56X-CC	513.8	3	3		A		A		P			P								
57X-CC	527.1	3	4				A					P								
58X-CC	534.9	2	4									P								
59X-CC	544.1	4	4	A																
64X-CC	594.6	1	1																	

Notes: D = dominant (>30%) and A = abundant (10%–30%) components of the assemblage are shown. Presence (P) and absence (A) are also shown for select species. Abundance is classified as 2 = rare; 3 = few; 4 = common; and 5 = abundant. Dissolution is given as 2 = some dissolution; 4 = moderate dissolution; and 5 = no dissolution.

Table 5. Relative abundance of benthic foraminiferal species and overall abundance of benthic foraminifers at Hole 1084A.

Core, section, interval	Depth (mbsf)	Abundance	*Anomalinoides globulosus*	*Astrononion novozealandicum*	*Astrononion stelligerum*	*Bolivina pseudoplicata*	*Bolivina subaenarensis*	*Bolivina seminuda*	*Bolivina* sp. 1	*Bulimina aculeata*	*Bulimina exilis*	*Bulimina marginata*	*Bulimina mexicana*	*Bulimina truncana*	*Cassidulina laevigata*	*Cassidulina minuta*	*Cassidulinoides* cf. *bradyi*	*Chilostomella ovoidea*	*Cibicidoides bradyi*	*Cibicidoides pachyderma*	*Cibicidoides wuellerstorfi*	*Eggerella bradyi*	*Ehrenbergina trigona*	*Epistominella exigua*	*Epistominella* sp. 1	*Fissurina* spp.	*Fursenkoina fusiformis*	*Fursenkoina* sp. 1	*Gavelonopsis lobatulus*	*Globocassidulina subglobosa*	*Gyroidinoides soldanii*	*Hoeglundina elegans*	*Karreriella bradyi*	*Laticarinina pauperata*	*Martinottiella communis*	*Melonis barleeanum*	*Melonis pompilioides*	*Nonion* sp. 1	*Nonionella turgida*	*Oolina hexagona*	*Oolina* spp.	*Oridorsalis umbonatus*	*Plectofrondicularia* cf. *inaequalis*	*Plectofrondicularia* cf. *raricosta*	*Plectofrondicularia* cf. *semicosta*	*Pleurostomella alternans*	*Praeglobobulimina/Globobulimina* group	*Pullenia bulloides*	*Pullenia subcarinata*	*Pyrgo* spp.	*Quadrimorphina allomorphinoides*	*Sigmoilinopsis schlumbergeri*	*Siphotextularia rolshauseni*	*Siphouvigerina* sp. 1	*Sphaeroidina bulloides*	*Stilostomella* spp.	*Trifarina angulosa*	*Uvigerina auberiana*	*Uvigerina hispida*	*Uvigerina hispidocostata*	*Uvigerina peregrina*	Unidentified	Number of specimens counted
175-1084A-																																																															
1H-CC	2.88	A								19	34				3		+	3		+	1					+					3					2		2	10			7					3		4		+							2			2	2	411
2H-CC	12.77	A						4		22	42		+		9		2	+			+							+		+						+		+	6			3					3		+		+							5				2	329
3H-CC	22.51	A								58	+				+		+	+		+				+	20			6		1	+								1			2					5			+								+		+	1	+	361
4H-CC	31.89	A						+		17	12				1		+							+		+		2											64			+																+		+	1		370
5H-CC	41.68	A								25	57	1	+		+		+			+						+		3		+	+								3			2					1		+	+				+				3			3		435
6H-CC	51.03	A								23	25				+			+		2		+						3								+			22			2					1	+	+	+		+						2			14	2	397
7H-CC	60.65	A								25	2	+	5	+	4		+		+	3	2			+		+		+		+	+								+			2		+			2	+	+	3		+			+			5		7	28	5	332
8H-CC	70.02	A						+		37	12			1	10		+	+		+	3			+		+		2		+	+					+	+	2	8		+	2					7		+	+								5			2	2	346
9H-CC	79.55	A								+	9				1		+			+	+							11		+	2							+	64			5					+	+		+								+		+	+	+	301
10H-CC	89.03	A								2	47				13		11									+		5			1							+	2			+					4											14					387
11H-CC	98.69	A								39	23				1		5			+	4							5		1	+								+			13					+	+		+								6				+	278
12H-CC	108.35	A						19		+	35				3		3			+	+						+	5											30								1											1		+			288
13H-CC	117.72	A						91			4																												5			+																					572
14H-CC	127.02	A						+		22	11				3		9				+					+				1	8								+			1					10	+		1								+		4	26		343
15H-CC	136.63	A						21		5	20				+	+					+							5		+								+	30			1					2			+										4	8	+	342
16H-CC	143.12	A									85						+											3		+									1			+					5														2	+	335
17H-CC	149.83	A								+	8		+		50		+	+										4		+	7				+				2			9		+			6	1	+	+										4	2	1	281
19X-CC	158.46	A									75				14		3											5		+														+			2																355
20X-CC	167.83	A									23		+		38		1				+					+		3			7										+	1	+	2			6			+						+		2		8	3	+	341
21X-CC	180.33	A									42				2		11				+					+					1											6	+		2		8	+	+											5	20	+	346
22X-CC	182.77	T									P				P		P																									P					P								P			P		P			11
23X-CC	195.46	A									86				+		3											2											+			+					3														+	4	307
24X-CC	206.98	A			+					51	+			+	8		+											1		+	3											5		1	+		5	+	1							9		+		10	+	3	352
25X-CC	219.65	A			+						4		3		2	+					+			+			+	3														2	+	3			3	1								52				5	16	3	258
26X-CC	222.61	A									2		+			3					4			2		1		2		+					+							6		5			9	+	+							34				11	5	13	295
27X-CC	235.79	A			+			1			35		3	2	4	2	+				+			20		+	+	4			2					+		2	1			1	+	+			1	1		1	2					11					1	2	300
28X-CC	248.62	A									23		2		5						4	+		9			4				4											3	+	+			3	4	+	2	4					5		21		2	+	4	264
29X-CC	254.47	A								12	26		+		+		1													+	2											7	+	1			4	4		+	1					6		+		14	14	4	285
30X-CC	265.89	A							+		10			+	8					3	+	+				+				7	17	+										4	+				1	1		1	+					8		1		20	6	6	305
31X-CC	271.74	A									67				+	+								+		2				4	2	+									+	3					4	1		+	+				+	5				2	2	4	317
32X-CC	283.18	A							1		44				10	+										+		+														4	3	+				+			2					21		+			6	6	335
33X-CC	294.69	A							31		46				+		1									+				+													2	+												3		1		2	6	4	344
34X-CC	304.37	A									30		2		+					+	19					1			+	+	+	4									+	2	1	+			4	+			+					3		8		12	5	5	363
35X-CC	313.19	A							+		62		+																		+					+						1	+				1	1							+	9		2		2	13	6	300
36X-CC	322.77	A									50				2						+					+				+	2	+			+							6		3			1	+			+					3		5		+	14	10	308
37X-CC	335.53	B																																																													0
38X-CC	344.79	C									25		+				2	+			12					2	+	+		5	1								1			5		2	7		6	11	+	2	5		+			+					3	6	295
39X-CC	354.30	A									29							+	+		44					+				+	2											11						6				+				5							287
40X-CC	364.31	A									+						10	+			26					2	+			3	2				+							9		+			+	20	+	+	6					9		2			3	6	307
41X-CC	373.95	A									4	6					7	+			12			15		2		+		+	11	+									+	14				+	+	16	+	1	+					3		+			1	+	311
42X-CC	382.44	A									90										+				+	+					+											2						2								+		2				1	317
43X-CC	393.57	A									15										2			10		+					45											+					1	12	+		2					4		2			+	5	415
44X-CC	403.19	A									21		6			+					18	1		+		3					14											13					+	2	1							2		3		+	7	6	290
45X-CC	412.78	A									48										34					1					7											4		+												3						1	260
46X-CC	422.12	R									53										14																					23																				9	64
47X-CC	429.04	A									85										+					+																+														13							316
48X-CC	439.49	A									3									+	47			3		+					6					2						4			+			15								2		4		+	11	1	264
49X-CC	450.97	B																																																													0
50X-CC	460.64	C		3							22										9			3		+					9				+	13					+	12	+		+			13	+	+					2	2		+				7	301
51X-CC	469.88	A		14							2		+						2	+	5	+		14		3			1	+	4					2					+	10	+				+	9	+	1					6	7		2			5	11	256
52X-CC	477.83	T		3							18										21			5		5														3				3			3			3						18		5			3	13	39

Table 5 (continued).

Core, section, interval	Depth (mbsf)	Abundance	*Anomalinoides globulosus*	*Astrononion novozealandicum*	*Astrononion stelligerum*	*Bolivina pseudoplicata*	*Bolivina subaenarensis*	*Bolivina seminuda*	*Bolivina* sp. 1	*Bulimina aculeata*	*Bulimina exilis*	*Bulimina marginata*	*Bulimina mexicana*	*Bulimina truncana*	*Cassidulina laevigata*	*Cassidulina minuta*	*Cassidulinoides* cf. *bradyi*	*Chilostomella ovoidea*	*Cibicidoides bradyi*	*Cibicidoides pachyderma*	*Cibicidoides wuellerstorfi*	*Eggerella bradyi*	*Ehrenbergina trigona*	*Epistominella exigua*	*Epistominella* sp. 1	*Fissurina* spp.	*Fursenkoina fusiformis*	*Fursenkoina* sp. 1	*Gavelonopsis lobatulus*	*Globocassidulina subglobosa*	*Gyroidinoides soldanii*	*Hoeglundina elegans*	*Karreriella bradyi*	*Laticarinina pauperata*	*Martinottiella communis*	*Melonis barleeanum*	*Melonis pompilioides*	*Nonion* sp. 1	*Nonionella turgida*	*Oolina hexagona*	*Oolina* spp.	*Oridorsalis umbonatus*	*Plectofrondicularia* cf. *inaequalis*	*Plectofrondicularia* cf. *raricosta*	*Plectofrondicularia* cf. *semicosta*	*Pleurostomella alternans*	*Praeglobobulimina*/*Globobulimina* group	*Pullenia bulloides*	*Pullenia subcarinata*	*Pyrgo* spp.	*Quadrimorphina allomorphinoides*	*Sigmoilinopsis schlumbergeri*	*Siphotextularia rolshauseni*	*Siphouvigerina* sp. 1	*Sphaeroidina bulloides*	*Stilostomella* spp.	*Trifarina angulosa*	*Uvigerina auberiana*	*Uvigerina hispida*	*Uvigerina hispidocostata*	*Uvigerina peregrina*	Unidentified	Number of specimens counted
53X-CC	485.73	A		4		+					5		2	2					5	14	8	+				1				1	1	+			+	8					+	4	+			+	2	4	+	3		2			+	+		11	2	3	4	11	329
54X-CC	496.68	A		+							37		+							1	2		+	+		2			+		3	+				7						2		1	+			7	1	+		2			+	3		13		10		2	328
55X-CC	503.54	A	+	1							+		2							8	14	1		4		2				+	2	2	+	5	+	2					+	8		+		+	+	2	2	+		6			11	+		3		4	2	11	333
56X-CC	513.78	A									14		6								4	1		29		3					4	+		+		4						7	+	+				5	+	+		4			2	5	+	3		3	1	2	306
57X-CC	527.14	A		3							13		4	1			+		+	8	4			10		5			1	3	+	2	+			2						8	+	3			2	4		1		+			2	3		3		6	3	8	355
58X-CC	535.19	A									52		2								1			+		+				+	3	+										24		+						+						1		6		4	1	4	395
59X-CC	544.08	A				2	27				+		6	6		+				2	3	2		8		1				+	3	9				5						4	+			+	+	+	+	2		4			2	+		4		2	+	3	452
60X-CC	555.48	Lith																																																													0
61X-CC	564.94	A				+	29				2		2	5			+		+	2	4	2		4		4			2	+	3	2	+	2	+	2						3	+			+	+	4	+	1			+		2	2		6		1	+	9	424
62X-CC	576.57	A					8				1		3	+			2		1	1	9	3				4					4	6			+	3						6						1	1			2			1	1		38				3	280
63X-CC	585.69	A	+				9						+	+			+		1	3	9	3	+	11		5				+	2		+		+	8					+	9	+				+		1	3		4			3	+		8		+		11	205
64X-CC	594.56	F					3												1	4	6	4		5		4				2	4	2	1			7						14						19				1			1	6		3		5		5	95
65X-CC	604.64	A	3		+		16						3	3					4	6	1	3		7		6				7	+		+		+	6					+	3				+	+	+		4	+	+	+		+	5		4		4	+	8	329

Notes: The relative abundance of benthic foraminiferal species is given as a percentage, where + = <1% and P = present (the relative abundance was not calculated because of small sample size). Absolute abundance (per ~20 cm^3 of sediment) of benthicforaminifers is given as A = abundant (>500 specimens); C = common (250–500 specimens); F = few (100–249 specimens); R = rare (50–99 specimens); T = trace (1–49 specimens); B = barren (no specimens); and Lith = lithified (not possible to count or classify benthic foraminifers).

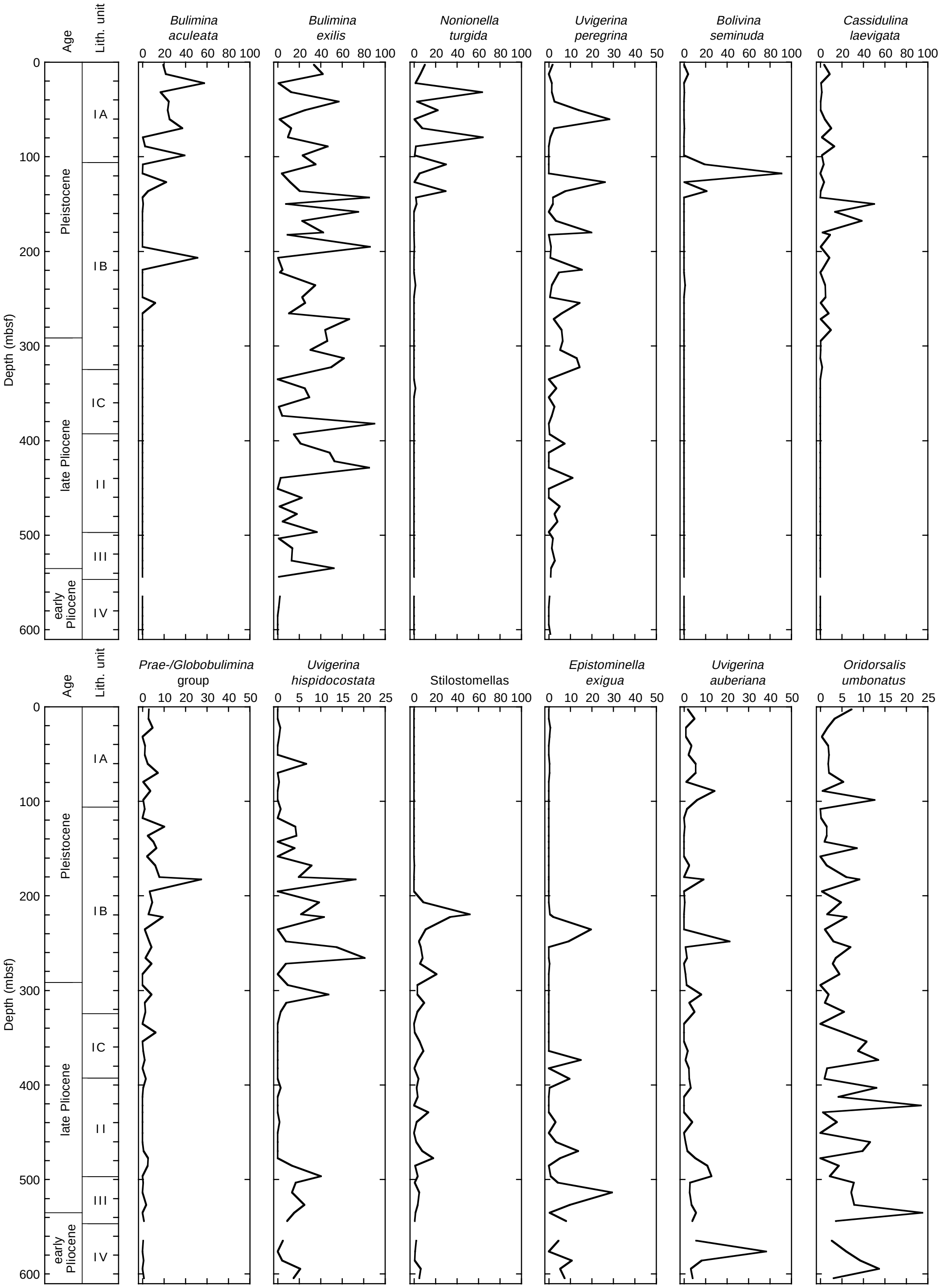

Figure 12. Relative abundances (in percentages) for selected benthic foraminiferal species. For description of lithostratigraphic units, see "Lithostratigraphy" section (this chapter). Continued next page.

The lowermost section of Hole 1084A reaches the lower Pliocene sediment and belongs to lithostratigraphic Unit IV (nannofossil ooze). The benthic foraminiferal assemblage in this interval is dominated by *Bolivina subaenarensis, M. barleeanum, O. umbonatus, P. bulloides,* and *Uvigerina auberiana* (Table 5; Fig. 12).

Radiolarians

Radiolarians are abundant and well preserved in almost all samples examined down to 175-1084A-53X-CC (Table 6). From Sample 175-1084A-54X-CC through 65X-CC, radiolarians are abundant and generally moderately preserved. Radiolarian fauna indicates a Quaternary to early Pliocene age for Hole 1084A. No apparent reworking was identified.

The radiolarian zones used for this hole are those of Caulet (1991) and Motoyama (1996). Moore's (1995) tropical zonation, which has been applied to previous holes from Sites 1075 to 1083, was not used for this hole because of the complete absence of diagnostic taxa *Buccinosphaera invaginata, Collosphaera tuberosa, Anthocyrtidium angulare,* and *Pterocanium prismatium,* and because of the scarcity of

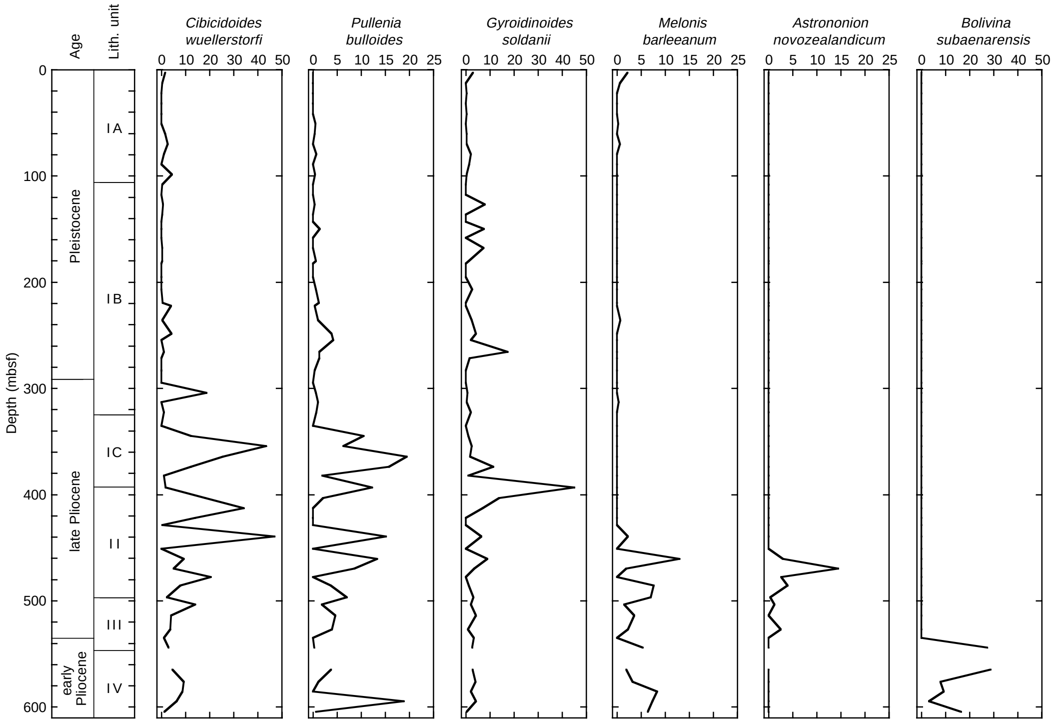

Figure 12 (continued).

Lamprocyrtis neoheteroporos. There are some difficulties in applying the established Antarctic zonations (Caulet, 1991; Lazarus, 1992) to the whole sedimentary sequence at Hole 1084A because of the absence of index species, such as *Prunopyle titan, Helotholus vema,* and *Amphymenium challengerae*, and because of apparent differences in stratigraphic ranges of *Eucyrtidium calvertense* and *Stichocorys peregrina.* The presence of *Axoprunum angelinum* and *Cycladophora pliocenica,* however, allows us to use a part of the Antarctic zones of Caulet (1991).

The absence of *A. angelinum* indicates that the uppermost cores (175-1084A-1H-CC through 8H-CC) are assigned to Zone NR1 of Caulet (1991).

Samples 175-1084A-9H-CC through 32X-CC belong to the Pleistocene Zone NR2 or Zone NR3/NR4 of Caulet (1991). Since *Phormostichoartus pitomorphus* was not identified, the zonal boundary between Zone NR2 and Zone NR3/4 was not determined. Caulet (1991) defined the bottom of the Zone NR3/NR4 by the last common occurrence of *C. pliocenica.* Considering the inconsistent occurrence of this species at Hole 1084A, the LO of the species in Sample 175-1084A-33X-CC is correlated with the bottom of Zone NR3/NR4, thereby approximating the Pliocene/Pleistocene boundary.

The FO of *C. davisiana* indicates an age of 2.7 Ma for Sample 175-1084A-48X-CC. Samples 175-1084A-33X-CC through 48X-CC between the LO of *C. pliocenica* and the FO of *C. davisiana* can be correlated with the *P. prismatium* zone of Moore (1995).

The presence of *S. pylomaticus* indicates that the age of the lowest sample (175-1084A-65X-CC) is no older than 5.2 Ma; thus, Samples 175-1084A-49X-CC through 65X-CC can be correlated to a zonal sequence from the lower part of the *Cycladophora sakaii* Zone to the *S. pylomaticus* Zone in the North Pacific (Motoyama, 1996).

Diatoms

Diatom counts and identifications were carried out using smear slides and acid-treated, sieved (20 µm) material from core-catcher samples from Hole 1084A (Table 7). Diatom preservation is moderate throughout Hole 1084A. As has been the case at Sites 1081 and 1082, overall diatom abundances are low or zero in the lower Pliocene sediments. Diatom abundances reach a maximum in the late Pliocene (Table 7; Fig. 13). In contrast to the other sites, diatom abundances, although highly variable, remain moderately high (common to abundant) throughout the Pleistocene (Table 7).

In addition to the "background" diatom assemblage composed of a mixture of upwelling-indicator (*Chaetoceros* resting spores and *Thalassionema nitzschioides* var. *nitzschioides*) and oceanic species (e.g., *Azpeitia nodulifer, A. tabularis, Hemidiscus cuneiformis,* and *Thalassiothrix* spp.), we recorded many more cold-water markers characteristic of the Southern Oceans (e.g. *Hemidiscus karstenii, Fragilariopsis kerguelensis, Proboscia barboi, Thalassiosira lentiginosa,* and *T. kolbei*) than at Sites 1081, 1082, and 1083. The Antarctic/subantarctic flora is present consistently between Samples 175-1084A-50X-CC (~460 mbsf) and 30X-CC (~266 mbsf; Fig. 13) and sporadically in Samples 175-1084A-6H-3, 80 cm, and 6H-CC. *Rhizosolenia hebetata,* a cold-water indicator, is observed in Samples 175-1084A-11H-CC and 12H-CC, 16H-CC through 19X-CC, and 25X-CC (Table 7). The intervals of cold-water flora may indicate periods of increased advection of subantarctic waters into the Benguela Oceanic Current (BOC) and concomitant intensified northward Benguela Current transport, an assumption that is also supported by the presence of the Antarctic radiolarian *C. pliocenica,* and by the sparse occurrence of the low–middle latitude nannofossil genus *Discoaster* (Fig. 13).

Chaetoceros resting spores and setae of *C. cinctus, C. debilis, C. diadema, C. lorenzianus, C. radicans,* and *C. constrictus/vanheurckii* are particularly abundant in Pleistocene sediments, and they may be regarded as indicators of high coastal upwelling productivity from the Lüderitz upwelling cell (see Shannon and Nelson, 1996). They are also abundant during highest overall abundance times in the late Pliocene within Subunit IC and Unit II (see "Lithostratigraphy" section, this chapter; Fig. 13). Within the late Pliocene (at an approximate age interval of 2–3 Ma), core-catcher Samples 175-1084A-37X-CC (~335 mbsf) through 51X-CC (470 mbsf) are rich in the pennate diatom *Thalassiothrix antarctica* (and probably other *Thalassiothrix* species as well), accompanied by lanceolate forms of *Thal-*

Table 6. Stratigraphic distribution of radiolarians at Hole 1084A.

Age	Zone	Core, section, interval	Depth (mbsf)	Abundance	Preservation	*Amphirhopalum ypsilon*	*Cycladophora cornutoides*	*Cycladophora davisiana*	*Eucyrtidium calvertense*	*Eucyrtidium teuscheri*	*Eucyrtidium acuminatum*	*Lamprocyclas hannai*	*Pterocanium praetextum eucolpum*	*Pterocanium trilobum*	*Spongurus pylomaticus*	*Theocorythium trachelium*	*Didymocyrtis tetrathalamus*	*Saturnalis circularis*	*Axoprunum angelinum*	*Lamprocyrtis nigriniae*	*Spongaster tetras tetras*	*Phormostichoartus corbula*	*Lamprocyrtis heteroporos*	*Lamprocyrtis neoheteroporos*	*Acanthodesmia viniculata*	*Eucyrtidium anomalum*	*Cycladophora pliocenica*	*Didymocyrtis avita*	*Cycladophora sakaii*	*Stichocorys peregrina*	*Dictyophimus* sp. B	*Phormostichoartus fistula*
		175-1084A-																														
Quaternary	NR1	1H-CC	2.88	A	G	P	+	P	P	P	+	P	P	P	P	P																
Quaternary	NR1	2H-CC	12.77	A	G	+	+	P	P	P	+	P	+	P	P	P																
Quaternary	NR1	3H-CC	22.51	A	G	P	P	P		P	P	P		P	P	P	P															
Quaternary	NR1	4H-CC	31.89	A	G	P		P	+	P	P	P	P	P	P	P	P															
Quaternary	NR1	5H-CC	41.68	A	M	+		P	P			P	+		P		P															
Quaternary	NR1	6H-CC	51.03	A	G			P		+	P	P	P	P	P	P	+	+														
Quaternary	NR1	7H-CC	60.65	A	G	P	+	P	P	P	P	P		P			P															
Quaternary	NR1	8H-CC	70.02	A	G		P	P		P	P	P	P	P			P															
Pleistocene	NR2–NR3/4	9H-CC	79.55	A	G		+	P		P	P	+	+	P	P	P	+		+	+	+											
Pleistocene	NR2–NR3/4	10H-CC	89.03	A	G	+	P	P	P	P	P	P	P		+	P			P													
Pleistocene	NR2–NR3/4	11H-CC	98.69	A	G			P	+		P		+	+	+	P			P													
Pleistocene	NR2–NR3/4	12H-CC	108.35	A	G	+		P	P	+	P	+		P		P	+		P			P										
Pleistocene	NR2–NR3/4	13H-CC	117.72	A	G		P	P	+	P	P	P		P					P			+										
Pleistocene	NR2–NR3/4	14H-CC	127.04	A	G	P		P	P	P	+	P		+	+	+			P													
Pleistocene	NR2–NR3/4	15H-CC	136.63	C	G			P	+		P	+	P	P	P				P				+	+								
Pleistocene	NR2–NR3/4	16H-CC	143.12	A	G	+	+	P	+	P	P	P	P	P		P			+													
Pleistocene	NR2–NR3/4	17H-CC	149.83	A	G	P	P	P	P		P	P	P	P	P		P		+			P			+							
Pleistocene	NR2–NR3/4	19X-CC	158.46	R	G		P	P		+	P	P		+					+													
Pleistocene	NR2–NR3/4	20X-CC	167.83	A	G	+		P	+	P	P	P		P	P	P	P		P													
Pleistocene	NR2–NR3/4	21X-CC	180.33	A	G			P	P	P		P		P	P	P	P		P													
Pleistocene	NR2–NR3/4	22X-CC	182.77	A	G			P	P	P		P		P	P	+	+		P	+				P								
Pleistocene	NR2–NR3/4	23X-CC	195.46	A	G	+	P	P		P	P	P		+	P			+	P			+	P			+						
Pleistocene	NR2–NR3/4	24X-CC	206.98	A	G	+	+	P	P	P	+	P	+	P	P	+	P		P													
Pleistocene	NR2–NR3/4	25X-CC	219.65	A	G	P	+	P	+	+	P	P		+		P	P	P	P													
Pleistocene	NR2–NR3/4	26X-CC	222.61	A	G	P	P	P	+	P	P	P		P		P	P		P				P									
Pleistocene	NR2–NR3/4	27X-CC	235.79	R	G	+	P	P			P	P		P	P		+		+													
Pleistocene	NR2–NR3/4	28X-CC	248.62	A	G	+	P	P		P	P	P		+		+	P	+	+					+								
Pleistocene	NR2–NR3/4	29X-CC	254.47	A	G		+	P	P	P		P	+	P	+	+		+	P				+									
Pleistocene	NR2–NR3/4	30X-CC	265.89	A	G		P	P	P	P	P	P		P	P				P				+									
Pleistocene	NR2–NR3/4	31X-CC	271.74	A	G			P	P	P	P	P	P	P	P	+	+		P			P	+	+								
Pleistocene	NR2–NR3/4	32X-CC	283.18	A	G			P	+	+	+	P		+	+	+			P				P									
Pliocene	*P. prismatium*	33X-CC	294.69	C	G	P		P	P	+	P	+			+			+	P				+				+	P				
Pliocene	*P. prismatium*	34X-CC	304.37	A	M	P	P	P	P	P	P	P		P	P		+	+	P					+								
Pliocene	*P. prismatium*	35X-CC	313.19	C	G			P		P	P	P		+	P				+			+					P					
Pliocene	*P. prismatium*	36X-CC	322.62	A	G	+	+	P	P	P	P	P		+	P		+		P			P		+			P					
Pliocene	*P. prismatium*	37X-CC	335.53	A	G			P		P					P			+									P	+				
Pliocene	*P. prismatium*	38X-CC	344.79	A	G	P	P	P	P	P	P	P	+	P		P			+				P									
Pliocene	*P. prismatium*	39X-CC	354.3	A	G	+	+	P	P	P		P			P								+									
Pliocene	*P. prismatium*	40X-CC	364.31	A	G	P	P	+	P	P	P	P	P	P	P		P		P			P	P	P								
Pliocene	*P. prismatium*	41X-CC	373.95	A	G			+	+	P		P			P				P				P				+					
Pliocene	*P. prismatium*	42X-CC	382.44	A	G	P	P	+	P	P		P		P	+		+		P				+				+					
Pliocene	*P. prismatium*	43X-CC	393.57	A	G		P	P	+	P	+	P					P		+				+									
Pliocene	*P. prismatium*	44X-CC	403.19	C	G	+	P	P	P	+	+				P	+	P		P													
Pliocene	*P. prismatium*	45X-CC	412.78	A	G	P	P		P	P			+		P		+		P				+									
Pliocene	*P. prismatium*	46X-CC	422.12	A	G		P	P		P				P									P				P		P			
Pliocene	*P. prismatium*	47X-CC	429.04	A	G		P	P	P	P		+			+			+	P				P						P			
Pliocene	*P. prismatium*	48X-CC	439.49	A	G		P	P		P	+	P		+	+				P			P	P						P			
Pliocene	*C. sakaii–S. pylomaticus*	49X-CC	450.97	C	G		P		+	P		+			+				+				P				P					
Pliocene	*C. sakaii–S. pylomaticus*	50X-CC	460.64	A	G		P		+	P		+		P	P		P		P				P				P					
Pliocene	*C. sakaii–S. pylomaticus*	51X-CC	469.88	A	G	P	P			+	+	+							P				P				P					
Pliocene	*C. sakaii–S. pylomaticus*	52X-CC	477.83	A	G	+	P		P	P	P	+	+	P	P		P		P				P				P	+				
Pliocene	*C. sakaii–S. pylomaticus*	53X-CC	485.73	A	G	+	P		P		P	P		P	P		+		P				P	+			P					
Pliocene	*C. sakaii–S. pylomaticus*	54X-CC	496.68	A	M	+	P		P	P	+	+			P				P				+				P					

Table 6 (continued).

Age	Zone	Core, section, interval	Depth (mbsf)	Abundance	Preservation	*Amphirhopalum ypsilon*	*Cycladophora cornutoides*	*Cycladophora davisiana*	*Eucyrtidium calvertense*	*Eucyrtidium teuscheri*	*Eucyrtidium acuminatum*	*Lamprocyclas hannai*	*Pterocanium praetextum eucolpum*	*Pterocanium trilobum*	*Spongurus pylomaticus*	*Theocorythium trachelium*	*Didymocyrtis tetrathalamus*	*Saturnalis circularis*	*Axoprunum angelinum*	*Lamprocyrtis nigriniae*	*Spongaster tetras tetras*	*Phormostichoartus corbula*	*Lamprocyrtis heteroporos*	*Lamprocyrtis neoheteroporos*	*Acanthodesmia viniculata*	*Eucyrtidium anomalum*	*Cycladophora pliocenica*	*Didymocyrtis avita*	*Cycladophora sakaii*	*Stichocorys peregrina*	*Dictyophimus* sp. B	*Phormostichoartus fistula*
Pliocene	*C. sakaii–S. pylomaticus*	55X-CC	503.54	A	M		+		P			P											P	+			P			P		
Pliocene	*C. sakaii–S. pylomaticus*	56X-CC	513.78	A	G		P			P					P		+		P				P	+			+					
Pliocene	*C. sakaii–S. pylomaticus*	57X-CC	527.14	A	M	+						+		+			P	+	P			P	P								P	
Pliocene	*C. sakaii–S. pylomaticus*	58X-CC	534.92	A	M				P			P			P				P			+	P	P						+		+
Pliocene	*C. sakaii–S. pylomaticus*	59X-CC	544.08	A	M				P			+			+				P				+							P	+	
Pliocene	*C. sakaii–S. pylomaticus*	60X-CC	555.48	A	G		+		+			P		+	P				P			+	P	+						P	+	
Pliocene	*C. sakaii–S. pylomaticus*	61X-CC	564.94	A	M				P	+	+	P		+	P			P	P				P							P	P	+
Pliocene	*C. sakaii–S. pylomaticus*	62X-CC	576.57	A	M		P		+			P		+	P	+	+	+	+				P							P	P	
Pliocene	*C. sakaii–S. pylomaticus*	63X-CC	585.69	A	M				P			+			P			P	P			+	P							P	+	
Pliocene	*C. sakaii–S. pylomaticus*	64X-CC	594.56	A	M				P			P			P			+	P			P	P							P		P
Pliocene	*C. sakaii–S. pylomaticus*	65X-CC	604.64	C	M							P			P			P	P				P							P	+	

Notes: Occurrence is indicated by P = present and + = one specimen per slide. Abundance: A = abundant; C = common; and R = rare. Preservation: G = good and M = moderate. *P. prismatium* = *Pterocanium prismatium; C. sakaii* = *Cycladophora sakaii;* and *S. pylomaticus* = *Spongurus pylomaticus*.

Table 7. Overall diatom abundance estimated from smear slides for Hole 1084A.

Core, section, interval (cm)	Depth (mbsf)	Overall abundance (smear slides)	Depth (mbsf)	Dominant assemblage	Cold-water marker species	Diatom and/or silicoflagellate datums
175-1084A-						
1H-CC	2.88	3.0	2.88	**Upw.** + **oceanic**		
2H-CC	12.77	4.5	12.77	**Upw.** + **oceanic**		
3H-CC	22.51	3.5	22.51	Upwelling		
4H-CC	31.89	4.0	31.89	Upw. + oceanic		
5H-CC	41.68	3.5	41.68	**Upw.** + **oceanic**		
6H-2, 10	42.50	2.5	42.50			
6H-3, 80	44.70	6.0	44.70	Upwelling	*F. kerguelensis, H. karstenii*	
6H-5, 110	47.90	6.0	47.90	Upwelling		
6H-6, 110	50.90	2.0	50.90			
6H-CC	51.03	3.5	51.03	Upw. + oceanic	*F. kerguelensis, H. karstenii*	
7H-CC	60.65	2.0	60.65			
8H-CC	70.02	3.0	70.02	Upw. + oceanic		
9H-CC	79.55	3.5	79.55	Upwelling		
10H-CC	89.03	4.0	89.03	Upw. + oceanic		
11H-CC	98.69	4.0	98.69	**Upw.** + **neritic** + **oceanic**	*R. hebetata* f. *hebetata*	<< LO *N. reinholdii* (0.65 Ma[a]) 0.69 Ma[b]
12H-CC	108.35	4.0	108.35	Upw. + oceanic	*R. hebetata + F. kerguelensis*	
13H-CC	117.72	6.0	117.72	Upwelling		
14H-CC	127.02	3.0	127.02	Oceanic		
15H-CC	136.63	4.5	136.63	Upw. + oceanic		
16H-CC	143.12	4.5	143.12	**Upw.** + **neritic** + **oceanic**	*R. hebetata* f. *hebetata*	<< LO *B. quadrangula* 0.8 Ma[b]
17H-CC	149.83	3.0	149.83		*R. hebetata* f. *hebetata*	
19X-CC	158.46	4.5	158.46	Upwelling	*R. hebetata* f. *hebetata*	
20X-CC	167.83	3.0	167.83	**Upw.** + **oceanic**		
21X-CC	180.33	4.0	180.33	Upw. + neritic + oceanic		
22X-CC	182.77	2.5	182.77			
23X-CC	195.46	4.0	195.46	Upw. + oceanic		
24X-CC	206.98	3.0	206.98	Upw. + oceanic		
25X-CC	219.65	3.5	219.65	**Upw.** + **neritic** + **oceanic**	*R. hebetata* f. *hebetata*	
26X-CC	222.61	3.0	222.61	Upw. + oceanic		
27X-CC	235.79	5.0	235.79	Upw. + oceanic		
28X-CC	248.62	5.0	248.62	Upw. + oceanic		
29X-CC	254.47	2.0	254.47			
30X-CC	265.89	3.5	265.89	Upw. + oceanic	*P. barboi*	<< LO *P. barboi* (1.58 Ma[a]) 1.68 Ma[b]
31X-CC	271.74	4.0	271.74	Upwelling	*H. karstenii, P. barboi*	
32X-CC	283.18	5.0	283.18	Upwelling	*H. karstenii, P. barboi*	
33X-CC	294.69	4.0	294.69	Upwelling	*H. karstenii, P. barboi, T. kolbei, T. lentiginosa*	<< ?LO *T. kolbei* (1.89 Ma[a])1.96 Ma[b]
34X-CC	304.37	3.0	304.37		*H. karstenii, P. barboi*	
35X-CC	313.19	4.5	313.19	Upw. + oceanic	*P. barboi*	
36X-CC	322.77	4.0	322.77	Oceanic	*P. barboi*	
37X-CC	335.53	6.0	335.53	Upwelling (spores + setae)	*H. karstenii, P. barboi*	
38X-CC	344.79	6.0	344.79	**Thalassionemataceae** + spores	*H. karstenii, P. barboi*	
39X-CC	354.30	6.0	354.30	**Thalassionemataceae** + spores	*H. karstenii, P. barboi*	
40X-CC	364.31	6.0	364.31	**Thalassionemataceae** + spores	*P. barboi*	
41X-CC	373.95	6.0	373.95	Thalassionemataceae	*P. barboi*	
42X-CC	382.44	6.0	382.44	Upwelling (spores + setae)	*P. barboi*	
43X-CC	393.57	6.0	393.57	**Thalassionemataceae** + spores	*P. barboi*	
44X-CC	403.19	5.0	403.19	Thalassionemataceae + spores	*P. barboi*	
45X-CC	412.78	6.0	412.78	Thalassionemataceae + **spores**	*H. karstenii*	
46X-CC	422.12	6.0	422.12	Thalassionemataceae + **spores**	*P. barboi*	
47X-CC	429.04	6.0	429.04	Upwelling (spores + setae)	*H. karstenii*	
48X-CC	439.49	6.0	439.49	**Thalassionemataceae** + spores	*P. barboi*	
49X-CC	450.97	5.0	450.97	Thalassionemataceae + **spores**	*P. barboi*	
50X-CC	460.64	5.0	460.64	**Thalassionemataceae** + spores	*P. barboi*	
51X-4, 70	466.00	5.0	466.00	Thalassionemataceae + **spores**		
51X-4, 100	466.30	4.5	466.30	Thalassionemataceae + **spores**		
51X-CC	469.88	4.5	469.88	Upw. + oceanic		<< FO *R. praebergonii* (3.0 Ma[a]) 3.12 Ma[b]
52X-CC	477.83	3.0	477.83	Thalassionemataceae + spores		
53X-CC	485.73	3.0	485.73	Oceanic		
54X-CC	496.68	2.5	496.68	Oceanic	*P. barboi*	
55X-CC	503.54	2.5	503.54	Oceanic	*P. barboi*	
56X-CC	513.78	2.0	513.78		*P. barboi*	
57X-CC	527.14	1.5	527.14			
58X-CC	535.19	2.0	535.19		*P. barboi*	
59X-4, 40	542.60	2.0	542.60			
59X-CC	544.08	0.0	544.08			
60X-4, 100	552.80	2.5	552.80	Oceanic		
60X-CC	555.48	0.0	555.48			
61X-4, 85	562.35	3.5	562.35	Upw. + oceanic		
61X-CC	564.94	1.5	564.94			
62X-CC	576.57	2.0	576.57			
63X-3, 120	580.40	3.5	580.40	Upw. + oceanic		
63X-CC	585.69	1.0	585.69			
64X-CC	594.56	1.0	594.56			
65X-CC	604.64	0.0	604.64			

Notes: For each sample, the dominant assemblage and the cold-water and biostratigraphic marker species are given. FO = first occurrence and LO = last occurrence.

[a] Ages adjusted to Berggren et al. (1995).

[b] Ages converted to Shackleton et al. (1995), as published in Wei (1994).

assionema nitzschioides. Most of the *Thalassiothrix* group specimens are fragmented. Species of the genus *Thalassiothrix* are characterized by narrow (1.5–6 µm), long (400 µm to 4 mm), straight to twisted cells. They form an interlocking meshwork (this could readily be seen under a binocular scope) within which abundant *Chaetoceros* spores, *Thalassionema nitzschioides,* and calcareous nannofossils are found. In addition, scattered specimens of *Actinocyclus curvatulus, A. octonarius, Actinoptychus senarius, Azpeitia nodulifera, Coscinodiscus* spp.*, Hemidiscus cuneiformis, H. karstenii, Nitzschia reinholdii, N. fossilis, Proboscia barboi,* and *Stephanopyxis* spp. are observed.

Site 1084 is located within the area of extension of the upwelling filaments in the frontal zone between the BCC and the BOC. The intervals of greatest diatom abundances in the late Pliocene are recorded by a mixed/*Thalassiothrix*-rich assemblage representative of two different oceanographic regimes that meet over Site 1084: (1) *Chaetoceros* spores and setae as a proxy of colder upwelling waters transported by the BCC and (2) mixed warm oceanic (e.g., *A. nodulifera* and *H. cuneiformis*) and Southern Ocean species (e.g., *T. antarctica* and *P. barboi*) as proxies of BOC waters. These intervals apparently represent mat deposits, which may be similar to the ones discovered in the eastern equatorial Pacific during Leg 138 (Kemp and Baldauf, 1993). The fact that these *Thalassiothrix*-rich sediments occur during persistent subantarctic water-mass influence at Site 1084 (Fig. 13) may relate to more vigorous surface circulation leading to the development of stronger frontal systems (among the BCC, the upwelling filaments, and the BOC), facilitating the concentration of diatom cells in the plankton and, consequently, greater downward flux through the water column (see Kemp et al., 1995, and references therein). Alternatively, silicate-rich subsurface waters were advected from the Southern Ocean, or by poleward undercurrents, or both.

Because of the mixture of warm, temperate, and Southern Ocean species and the occasional lack of biostratigraphic markers from either oceanographic regime, diatom biostratigraphic zonations are difficult to apply to Hole 1084A; consequently, they are not given here. Instead, biostratigraphic events, such as the FO or LO of a species, have been assigned to the sample containing the first or last observed specimens (Table 7; Fig. 11).

PALEOMAGNETISM

The investigation of magnetic properties at Site 1084 included the measurement of bulk susceptibility of whole-core sections and of the natural remanent magnetization (NRM) of archive-half sections and discrete samples. The Tensor tool was used to orient Cores 175-1084A-4H through 17H, Cores 175-1084B-16H through 20H, and Cores 175-1084C-16H through 22H (Table 8). Cores 175-1084B-4H through 15H and 175-1084C-4H through 15H were not oriented because of technical problems with the Tensor tool.

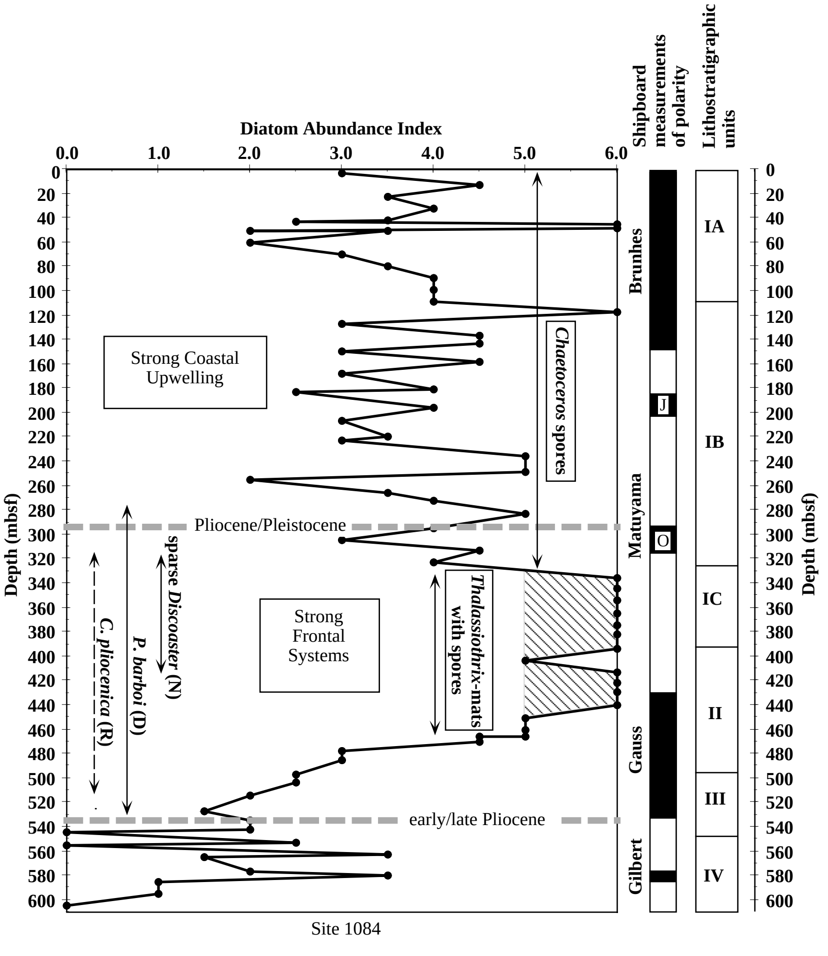

Figure 13. Overall diatom abundance vs. depth at Hole 1084A. Shipboard measurements of polarity and lithographic units are given on the right-hand side. The time interval of subantarctic influence in the late Pliocene is exemplified by the presence of *Proboscia barboi* (diatom) and *Cycladophora pliocenica* and by the sparse occurrence of *Discoaster* nannofossil species. We believe that a strong coastal upwelling system dominated over Site 1084 in the Pleistocene, whereas strong frontal systems (among the BCC, the up-welling filaments, and the BOC) dominated the late Pliocene, as exemplified by *Chaetoceros* resting spores and *Thalassiothrix*-rich sediments, respectively.

Natural Remanent Magnetization, Magnetic Susceptibility, and Magnetic Overprint

Measurements of NRM were made on all archive-half core sections from Holes 1084A, 1084B, and 1084C. APC sections from Hole 1084A were demagnetized by AF at 10 and 20 mT. XCB sections from Hole 1084A and all sections from Holes 1084B and 1084C were demagnetized by AF at 20 mT only. All discrete samples, one per section from Hole 1084A, were demagnetized by AF at 10, 20, 25, and 30 mT. Magnetic susceptibility measurements were made on whole cores from all holes as part of the MST analysis (see "Physical Properties" section, this chapter).

Magnetic susceptibility ranges between 0 and 8×10^{-5} (SI volume units), and intensity of NRM after 20-mT demagnetization ranges between ~10^{-2} and ~10^{-4} A/m (Fig. 14). Long-term changes of the remanent intensity are similar to those of the magnetic susceptibility; highs occur from ~220 to 330 mbsf and from ~500 to 600 mbsf. The exception is in the upper 100 mbsf where the remanent intensity is high, but the magnetic susceptibility is low.

A magnetic overprint was generally removed by 20-mT demagnetization, and a primary NRM was recovered for all APC cores (Fig. 14). For XCB cores, however, a significant magnetic overprint remained after AF demagnetization. Declinations of archive-half cores cluster around –20°, independent of the orientation of the sediments, even where the sediments are extensively biscuited (Figs. 14A, 15A). This phenomenon is similar to that observed at Sites 1081 and 1082 (see "Paleomagnetism" sections, "Site 1081" and "Site 1082" chapters, this volume), where the magnetic overprint was attributed to the coring process. Declinations of discrete samples taken from the working halves cluster around 180° (Figs. 14A, 15B). This direction is nearly opposite to declinations from the archive halves, indicating a magnetic overprint of a nearly radial-inward direction. Clustering of declinations is weaker in discrete samples than in half-core samples, suggesting that a primary magnetization was preserved in part of the center of cores. In contrast, inclinations showed distinct polarity biases after 20-mT demagnetization. The inclinations are deflected downward from the downward-oriented magnetic overprint, causing upward inclinations to be shallower than expected and downward inclinations to be steeper than expected. The groupings of normal and reversed polarities are more distinct in the discrete samples (Fig. 16).

The inclinations from APC half-core measurements are steeper than those from discrete samples (Figs. 14, 16). The average inclination of discrete samples during the Brunhes Chron agrees with that expected from the geocentric axial dipole model (–44° at this site), with the correction for the inclination anomaly (+3°) caused by nondipole components (Merrill and McElhinny, 1983). The steeper inclinations from half-core measurements may be related to deformation of sediments along the rim of cores (see "Paleomagnetism" section, "Site 1083" chapter, this volume).

Magnetostratigraphy

We identified the polarity of the NRM from the declinations and inclinations of APC cores and from the inclinations of XCB cores. All major polarity chrons from the Brunhes to the latter part of the Gilbert (~4.4 Ma) were identified at Hole 1084A. Magnetostratigraphic interpretation is summarized in Table 9. The time scale of Berggren et al. (1995) was used. The identification of the Jaramillo Subchron in XCB cores from Hole 1084A at depth was aided by its identification in the APC cores from Hole 1084C, which contained less magnetic overprinting, and supports the polarity interpretations based on inclinations from XCB cores.

Transitional records of the Brunhes/Matuyama polarity change were obtained from Holes 1084B and 1084C. At Hole 1084A, the transition record was unfortunately missing because of a gap in recovery between cores.

Table 8. Tensor tool–orientation data for cores from Holes 1084A, 1084B, and 1084C.

Core	MTF (°)	Inclination angle
175-1084A-		
4H	235	0.47
5H	116	0.96
6H	241	0.73
7H	49	1.57
8H	246	0.67
9H	280	1.27
10H	253	0.64
11H	86	0.40
12H	87	0.69
13H	31	0.62
14H	40	0.62
15H	209	0.99
16H	104	1.68
17H	89	1.82
175-1084B-		
16H	293	0.88
17H	353	1.07
18H	299	0.64
19H	34	0.82
20H	146	1.01
175-1084C-		
16H	333	0.24
17H	305	0.52
18H	258	0.77
19H	163	0.73
20H	79	0.56
21H	165	0.56
22H	319	0.47

Note: The orientation parameter (MTF) is the angle in degrees between magnetic north and the double line marked on the center of the working half of the core. The local declination anomaly is 17°W.

In spite of the high sedimentation rate of ~200 m/m.y., no short polarity-reversal event was detected during the Brunhes Chron. Most anomalous directions of NRM seen in Figure 14 were caused by physical disturbance of the sediments that occur at core or section boundaries. Some anomalous directions occur in the middle of sections, but they do not duplicate between holes.

COMPOSITE SECTION

Three holes were cored at Site 1084 with the APC/XCB to a maximum depth of 604 mbsf. MST measurements of magnetic susceptibility and GRAPE density were taken at 4-cm resolution for all cores, except the upper 11 cores of Hole 1084A, which were measured at 2-cm intervals. Measurements of spectral reflectance using the Minolta spectrophotometer were done using the same intervals. Quantitative and graphic correlation of the physical parameter measurement of adjacent holes were used to establish depth continuity of the stratigraphic sequence. This process is used to determine intercore depth offsets of adjacent holes and to establish a common composite depth scale (expressed as meters composite depth, or mcd). The stratigraphic sequence was demonstrated to be a continuous from the core top to 175 mcd (Fig. 17; Table 10).

Cores recovered from Site 1084 show a high number of small voids of a few centimeters in size, beginning with Cores 175-1084A-8H, 175-1084B-8H, and 175-1084C-8H. The abundance of voids below 75 mcd is reflected in the MST data collected (see "Physical Properties" section, this chapter). The scatter introduced in the physical properties logs partly masks features suitable for interhole correlation. Thus, total color reflectance (lightness L*) was primarily used to construct the composite section. Magnetic susceptibility and GRAPE density were also used to supplement the correlations. To establish the composite depth record, Gaussian smoothing was applied to the data over a 31-cm window.

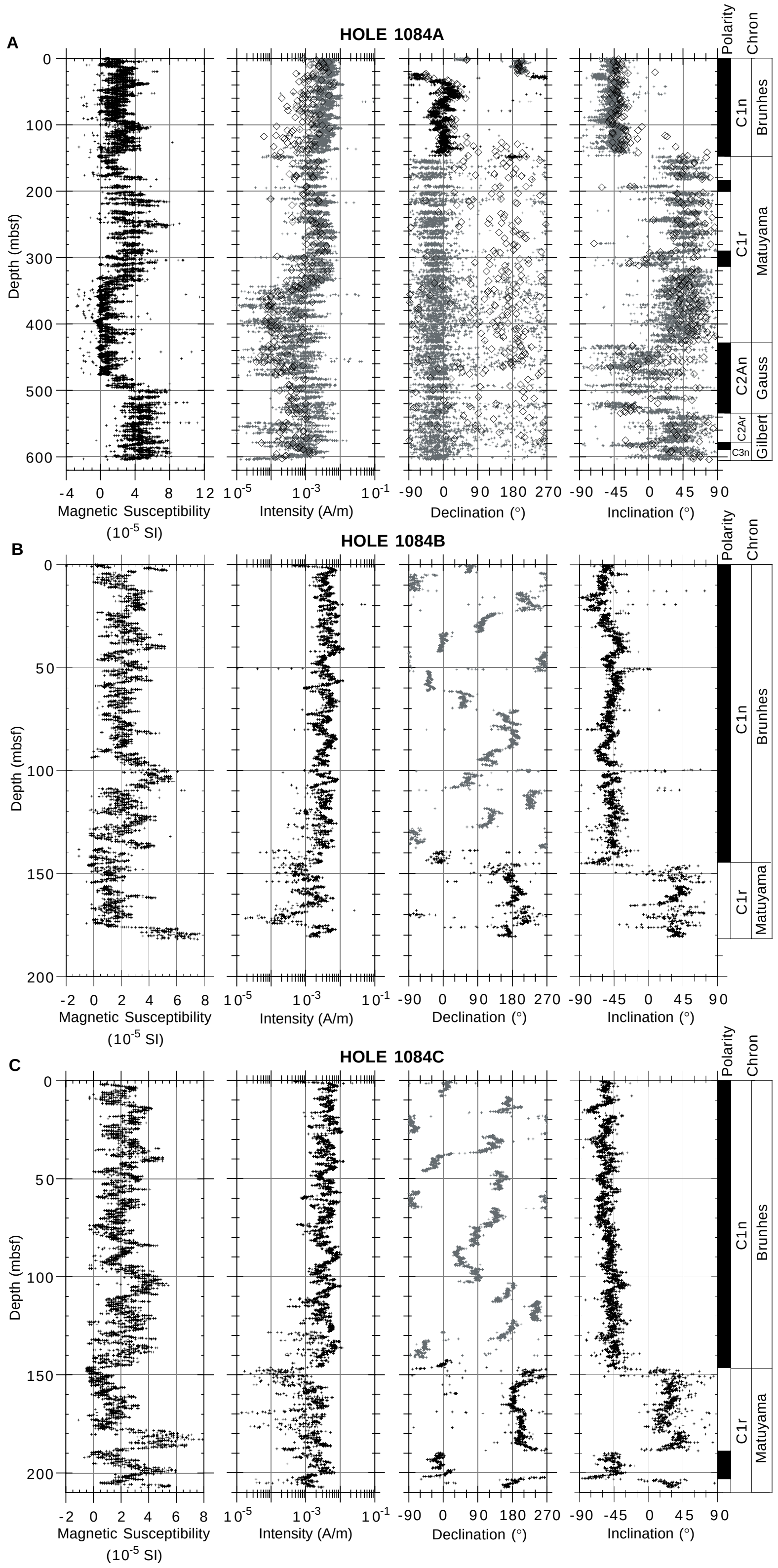

Figure 14. Magnetic susceptibility (volumetric SI) and NRM intensity, declination, inclination, and magnetostratigraphic interpretation after 20-mT demagnetization for (**A**) Hole 1084A, (**B**) Hole 1084B, and (**C**) Hole 1084C. Black symbols = Tensor corrected; gray symbols = uncorrected; open diamonds = discrete samples. Polarity shading: black = normal, white = reversed, and gray = ambiguous.

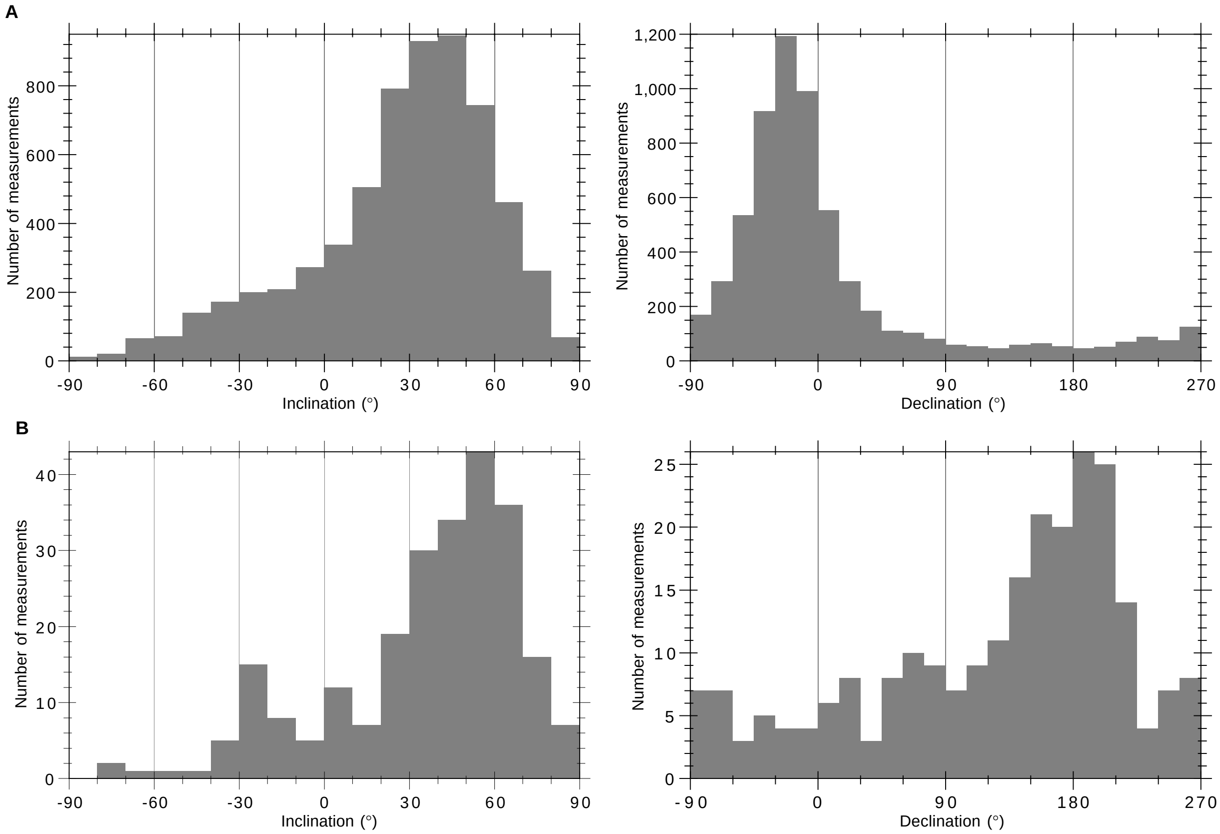

Figure 15. Distribution of inclination and declination for all XCB cores from Hole 1084A. **A.** Half-core measurements. **B.** Discrete samples.

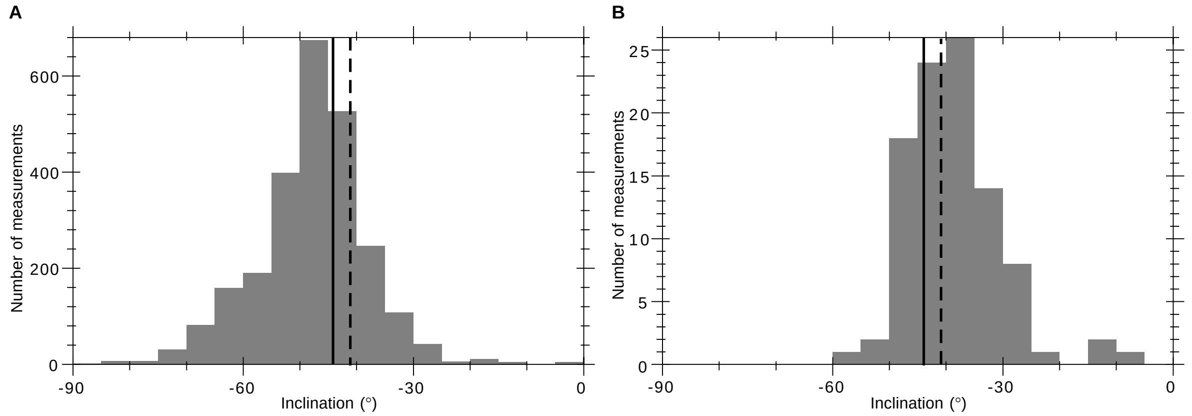

Figure 16. Distribution of inclination during the Brunhes Chron from Cores 175-1084A-1H through 16H. **A**. Half-core measurements. **B**. Discrete samples. Solid line = the inclination expected from the geocentric axial dipole model at this site; dashed line = the inclination expected after correcting for the anomaly caused by nondipole components (+3°; Merrill and McElhinny, 1983).

Table 9. Magnetostratigraphic interpretations for Site 1084.

Polarity chron	Age (Ma)	Depth (mbsf) Hole 1084A	Hole 1084B	Hole 1084C	Polarity epoch
C1n/C1r.1r	0.78	147	145	147	Brunhes/Matuyama
C1r.1n	0.99-1.07	185-200		189-203	Jaramillo
C2n	1.77-1.95	293-315			Olduvai
C2An.1n (top)	2.58	430			Gauss
C2Ar (top)	3.58	535			Gilbert
C3n.1n	4.18-4.29	575-585			Cochiti

Note: Time scale used is that of Berggren et al. (1995).

Once converted to the mcd scale, a complete spliced sedimentary sequence of magnetic susceptibility and color reflectance was constructed (Fig. 18). On the mcd scale, features of the magnetic susceptibility appear to be inversely related to features in the color reflectance data. By using Table 11 as a reference, a chronologically complete downcore record can be constructed by sampling adjacent holes and filling intercore gaps documented in the primary sampling hole.

Documentation of the composite section was generally good to very good; however, the noise in the deeper portions of the hole made parts of the composite section more speculative. Growth of the mcd scale relative to the mbsf scale drilled was ~17% (Fig. 19).

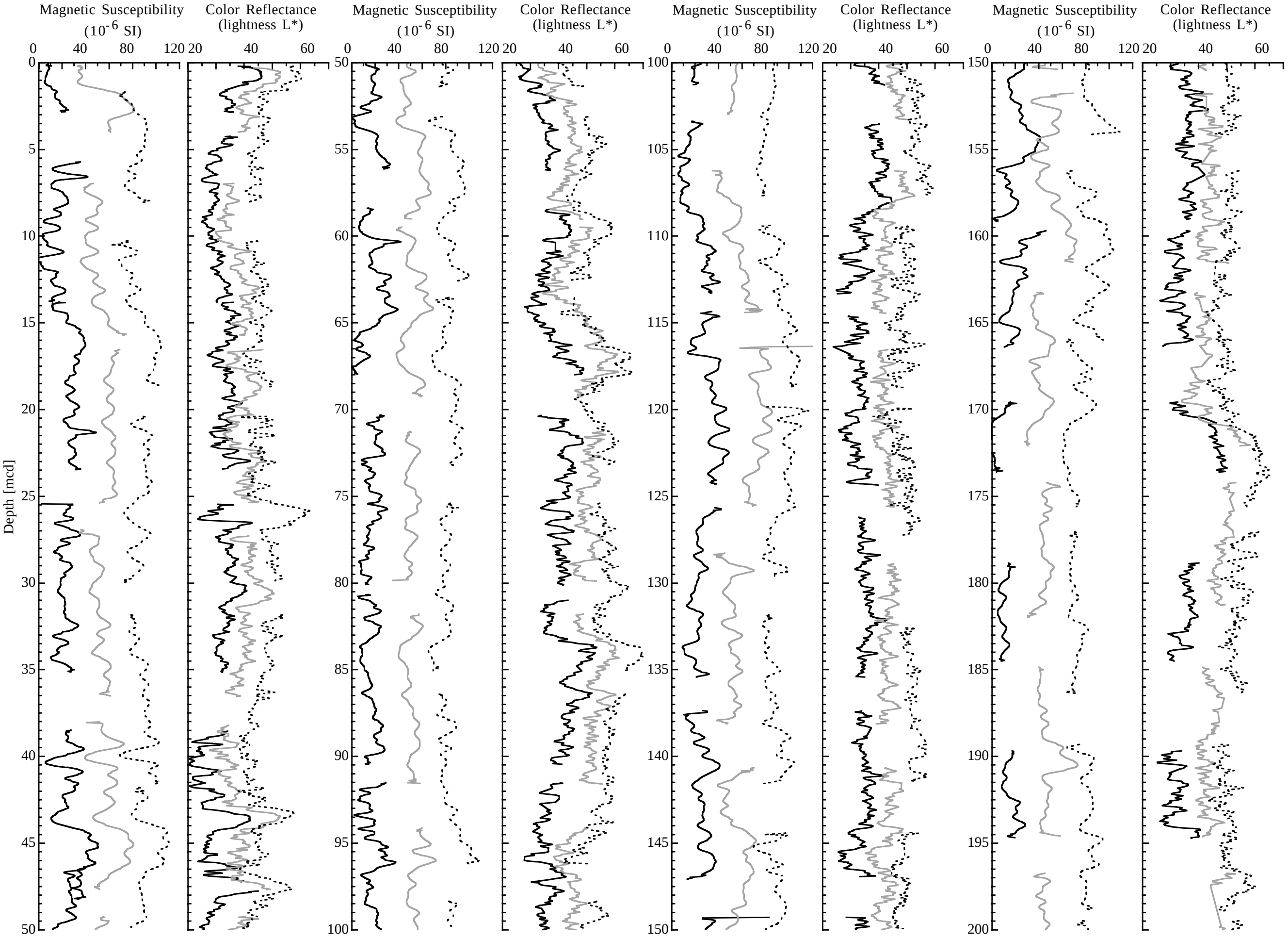

Figure 17. Composite section for Site 1084. Magnetic susceptibility and the total color reflectance (lightness L*) data are plotted for Holes 1084A (solid black line), 1084B (gray line), and 1084C (dashed line). The downhole logs are shown in meters composite depth (mcd). Offsets of integer multiples 1.5 times the standard deviation of the Hole 1084A data have been applied to Holes 1084B and 1084C for clarity in viewing the composite sections.

INORGANIC GEOCHEMISTRY

Thirty interstitial water samples were gathered from Hole 1084A between 1.4 and 599.90 mbsf. Whole-round samples were sampled at a frequency of one sample per core to 101.1 mbsf, and every third core thereafter to total depth (Table 12). The interstitial water chemistry at this site is dominated by the extremely high organic carbon concentrations in the sediment, which results in the generation of unusual chemical profiles. At this site we recorded the second highest concentrations of alkalinity and ammonium ever measured in the history of ocean drilling. Only Site 688 (Leg 112, Peruvian margin) recorded more extreme interstitial water variations; the alkalinity and ammonium values found here at Site 1084 exceed those found in the Santa Barbara Basin, Saanich Inlet, Oman Margin, and any other high organic region cored by DSDP or ODP.

Alkalinity, Sulfate, and Ammonium

Downcore profiles of alkalinity, sulfate, and ammonium (Fig. 20) through the upper 100 mbsf reflect the degradation of organic matter. Because of the extremely high total organic carbon (TOC) values at this site (see “Organic Geochemistry” section, this chapter), the rate of increase is very high. Alkalinity increases to a maximum value of 172 mM at 93 mbsf (approximately the boundary between lithostratigraphic Subunits IA and IB; see “Lithostratigraphy” section, this chapter) and remains at values >150 mM to ~220 mbsf before decreasing to the bottom of the hole. Within the uppermost 5.9 mbsf, sulfate is completely consumed. This is the shallowest depth of complete sulfate removal observed so far on this leg. Ammonium reaches a maximum of ~50 mM through the depth range of 130 to 250 mbsf before decreasing to the bottom of the hole. At previous sites on this leg we noted a more or less linear increase of dissolved ammonium with depth, a trend we attributed to the combined processes of organic matter degradation and clay mineral exchange. At Site 1084, in contrast, a broad ammonium maximum at depths between 100 and 300 mbsf reflects the continuing vigorous degradation of organic matter down to ~150–200 mbsf.

Calcium, Magnesium, and Strontium

The concentration of dissolved Sr^{2+} increases within the uppermost 10 mbsf from a value near that of average seawater to ~125 µM (Fig. 21). This slight and shallow increase suggests that biogenic calcite dissolution is occurring only to a minor extent. Through lithostratigraphic Subunit IA (see “Lithostratigraphy” section, this chapter) from 10 to 131 mbsf, dissolved Sr^{2+} concentrations stay approximately constant, suggesting no further dissolution. Through the remainder of lithostratigraphic Unit I and continually through Units

Table 10. Offsets applied to cores from Holes 1084A, 1084B, and 1084C.

Core	Depth (mbsf)	Offset (m)	Composite depth (mcd)
175-1084A-			
1H	0.0	0.00	0.00
2H	3.0	1.18	4.18
3H	12.5	1.24	13.74
4H	22.0	3.38	25.38
5H	31.5	6.92	38.42
6H	41.0	5.29	46.29
7H	50.5	7.81	58.31
8H	60.0	10.27	70.27
9H	69.5	11.10	80.60
10H	79.0	12.44	91.44
11H	88.5	14.81	103.31
12H	98.0	16.26	114.26
13H	107.5	18.08	125.58
14H	117.0	20.27	137.27
15H	126.5	22.71	149.21
16H	136.0	23.60	159.60
17H	145.5	23.99	169.49
18X	149.5	10.29	159.79
19X	152.5	26.27	178.77
20X	162.2	27.17	189.37
21X	171.8	29.00	200.80
22X	181.5	29.00	210.50
23X	191.2	29.00	220.20
24X	200.8	29.00	229.80
25X	210.4	29.00	239.40
26X	220.1	29.00	249.10
27X	229.7	29.00	258.70
28X	239.3	29.00	268.30
29X	248.9	29.00	277.90
30X	258.5	29.00	287.50
31X	268.2	29.00	297.20
32X	277.8	29.00	306.80
33X	287.4	29.00	316.40
34X	297.0	29.00	326.00
35X	306.6	29.00	335.60
36X	316.3	29.00	345.30
37X	325.9	29.00	354.90
38X	335.6	29.00	364.60
39X	345.2	29.00	374.20
40X	354.8	29.00	383.80
41X	364.4	29.00	393.40
42X	374.1	29.00	403.10
43X	383.7	29.00	412.70
44X	393.3	29.00	422.30
45X	402.9	29.00	431.90
46X	412.6	29.00	441.60
47X	422.2	29.00	451.20
48X	431.9	29.00	460.90
49X	441.6	29.00	470.60
50X	451.2	29.00	480.20
51X	460.8	29.00	489.80
52X	470.0	29.00	499.00
53X	479.7	29.00	508.70
54X	489.4	29.00	518.40
55X	499.1	29.00	528.10
56X	508.7	29.00	537.70
57X	518.3	29.00	547.30
58X	528.0	29.00	557.00
59X	537.7	29.00	566.70
60X	547.3	29.00	576.30
61X	557.0	29.00	586.00
62X	566.6	29.00	595.60
63X	576.2	29.00	605.20
64X	585.9	29.00	614.90
65X	595.5	29.00	624.50
175-1084B-			
1H	0.0	0.09	0.09
2H	4.1	2.77	6.87
3H	13.6	2.85	16.45
4H	23.1	3.73	26.83
5H	32.6	5.33	37.93
6H	42.1	7.07	49.17
7H	51.6	7.81	59.41
8H	61.1	10.09	71.19
9H	70.6	11.11	81.71
10H	80.1	13.94	94.04
11H	89.6	16.54	106.14
12H	99.1	17.04	116.14
13H	108.6	19.6	128.2
14H	118.1	22.47	140.57
15H	127.6	23.72	151.32
16H	137.1	25.57	162.67
17H	146.6	27.53	174.13
18H	156.1	28.69	184.79
19H	165.6	31.05	196.65
20H	175.1	30.52	205.62
175-1084C-			
1H	0.0	0.13	0.13
2H	8.1	2.09	10.19
3H	17.6	2.71	20.31
4H	27.1	4.67	31.77
5H	36.6	5.11	41.71
6H	46.1	6.95	53.05
7H	55.6	7.85	63.45
8H	65.1	10.23	75.33
9H	74.6	11.74	86.34
10H	84.1	13.64	97.74
11H	93.6	15.71	109.31
12H	103.1	16.66	119.76
13H	112.6	19.15	131.75
14H	122.1	22.21	144.31
15H	131.6	24.54	156.14
16H	141.1	24.77	165.87
17H	150.6	26.38	176.98
18H	160.1	29.13	189.23
19H	169.6	29.79	199.39
20H	179.1	29.79	208.89
21H	188.6	29.79	218.39
22H	198.1	29.79	227.89
21H	188.6	19.20	207.80
22H	198.1	19.20	217.30

Note: The offsets transform ODP standard depth values in meters below seafloor (mbsf) to meters composite depth (mcd).

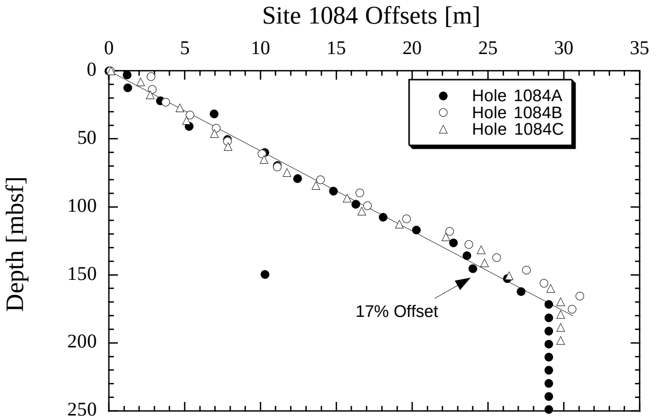

Figure 18. Core offsets applied to Site 1084 cores plotted against standard ODP meters below seafloor (mbsf). A linear 17% growth of meters composite depth (mcd) compared with mbsf is indicated by a line.

II, III, and IV from 131 mbsf to the bottom of the hole, dissolved Sr^{2+} increases to a maximum of 464 µM. This deep increase records the dissolution of biogenic calcite, which releases Sr^{2+} to the interstitial waters.

Thus, through Subunit IA there appears to be calcite dissolution only in the uppermost 10 mbsf. From the seafloor to 73 mbsf, the concentration of dissolved Ca^{2+} decreases sharply, whereas that of Mg^{2+} increases through the same region. This is unlike observations at the previous Leg 175 sites, where Ca^{2+} and Mg^{2+} decreased in approximately equal proportions because of dolomitization. We interpret the Ca^{2+} profile at Site 1084 as recording precipitation of calcium carbonate driven by the high alkalinity. Below this depth, from 100 mbsf to the bottom of the hole, the increase in dissolved Ca^{2+} is consistent with the similar increase in dissolved Sr^{2+}, both of which are caused by deep dissolution of biogenic calcite. We are unsure about the cause of the initial increase in Mg^{2+}. We hypothesize that the deeper decrease in Mg^{2+} reflects ion exchange by clay minerals. The shallow increase in dissolved Mg^{2+} may also record ion exchange, or perhaps complexation of the cations with bicarbonate (J. Gieskes, pers. comm., 1997).

Table 11. List of splice tie points used to create the continuous “spliced” stratigraphic sequence for Site 1084.

Hole, core, section, interval (cm)	Depth (mbsf)	Composite depth (mcd)	Whether tied	Hole, core, section, interval (cm)	Depth (mbsf)	Composite depth (mcd)	Offset (m)
1084A-1H-2, 16	1.66	1.66	Tie to	1084C-1H-2, 2.5	1.53	1.66	0.13
1084C-1H-4, 32	4.82	4.95	Tie to	1084A-2H-1, 76.5	3.77	4.95	1.18
1084A-2H-7, 24	12.24	13.42	Tie to	1084C-2H-3, 22.5	11.33	13.42	2.77
1084C-2H-3, 124	12.34	14.43	Tie to	1084A-3H-1, 68.5	13.19	14.43	–0.11
1084A-3H-6, 54	20.54	21.78	Tie to	1084C-3H-1, 147	19.07	21.78	1.67
1084C-3H-5, 68	24.28	26.99	Tie to	1084A-4H-2, 10.5	23.61	26.99	2.75
1084A-4H-6, 84	30.34	33.72	Tie to	1084C-4H-2, 43.5	29.05	33.72	3.37
1084C-4H-5, 100	34.10	38.77	Tie to	1084A-5H-1, 34.5	31.85	38.77	3.57
1084A-5H-6, 118	40.08	47.00	Tie to	1084C-5H-4, 78.5	41.89	47.00	4.79
1084C-5H-5, 4	42.64	47.75	Tie to	1084A-6H-2, 6	42.46	47.75	6.55
1084A-6H-7, 68	50.48	55.77	Tie to	1084C-6H-2, 121	48.82	55.77	5.03
1084C-6H-6, 48	54.08	61.03	Tie to	1084A-7H-2, 122	53.22	61.03	5.43
1084A-7H-5, 124	57.22	65.03	Tie to	1084C-7H-2, 8	57.18	65.03	7.07
1084C-7H-6, 84	63.94	71.79	Tie to	1084A-8H-2, 1	61.52	71.79	7.29
1084A-8H-7, 64	69.54	79.81	Tie to	1084C-8H-3, 148	69.58	79.81	7.79
1084C-8H-4, 128	70.88	81.11	Tie to	1084A-9H-1, 50.5	70.01	81.11	7.75
1084A-9H-7, 12	78.52	89.62	Tie to	1084C-9H-3, 28	77.88	89.62	10.21
1084C-9H-7, 76	84.36	96.10	Tie to	1084A-10H-4, 16	83.66	96.10	9.75
1084A-10H-7, 56	88.56	101.00	Tie to	1084C-10H-4, 12	87.36	101.00	10.59
1084C-10H-6, 36	90.60	104.24	Tie to	1084A-11H-2, 76	89.43	104.24	12.23
1084A-11H-6, 44	95.11	109.92	Tie to	1084C-11H-1, 59.5	94.21	109.92	12.53
1084C-11H-6, 104	101.73	117.44	Tie to	1084A-12H-3, 142	101.18	117.44	12.99
1084A-12H-8, 64	107.90	124.16	Tie to	1084C-12H-3, 140	107.50	124.16	13.92
1084C-12H-5, 40	109.50	126.16	Tie to	1084A-13H-1, 57	108.08	126.16	14.98
1084A-13H-7, 12	116.62	134.70	Tie to	1084C-13H-2, 145	115.55	134.70	16.33
1084C-13H-6, 24	120.34	139.49	Tie to	1084A-14H-2, 72	119.22	139.49	17.31
1084A-14H-6, 144	125.97	146.24	Tie to	1084C-14H-2, 42.5	124.03	146.24	16.41
1084C-14H-5, 84	128.94	151.15	Tie to	1084A-15H-2, 44	128.44	151.15	19.50
1084A-15H-6, 44	134.54	157.25	Tie to	1084C-15H-1, 110.5	132.74	157.25	19.87
1084C-15H-6, 136	140.46	165.00	Tie to	1084A-16H-4, 89	141.40	165.00	22.46
1084A-16H-4, 100	141.50	165.10	Tie to	1084B-16H-3, 40	139.53	165.10	22.86
1084B-16H-6, 56	143.36	168.93	Tie to	1084C-16H-3, 5	144.16	168.93	24.54
1084C-16H-7, 80	150.90	175.67					

Note: The tie points are listed in standard ODP meters below seafloor (mbsf) and meters composite depth (mcd).

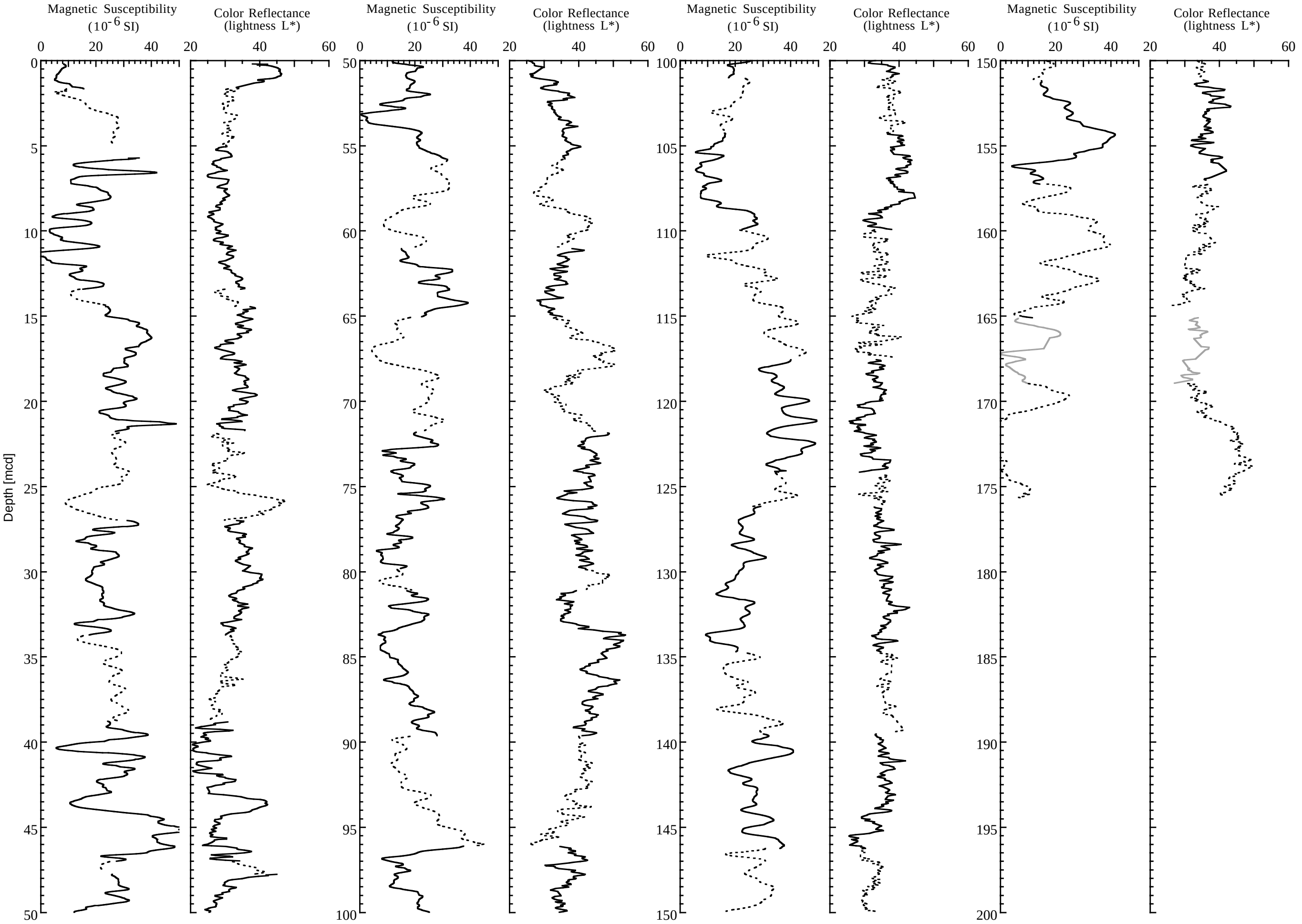

Figure 19. Spliced records for magnetic susceptibility and total color reflectance (lightness L*) plotted in meters composite depth (mcd). Cores from all three holes at Site 1084 have been used for the spliced record: solid black line = Hole 1084A, gray line = Hole 1084B, and dashed line = Hole 1084C.

Table 12. Interstitial water composition for Hole 1084A.

Core, section, interval (cm)	Depth (mbsf)	pH	Alkalinity (mM)	Salinity	Cl^- (titr) (mM)	Cl^- (IC) (mM)	SO_4^{2-} (mM)	Na^+ (mM)	Mg^{2+} (mM)	Ca^{2+} (mM)	K^+ (mM)	H_4SiO_4 (µM)	NH_4^+ (mM)	PO_4^{3-} (µM)	Sr^{2+} (µM)
175-1084A-															
1H-1, 140-150	1.40	7.48	4.068	35.5	553	589	29.27	472	55.22	10.76	11.86	466	0.34	8	93
2H-2, 140-150	5.90	8.02	56.721	36.0	553	563	0.05	476	56.09	5.12	11.32	740	5.98	155	110
2H-5, 140-150	10.40	7.14		37.0	548	593	0.00	406	61.00	4.32	11.39	762	8.56	254	126
3H-3, 140-150	16.90	7.85	91.901	38.5	544	596	0.07	488	63.94	3.94	12.73	818	13.80	341	128
4H-3, 140-150	26.40	7.72	114.024	40.0	541	581	0.00	493	70.18	4.11	13.23	840	15.60	435	124
5H-3, 130-140	35.80	7.45	123.262	40.5	538	575	0.88	496	72.36	4.19	13.82	808	19.86	546	123
6H-3, 130-140	45.20	7.30	136.298	41.0	540	567	0.38	507	74.27	4.11	13.70	901	23.75	534	128
7H-4, 135-145	55.88	7.64	138.974	41.0	540	556	0.00	513	73.01	2.74	14.29	835	27.94	435	111
8H-3, 130-140	64.30	8.29	152.985	41.0	536	572	0.00	511	78.96	3.08	14.19	823	30.64	482	126
9H-3, 130-140	73.80	7.52	154.244	42.0	537	579	0.00	523	74.44	2.27	14.64	808	35.85	417	102
10H-5, 140-150	86.40	7.43	160.224	42.0	535	549	0.00	530	72.53	2.63	14.70	850	36.21	441	113
11H-4, 140-150	93.07	8.21	171.667	42.5	537	578	0.00	537	75.38	2.86	14.66	845	38.42	540	122
12H-3, 140-150	101.16	7.45	162.526	42.5	537	579	0.00	540	68.71	3.15	15.35	765	42.44	499	128
15H-3, 140-150	130.90	7.45	155.389	41.5	537	585	0.00	543	63.62	2.41	16.68	855	47.95	400	111
19X-2, 140-150	155.40	7.63	162.109	42.0	532	589	0.40	555	59.92	2.46	14.94	959	49.03	376	147
23X-2, 118-128	193.88	7.85	166.144	41.5	531	578	0.00	549	62.75	3.41	15.91	995	50.40	423	160
26X-1, 140-150	221.50	7.92	159.546	41.5	540	581	0.00	556	58.79	4.54	16.87	1003	49.81	295	187
29X-3, 140-150	253.30	7.95	144.675	40.5	540	565	0.00	556	52.25	4.02	15.78	1010	48.55	207	205
32X-3, 140-150	281.64	7.21	131.575	39.0	538	570	0.00	554	45.47	4.53	15.92	1117	45.01	172	228
35X-3, 140-150	310.91	7.97	115.721	38.0	541	552	0.00	550	41.33	4.90	14.90	1066	43.22	148	246
38X-3, 140-150	340.00	7.96	102.146	38.0	542	551	0.00	548	35.96	4.84	14.70	1180	41.54	123	254
41X-3, 140-150	368.80	7.03	94.875	36.5	544	546	0.00	552	31.23	5.35	14.06	1328	39.26	112	291
44X-3, 140-150	397.70	7.16	77.983	36.0	544	553	0.03	536	30.33	6.03	13.80	1350	32.67	61	264
47X-4, 140-150	427.05	7.95	75.788	35.5	547	550	0.06	543	26.74	6.52	13.58	1413	34.16	47	312
50X-4, 140-150	457.10	6.84	63.928	35.0	548	551	0.00	540	23.63	5.85	13.24	1440	33.86	36	330
53X-3, 140-150	483.19	6.29	57.204	35.0	549	557	0.11	535	23.14	6.51	12.38	1316	31.01	24	337
56X-2, 140-150	511.60	7.01	48.215	35.0	553	568	0.00	533	21.59	6.64	12.31	1273	29.90	15	365
59X-2, 140-150	540.60	7.95		34.0	549	548	0.11	483	20.28	7.34	11.06	1263	26.85	10	401
62X-4, 140-150	571.30	6.84	38.290	34.0	556	560	0.00	528	19.13	8.37	10.65	1328	24.42	10	453
65X-3, 140-150	599.90	6.83	28.067	33.5	559	564	0.20	525	18.41	8.10	9.84	1387	22.63	10	464

Notes: Cl^- (titr) = analyzed by titration and Cl^- (IC) = analyzed by ion chromatography. Empty cells = not analyzed.

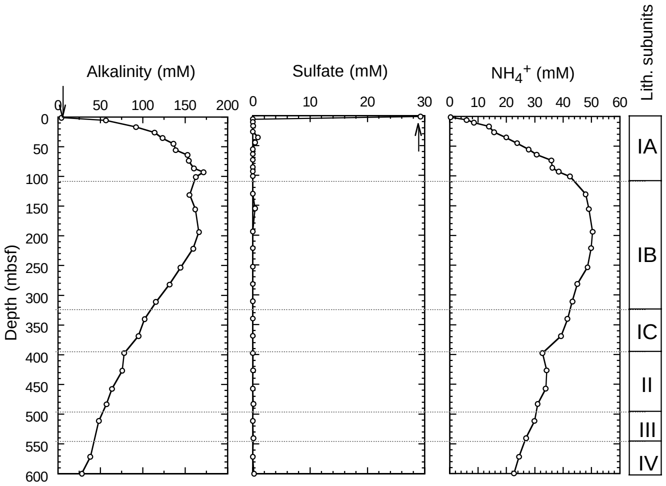

Figure 20. Downcore profiles of dissolved alkalinity, sulfate, and ammonium at Site 1084. Lithostratigraphic subunits shown on right-hand bar. Arrows = mean ocean-bottom-water values taken from Millero and Sohn (1992). Notice change in scale of ammonium axis (in mM) compared with previous Leg 175 sites (in µM).

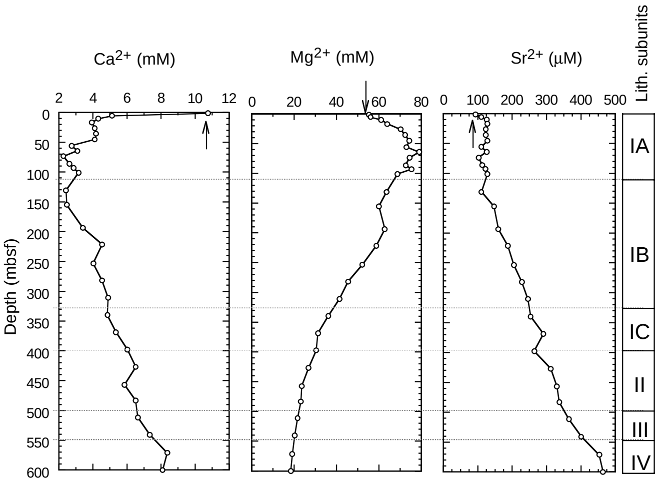

Figure 21. Downcore profiles of Ca^{2+}, Mg^{2+}, and Sr^{2+} at Site 1084. Lithostratigraphic subunits shown on right-hand bar. Arrows = mean ocean-bottom-water values taken from Millero and Sohn (1992).

Silica and Phosphate

Dissolved silica is present in interstitial waters from Site 1084 at concentrations greater than representative bottom-water values (Fig. 22), indicating dissolution of biogenic opal. The concentration of dissolved silica continues to increase slightly with depth. Most notably, a local increase through lithostratigraphic Subunit IC and Unit II corresponds well with the increase in diatoms through this depth interval (see "Biostratigraphy and Sedimentation Rates" section, this chapter), as shown in the shaded region of Fig. 22. Below these diatomaceous sequences (see "Lithostratigraphy" section, this chapter), although dissolved silica continues to increase, the rate of the increase is similar to the rate through the nondiatomaceous lithostratigraphic units.

Because of remineralization of organic matter, dissolved phosphate concentrations increase with depth through Subunit IA and reach a maximum of nearly 50 µM at several intervals in this unit (Fig. 22). Through the remainder of the sequence, dissolved phosphate decreases to extremely low concentrations (~10 µM) reflecting the strong uptake of dissolved phosphate into diagenetic phases.

Sodium and Potassium

Concentrations of dissolved Na^+ and dissolved K^+ both increase from seawater values to maximum values at depth in lithostratigraphic Subunit IB before decreasing with depth to the bottom of the hole

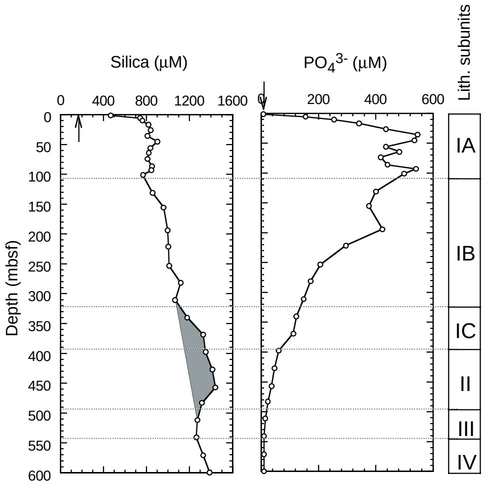

Figure 22. Downcore profiles of dissolved silica and phosphate at Site 1084. Lithostratigraphic subunits shown on right-hand bar. Shaded region = zone of increased dissolved silica caused by the greater abundance of diatoms through the interval. Arrows = mean ocean-bottom-water values taken from Millero and Sohn (1992).

(Fig. 23). These profiles are broadly similar to those of alkalinity, ammonium, and, to a lesser extent, phosphate. In this context, it is important to recall that the Na^+ concentration is not directly measured but is determined by charge balance. Because ammonium has the same ionic charge as Na^+ and K^+, its role may prove particularly relevant, and these positively charged species may all be responding to ion exchange with clay minerals.

Salinity and Chloride

Because of the large increases in alkalinity, ammonium, Mg^{2+}, phosphate, Na^+, and K^+ through the upper 100 mbsf, as described above, salinity values increase to a maximum of 42.5 from ~90 to 100 mbsf (Fig. 24). Concentrations of dissolved $Cl^–$ show a downcore pattern that is different from the previous Leg 175 sites; they exhibit a strong decrease from the seafloor down to a minimum of 531 mM at ~200 mbsf. Below this depth, dissolved $Cl^–$ increases to a maximum value at the bottom of the hole. We are unsure of the processes controlling this distribution, although water exclusion during clay mineral formation may play a role. The decrease in dissolved $Cl^–$ is not caused by clathrate dissolution during coring and recovery because such dissolution would also decrease the salinity, and there is no other independent evidence of clathrate presence (see "Organic Geochemistry" and "Lithostratigraphy" sections, this chapter).

ORGANIC GEOCHEMISTRY

Calcium carbonate and organic carbon concentrations were measured on sediment samples from Hole 1084A (Table 13). Organic matter atomic carbon/nitrogen (C/N) ratios and Rock-Eval pyrolysis analyses were employed to determine the type of organic matter contained within the sediments. Elevated amounts of gas were encountered, and routine monitoring of the sedimentary gases was done for drilling safety.

Inorganic and Organic Carbon Concentrations

Concentrations of carbonate carbon in Site 1084 sediments range between 8.2 and <0.1 wt%, corresponding to 68.7 and 0.5 wt% $CaCO_3$ (Table 13). The carbonate concentrations vary in two ways: (1) closely spaced changes related to light–dark color fluctuations and (2) more gradual downhole increases and decreases (Fig. 25). Sediments at this site are divided into four lithostratigraphic units (see "Lithostratigraphy" section, this chapter). Unit I is further divided in three subunits. Subunit IA comprises Pleistocene nannofossil clays and oozes and averages 39 wt% $CaCO_3$. Subunit IB is a Pliocene–Pleistocene diatom-bearing clayey nannofossil ooze that averages 26 wt% $CaCO_3$. Subunit IC is a Pliocene diatomaceous clay that contains an average of 14 wt% $CaCO_3$. Unit II, a Pliocene clay-rich nannofossil diatom ooze, averages 29 wt% $CaCO_3$. Unit III is a Pliocene nannofossil clay in which $CaCO_3$ concentrations average 42 wt%. Unit IV is a Pliocene nannofossil ooze averaging 46 wt% $CaCO_3$. The variations in concentrations reflect varying combinations of changes in delivery of calcareous material, dilution by noncalcareous components, and carbonate dissolution fueled by oxidation of organic matter.

TOC determinations were done on selected samples from Hole 1084A sediments to estimate the amounts of organic matter in the different lithostratigraphic units (Table 13). Like $CaCO_3$ concentrations, TOC concentrations change in both short-term and longer term pat-

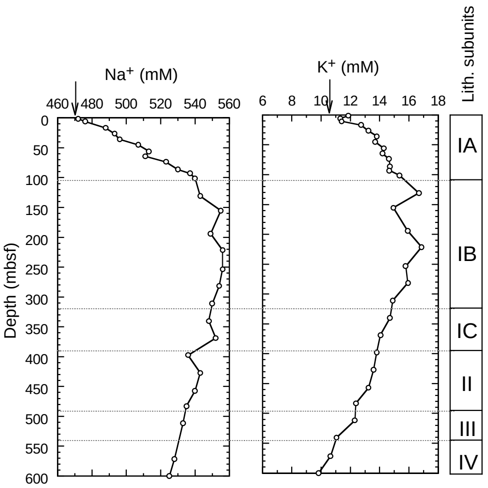

Figure 23. Downcore profiles of dissolved Na^+ and K^+ at Site 1084. Lithostratigraphic subunits shown on right-hand bar. Arrows = mean ocean-bottom-water values taken from Millero and Sohn (1992).

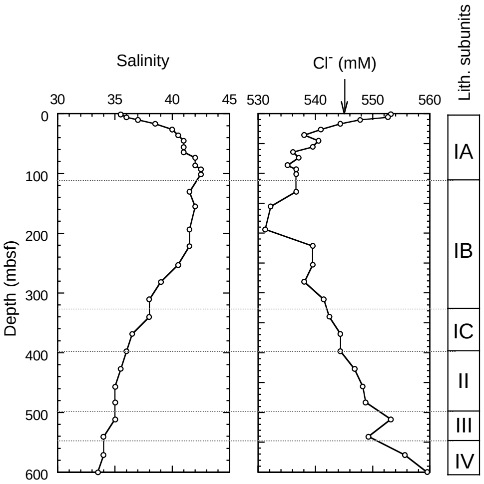

Figure 24. Downcore profiles of salinity and dissolved $Cl^–$ at Site 1084. Lithostratigraphic subunits shown on right-hand bar. Arrow = mean ocean-bottom-water value taken from Millero and Sohn (1992).

Table 13. Percentages of inorganic and total carbon, total nitrogen, and total sulfur in sediment samples from Hole 1084A.

Core, section, interval (cm)	Depth (mbsf)	IC (wt%)	$CaCO_3$ (wt%)	TC (wt%)	TOC (wt%)	TN (wt%)	TS (wt%)	C/N (atomic)
175-1084A-								
Subunit IA - Pleistocene nannofossil clay and ooze								
1H-2, 46-47	1.96	5.32	44.3	11.15	5.84	0.66	0.73	10.4
2H-2, 46-47	4.96	1.94	16.2	8.87	6.93	0.72	1.31	11.3
2H-4, 46-47	7.96	0.57	4.7	8.92	8.35	0.84	1.45	11.6
2H-6, 46-47	10.96	3.12	26.0					
3H-2, 46-47	14.46	3.98	33.1					
3H-4, 46-47	17.46	5.20	43.3	10.67	5.47	0.56	1.08	11.5
3H-5, 4-5	18.54	3.83	31.9	11.77	7.94	0.73	1.50	12.7
3H-5, 4445	18.94	4.24	35.3	12.06	7.82	0.73	1.32	12.6
3H-5, 79-80	19.29	2.96	24.7	12.63	9.67	0.87	1.68	13.0
3H-5, 119-120	19.69	2.76	23.0	12.51	9.75	0.87	1.82	13.1
3H-6, 4-5	20.04	1.75	14.6	13.39	11.64	1.04	2.00	13.0
3H-6, 29-30	20.29	1.06	8.8	14.29	13.23	1.14	2.13	13.5
3H-6, 69-70	20.69	1.46	12.2	12.75	11.29	1.02	2.33	13.0
3H-6, 109-110	21.09	4.14	34.5	12.45	8.31	0.77	1.53	12.6
3H-6, 144-145	21.44	4.85	40.4	12.44	7.59	0.70	1.30	12.8
3H-7, 4-5	21.54	4.60	38.3	12.40	7.80	0.70	1.38	13.0
3H-7, 34-35	21.84	5.78	48.1	11.79	6.01	0.56	1.11	12.6
3H-7, 66-67	22.16	4.76	39.7	12.17	7.41	0.66	1.32	13.0
4H-2, 46-47	23.96	4.16	34.7	11.67	7.51	0.65	1.42	13.5
4H-4, 46-47	26.96	5.06	42.2					
5H-6, 46-47	39.36	0.62	5.2	18.63	18.01	1.39	3.25	15.2
6H-2, 46-47	42.86	4.17	34.8					
6H-4, 46-47	45.76	2.41	20.1	10.12	7.72	0.60	1.88	15.0
6H-6, 46-47	48.76	6.25	52.1					
7H-2, 46-47	52.46	7.05	58.7					
7H-4, 46-47	54.99	4.36	36.3	12.75	8.39	0.67	1.76	14.6
7H-6, 46-47	57.94	7.88	65.6					
8H-2, 46-47	61.96	6.78	56.5					
8H-4, 46-47	64.86	6.37	53.1	11.06	4.69	0.45	1.07	12.2
8H-6, 46-47	67.86	6.59	54.9					
9H-2, 46-47	71.46	6.76	56.3					
9H-4, 46-47	74.36	8.25	68.7	11.70	3.45	0.31	0.49	12.9
9H-6, 46-47	77.36	6.95	57.9					
10H-2, 46-47	80.96	6.43	53.5					
10H-4, 46-47	83.96	6.83	56.9	13.32	6.48	0.51	1.07	15.0
10H-6, 46-47	86.96	6.35	52.9					
11H-2, 46-47	89.13	6.70	55.8					
11H-4, 46-47	92.13	7.97	66.4	11.80	3.83	0.33	0.61	13.5
11H-6, 46-47	95.13	6.77	56.4					
12H-2, 46-47	98.72	6.75	56.2					
12H-4, 46-47	101.72	4.34	36.2	14.38	10.04	0.71	1.75	16.6
12H-6, 46-47	104.72	1.12	9.3					
Subunit IB - Pliocene-Pleistocene diatom-bearing clayey nannofossil ooze								
13H-2, 46-47	109.46	2.48	20.7					
13H-4, 46-47	112.46	3.45	28.7	8.62	5.17	0.42	1.38	14.3
13H-6, 46-47	115.46	2.99	24.9					
14H-2, 46-47	118.96	3.47	28.9					
14H-4, 46-47	121.96	4.81	40.1	10.58	5.77	0.48	1.32	14.1
14H-5, 83-84	123.86	3.93	32.7	9.68	5.75	0.51	1.32	13.1
14H-5, 137-138	124.40	3.42	28.5	11.80	8.38	0.64	1.59	15.3
14H-6, 46-47	124.99	5.09	42.4	13.01	7.92	0.61	1.17	15.1
15H-2, 46-47	128.46	4.44	37.0					
15H-4, 46-47	131.56	4.94	41.1	11.04	6.10	0.49	1.36	14.6
15H-6, 46-47	134.56	4.27	35.6					
16H-2, 53-54	138.03	2.05	17.1					
16H-4, 46-47	140.96	2.60	21.6	8.43	5.83	0.44	1.07	15.4
17H-2, 46-47	147.46	8.10	67.5	11.64	3.54	0.26	0.14	15.9
19X-2, 46-47	154.46	6.26	52.1					
19X-4, 46-47	157.46	3.94	32.8	11.80	7.86	0.57	1.29	16.2
20X-2, 46-47	162.94	1.55	12.9					
20X-4, 46-47	164.84	3.43	28.5	8.64	5.22	0.56	0.90	10.8
21X-2, 46-47	173.76	2.94	24.5					
21X-4, 46-47	176.76	3.95	32.9	7.77	3.82	0.32	0.79	13.9
21X-5, 50-51	178.30	4.19	34.9	8.78	4.59	0.42	1.08	12.7
21X-5, 85-86	178.65	3.13	26.0	8.46	5.33	0.53	1.96	11.8
21X-5, 120-121	179.00	2.45	20.4	8.79	6.33	0.55	1.75	13.5
21X-6, 29-30	179.59	3.03	25.2	8.76	5.74	0.53	1.40	12.7
21X-6, 46-47	179.76	2.61	21.8					
21X-6, 59-60	179.89	2.59	21.6	8.86	6.27	0.55	1.61	13.4
21X-6, 80-81	180.10	3.07	25.6	8.85	5.78	0.58	1.62	11.8
22X-1, 14-15	181.64	0.10	0.9	10.67	10.57	0.84	2.02	14.7
22X-1, 44-45	181.94	0.38	3.2	10.40	10.02	0.79	2.01	14.9
22X-1, 48-49	181.98	0.73	6.1	10.80	10.07	0.80	1.78	14.7
22X-1, 93-94	182.43	0.41	3.4	12.60	12.19	0.93	1.96	15.3
23X-2, 46-47	193.16	2.31	19.3	10.01	7.70	0.52	1.32	17.3
24X-2, 46-47	202.76	4.78	39.8					
24X-4, 46-47	204.69	2.12	17.6	9.81	7.69	0.62	1.88	14.6
25X-2, 46-47	212.36	1.70	14.1					
25X-2, 148-149	213.38	0.96	8.0	13.14	12.18	0.87	2.46	16.4
25X-4, 46-47	215.36	1.58	13.1	16.43	14.86	1.06	2.47	16.4
25X-6, 46-47	218.33	4.66	38.8					
26X-2, 46-47	222.06	1.96	16.3	7.82	5.86	0.56	1.80	12.3
27X-2, 46-47	230.58	5.17	43.1					
27X-4, 46-47	232.87	2.81	23.4	7.88	5.07	0.52	1.54	11.5
28X-2, 46-47	241.26	4.59	38.2					
28X-4, 46-47	244.26	4.54	37.9	9.72	5.18	0.45	1.21	13.3

Table 13 (continued).

Core, section, interval (cm)	Depth (mbsf)	IC (wt%)	$CaCO_3$ (wt%)	TC (wt%)	TOC (wt%)	TN (wt%)	TS (wt%)	C/N (atomic)
28X-6, 46-47	247.26	2.65	22.1					
29X-2, 46-47	250.86	1.36	11.4					
29X-4, 46-47	253.86	1.18	9.9	9.94	8.76	0.71	1.76	14.5
30X-2, 46-47	260.46	5.66	47.2					
30X-4, 46-47	263.17	3.24	27.0	10.56	7.33	0.65	1.35	13.2
31X-2, 46-47	270.16	4.98	41.5					
32X-2, 46-47	279.35	4.18	34.8					
32X-4, 46-47	282.20	2.12	17.6	7.27	5.15	0.47	1.24	12.8
33X-2, 46-47	289.36	1.57	13.1					
33X-4, 46-47	292.23	1.13	9.4	9.10	7.97	0.64	2.32	14.6
34X-2, 46-47	298.96	3.07	25.6	6.28	3.21	0.31	0.86	12.2
34X-4, 46-47	301.56	1.63	13.6					
35X-2, 46-47	308.56	2.91	24.2					
35X-4, 46-47	311.47	0.99	8.2	7.26	6.27	0.52	1.68	14.2
36X-2, 46-47	318.26	5.77	48.1					
36X-4, 46-47	321.17	4.60	38.3	8.46	3.86	0.41	1.45	11.1
Subunit IC - Pliocene diatomaceous clay								
37X-2, 46-47	327.86	1.57	13.1					
37X-4, 46-47	330.86	0.11	0.9	7.58	7.47	0.55	1.85	15.9
37X-6, 46-47	333.86	0.15	1.3					
38X-2, 46-47	337.56	0.35	2.9					
38X-4, 46-47	340.56	3.03	25.2	8.24	5.22	0.44	1.27	13.8
38X-6, 46-47	343.47	3.35	27.9					
39X-2, 46-47	347.16	0.14	1.2					
39X-4, 46-47	350.16	0.54	4.5	5.57	5.03	0.38	1.01	15.6
39X-6, 46-47	353.16	1.64	13.6					
40X-2, 46-47	356.76	1.05	8.8					
40X-4, 46-47	359.76	4.62	38.5	7.27	2.66	0.23	0.31	13.6
40X-6, 46-47	362.59	2.27	18.9					
41X-2, 46-47	366.36	0.06	0.5					
41X-4, 46-47	369.36	2.22	18.5	5.94	3.72	0.31	0.94	13.9
41X-6, 46-47	372.36	2.80	23.3					
42X-2, 46-47	376.06	3.38	28.1					
42X-4, 46-47	379.06	1.18	9.8	4.90	3.72	0.40	0.83	11.0
42X-6, 46-47	381.94	1.60	13.3					
43X-4, 46-47	388.66	0.51	4.2	7.13	6.62	0.56	1.88	13.7
43X-6, 46-47	391.66	2.49	20.7					
Unit II - Pliocene clay-rich nannofossil diatom ooze and diatomaceous nannofossil ooze								
44X-2, 46-47	395.26	2.17	18.1					
44X-4, 26-27	398.06	2.37	19.7	5.63	3.26	0.25	0.52	15.1
44X-6, 46-47	401.26	2.86	23.8					
45X-2, 46-47	404.86	0.90	7.5					
45X-4, 46-47	407.86	1.57	13.1	5.34	3.77	0.37	1.58	11.8
46X-2, 46-47	413.64	2.95	24.6					
46X-4, 46-47	416.64	4.65	38.7	7.18	2.53	0.25	0.87	11.7
46X-6, 46-47	419.64	4.69	39.1					
47X-2, 46-47	423.11	5.62	46.8					
47X-4, 46-47	426.11	2.74	22.9	6.49	3.75	0.33	0.84	13.3
47X-6, 46-47	428.19	1.68	14.0					
48X-2, 46-47	433.86	2.82	23.5					
48X-4, 46-47	436.86	1.49	12.4	4.23	2.74	0.28	0.94	11.6
49X-2, 46-47	443.56	3.70	30.8					
49X-4, 46-47	446.56	1.33	11.1					
49X-6, 46-47	449.56	3.70	30.9	6.47	2.77	0.28	0.90	11.7
50X-2, 46-47	453.16	1.57	13.1	6.07	4.51	0.41	1.43	12.9
50X-4, 46-47	456.16	4.03	33.6					
50X-6, 46-47	457.95	6.53	54.4	7.76	1.23	0.34	0.58	4.3
51X-2, 46-47	462.76	5.31	44.3					
51X-4, 46-47	465.76	2.05	17.1	5.86	3.81	0.36	1.24	12.5
51X-6, 46-47	468.76	7.11	59.3					
52X-2, 46-47	471.96	4.80	40.0					
52X-4, 46-47	474.96	5.42	45.1	7.56	2.14	0.22	0.44	11.2
53X-2, 46-47	480.75	3.56	29.7	9.99	6.43	0.74	1.67	10.2
53X-4, 46-47	483.75	5.20	43.4					
Unit III - Pliocene nannofossil clay								
54X-2, 46-47	490.72	3.60	30.0	7.12	3.52	0.37	1.01	11.2
54X-4, 46-47	493.72	5.28	43.9					
55X-2, 46-47	501.06	4.16	34.7	7.92	3.76	0.36	1.02	12.1
56X-2, 46-47	510.66	2.97	24.7	7.73	4.76	0.43	1.28	12.9
57X-2, 46-47	520.26	6.48	54.0					
57X-4, 46-47	523.26	4.32	36.0	11.66	7.34	0.58	1.65	14.8
57X-6, 46-47	526.26	5.77	48.0					
58X-2, 46-47	529.96	6.78	56.5					
58X-4, 46-47	532.96	5.82	48.5	7.65	1.83	0.26	0.54	8.4
59X-2, 46-47	539.66	5.58	46.4					
59X-4, 46-47	542.66	5.12	42.7	11.23	6.11	0.49	1.41	14.6
Unit IV - Pliocene nannofossil ooze								
60X-2, 46-47	549.26	5.18	43.1					
60X-4, 46-47	552.26	5.46	45.5	7.37	1.91	0.36	0.63	6.2
61X-2, 46-47	558.96	4.97	41.4					
61X-4, 46-47	561.96	4.10	34.2	8.36	4.26	0.53	1.39	9.5
62X-2, 46-47	567.36	5.90	49.2					
62X-4, 46-47	570.36	4.26	35.5	6.98	2.72	0.48	0.90	6.6
62X-6, 46-47	573.36	5.18	43.2					
63X-2, 46-47	578.16	5.02	41.8					
63X-4, 46-47	581.16	5.91	49.2	8.75	2.84	0.39	0.58	8.5
63X-6, 46-47	584.16	7.22	60.2					

Table 13 (continued).

Core, section, interval (cm)	Depth (mbsf)	IC (wt%)	$CaCO_3$ (wt%)	TC (wt%)	TOC (wt%)	TN (wt%)	TS (wt%)	C/N (atomic)
64X-2, 50-51	587.90	6.72	56.0					
64X-4, 46-47	590.86	5.41	45.1	8.38	2.97	0.30	1.21	11.4
64X-6, 46-47	593.86	3.90	32.5					
65X-2, 46-47	597.46	3.74	31.2					
65X-4, 46-47	600.46	6.91	57.5	9.45	2.54	0.26	0.52	11.3
65X-6, 46-47	603.46	7.87	65.5					

Notes: IC = inorganic carbon; $CaCO_3$ = calcium carbonate; TC = total carbon; TOC = total organic carbon; TN = total nitrogen; TS = total sulfur; and C/N = carbon/nitrogen ratio. TOC concentrations are calculated from the difference between IC and TC concentrations. C/N ratios are calculated from TOC and TN concentrations and are given as atom/atom ratios.

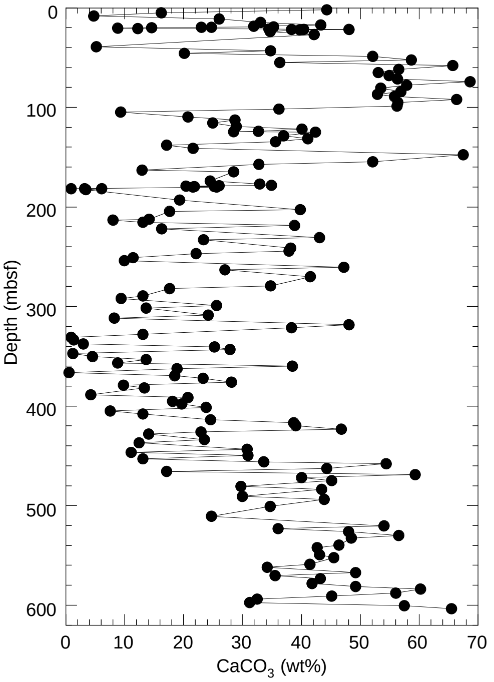

Figure 25. Concentrations of $CaCO_3$ in sediments from Hole 1084A. Variations reflect light–dark color cycles and different lithologic units.

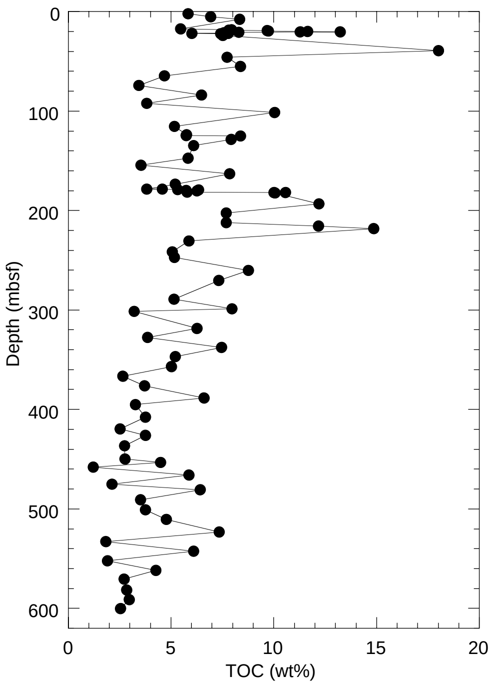

Figure 26. Concentrations of TOC in sediments from Hole 1084A. Variations reflect light–dark color cycles.

terns (Fig. 26). Dark-colored sediments have higher TOC values than light-colored layers. TOC concentrations also differ in Hole 1084A lithostratigraphic units, averaging 8.21 wt% in Subunit IA, 7.00 wt% in Subunit IB, 4.92 wt% in Subunit IC, 3.36 wt% in Unit II, 4.55 wt% in Unit III, and 2.87 wt% in Unit IV. The high TOC concentrations in the subunits of Unit I are a consequence of the elevated paleoproductivity of the Benguela Current upwelling system, which has delivered abundant organic matter to the sediments, and the high accumulation rate of sediments (see "Biostratigraphy and Sedimentation Rates" section, this chapter), which enhances preservation of the organic matter.

Organic Matter Source Characterization

Organic C/N ratios were calculated for sediment samples from the different Site 1084 lithostratigraphic units using TOC and total nitrogen concentrations (Table 13). The C/N ratios vary from 17.3 to 4.3 (Fig. 27). Most of these C/N ratios are intermediate between unaltered algal organic matter (5–8) and fresh land-plant material (25–35; e.g., Emerson and Hedges, 1988; Meyers, 1994). The means of the C/N ratios are Subunit IA, 13.1; Subunit IB, 14.0; Subunit IC, 14.0; Unit II, 11.5; Unit III, 12.3; and Unit IV, 8.9. Because of their setting under a major upwelling system and offshore from a coastal desert, it is likely that these organic carbon–rich sediments contain mostly ma-

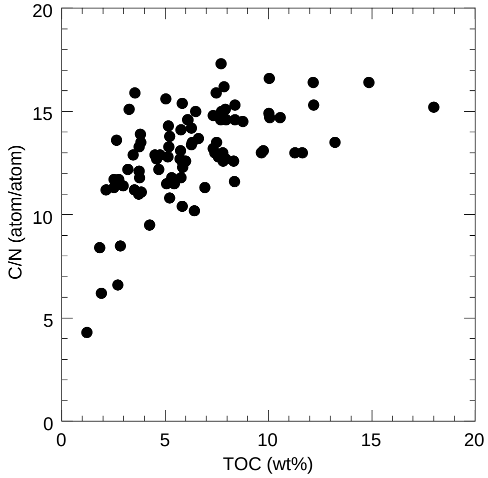

Figure 27. Comparison of organic matter C/N ratios and TOC concentrations of sediments from Hole 1084A. The correspondence between increases in both parameters indicates that preservation of marine organic matter during early diagenesis is important to enhancing the organic carbon richness of sediments on the Walvis Ridge.

rine-derived organic matter with only a minor contribution of detrital continental organic matter. The C/N ratios that are higher than fresh algal organic matter indicate that preferential loss of nitrogen-rich, proteinaceous matter and consequent elevation of C/N ratios occurred during settling of organic matter to the seafloor. Such early diagenetic alteration of C/N ratios is commonly seen under areas of elevated marine productivity such as upwelling systems (Meyers, 1997).

A Van Krevelen–type plot of the hydrogen index (HI) and oxygen index (OI) values indicates that the sediments contain type II (algal) organic matter (Fig. 28) that has been altered by microbial processing during early diagenesis. Well-preserved type II organic matter has high HI values (Peters, 1986); these values can be lowered by microbial oxidation (Meyers, 1997). Hole 1084A sediments deviate from the pattern observed at other Leg 175 sites in which lower HI values correlate with lower TOC values (Fig. 29). Because oxidation typically lowers both HI and TOC values (Meyers, 1997), the absence of this relationship suggests that, in addition to aerobic and anaerobic degradation, the marine organic matter has been subject to variable amounts of dilution. Evidence of substantial amounts of in situ organic matter degradation exists in the rapid depletion of sulfate and the exceptionally large increases in alkalinity and ammonia in the interstitial waters of Site 1084 sediments (see "Inorganic Geochemistry" section, this chapter).

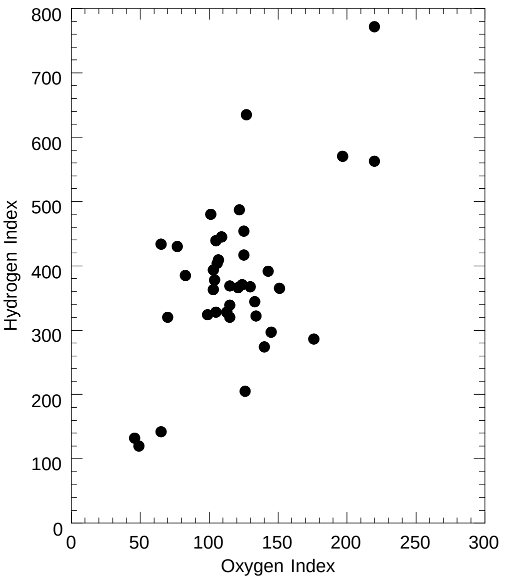

Figure 28. Rock-Eval Van Krevelen–type diagram of sediments from Hole 1084A. Organic matter appears to be type II algal material that has been variably oxidized. HI = milligrams of hydrocarbons per gram of organic carbon; OI = milligrams of CO_2 per gram of organic carbon.

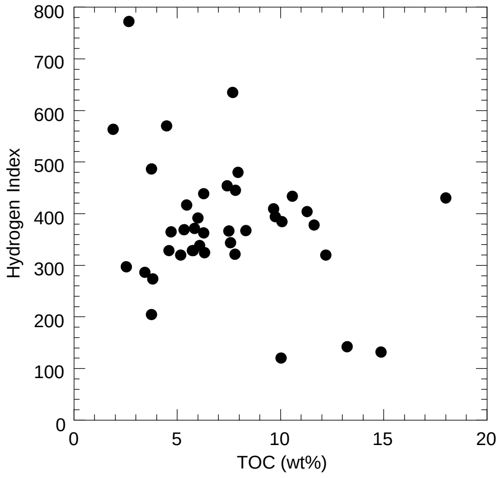

Figure 29. Comparison of Rock-Eval HI values and TOC concentrations of sediments from Hole 1084A. The correspondence between increases in both parameters (in the center of the scatter plot) indicates that preservation of marine organic matter is important to enhancing the organic carbon richness of sediments on the Walvis Ridge. The outliers call for additional explanation.

The sediment samples have low Rock-Eval T_{max} values (Table 14), showing that their organic matter is thermally immature with respect to petroleum generation (Peters, 1986) and therefore is unlikely to contain much detrital organic matter derived from erosion of ancient, thermally mature sediments from Africa.

Headspace Gases

High amounts of hydrogen sulfide, methane, and CO_2 were found in sediments from Site 1084. The odor of hydrogen sulfide was noted through most of the sequence, and detectable concentrations of this gas were found in upper parts of Hole 1084A (Table 15). Much of the sedimentary sequence had an offensive odor, which may have resulted from microbial organo-sulfur gases such as dimethyl sulfide and CS_2. Total gas pressures became great enough in sediments below

Table 14. Results of Rock-Eval pyrolysis analyses of sediments from Hole 1084A.

Core, section, interval (cm)	Depth (mbsf)	TOC (wt%)	S_1	S_2	S_3	T_{max} (°C)	HI	OI
175-1084A-								
1H-2, 46-47	1.96	5.84	3.34	21.71	7.25	406	371	124
3H-4, 46-47	17.46	5.47	3.49	22.84	6.86	409	417	125
3H-5, 4-5	18.54	7.94	3.78	38.15	8.09	407	480	101
3H-5, 44-45	18.94	7.82	3.45	34.82	8.53	708	445	109
3H-5, 79-80	19.29	9.67	4.45	39.64	10.42	404	409	107
3H-5, 119-120	19.69	9.75	4.87	38.47	10.10	410	394	103
3H-6, 4-5	20.04	11.64	5.23	44.04	12.20	404	378	104
3H-6, 29-30	20.29	13.23	1.81	18.91	8.69	415	142	65
3H-6, 69-70	20.69	11.29	9.03	45.66	12.08	399	404	106
3H-6, 109-110	21.09	8.31	3.32	30.54	10.82	411	367	130
3H-6, 144-145	21.44	7.59	2.61	26.13	10.10	410	344	133
3H-7, 4-5	21.54	7.80	4.42	25.16	10.47	400	322	134
3H-7, 34-35	21.84	6.01	4.09	23.59	8.64	407	392	143
3H-7, 66-67	22.16	7.41	5.72	33.66	9.28	399	454	125
4H-2, 46-47	23.96	7.51	3.21	27.49	9.14	402	366	121
5H-6, 46-47	39.36	18.01	8.63	77.54	14.01	407	430	77
8H-4, 46-47	64.86	4.69	2.07	17.16	7.09	410	365	151
9H-4, 46-47	74.36	3.45	1.24	9.89	6.08	411	286	176
13H-4, 46-47	112.46	5.17	1.91	16.59	5.99	412	320	115
15H-4, 46-47	131.56	6.10	1.88	20.73	7.02	410	339	115
21X-4, 46-47	176.76	3.82	1.14	10.49	5.38	411	274	140
21X-5, 50-51	178.30	4.59	1.15	15.10	5.21	415	328	113
21X-5, 85-86	178.65	5.33	1.50	19.69	6.18	412	369	115
21X-5, 120-121	179.00	6.33	1.68	20.55	6.28	409	324	99
21X-6, 29-30	179.59	5.74	1.40	18.86	6.06	415	328	105
21X-6, 59-60	179.89	6.27	2.12	22.77	6.51	400	363	103
21X-6, 80-81	180.10	5.78	1.37	18.98	6.56	411	328	113
22X-1, 14-15	181.64	10.57	3.84	45.95	6.97	405	434	65
22X-1, 44-45	181.94	10.02	0.93	12.07	4.92	412	120	49
22X-1, 48-49	181.98	10.07	5.11	38.82	8.41	399	385	83
22X-1, 93-94	182.43	12.19	3.41	39.09	8.56	407	320	70
23X-2, 46-47	193.16	7.70	4.39	48.96	9.78	408	635	127
25X-4, 46-47	215.36	14.86	1.69	19.76	6.88	412	132	46
35X-4, 46-47	311.47	6.27	1.66	27.58	6.62	414	439	105
40X-4, 46-47	359.76	2.66	2.37	20.54	5.86	398	772	220
45X-4, 46-47	407.86	3.76	0.68	7.74	4.78	411	205	126
50X-2, 46-47	453.16	4.50	1.12	13.93	4.82	402	570	197
55X-2, 46-47	501.06	3.75	1.54	18.30	4.61	399	487	122
60X-4, 46-47	552.26	1.91	0.62	10.78	4.44	422	563	220
65X-4, 46-47	600.46	2.54	0.44	7.56	3.69	417	297	145

Notes: TOC = total organic carbon; HI = hydrogen index; and OI = oxygen index. Units of the various Rock-Eval parameters are given in the "Organic Geochemistry" section of the "Explanatory Notes" chapter (this volume).

Table 15. Results of headspace gas analyses of sediments from Hole 1084A.

Core, section, interval (cm)	Depth (mbsf)	C_1 (ppmv)	CO_2 (ppmv)	C_2= (ppmv)	C_2 (ppmv)	H_2S (ppmv)	C_3= (ppmv)	C_3 (ppmv)	C_1/C_2
175-1084A-									
1H-2, 0-5	1.50	3.2	2,111						
2H-3, 0-5	6.00	3,248	24,605						
2H-6, 0-5	10.50	26,991	63,842	0.2	0.5	26			53,982
3H-4, 0-5	17.00	45,832	59,528	0.2	0.8	27	0.2	0.6	57,290
4H-4, 0-5	26.50	64,469	82,735	0.2	1.0				64,469
5H-4, 0-5	35.90	27,032	107,765	0.7	2.8		0.7	2.2	9,654
6H-4, 0-5	45.30	68,458	135,912		1.3			1.2	52,660
7H-5, 0-5	55.98	12,536	133,617	1.2	4.6		1.2	3.7	2,725
8H-4, 0-5	64.40	27,128	209,240	0.3	1.7	23		1.3	15,958
9H-4, 0-5	73.90	13,600	193,132	0.6	2.2		0.3	1.6	6,182
10H-6, 0-5	86.50	9,520	177,778	1.1	3.8		1.1	3.0	2,505
11H-5, 0-5	93.17	20,142	213,686	0.7	2.0		0.7	1.6	10,071
12H-4, 0-5	101.26	4,277	221,269	0.7	3.2		0.5	3.0	1,337
13H-4, 0-5	112.00	13,617	248,365	0.4	1.4		0.4	1.4	9,726
14H-4, 0-5	121.50	9,722	273,365	0.9	2.4			2.5	4,051
15H-4, 0-5	131.10	3,852	172,859	0.6	1.7			1.9	2,266
16H-5, 0-5	142.00	3,783	206,605	0.4	1.4		0.3	1.8	2,702
17H-3, 0-5	148.50	1,862	201,350		0.5				3,724
19X-3, 0-5	155.50	1,605	161,340	0.2	0.6			0.6	2,675
20X-4, 0-5	164.38	1,403	138,253	0.5	1.5			1.8	935
21X-3, 0-5	174.80	2,573	229,659	0.2	0.8			0.8	3,216
22X-1, 0-5	181.50	8,311	117,098	2.5	5.9		2.2	6.7	1,409
23X-3, 0-5	193.98	2,964	157,018	0.3	1.0		0.2	1.0	2,964
24X-2, 0-5	202.30	2,590	220,395	0.4	1.3		0.3	1.5	1,992
25X-4, 0-5	214.90	2,336	298,177	2.5	9.8		2.0	11.8	238
26X-2, 0-5	221.60	2,387	226,388	0.6	2.5		0.5	3.2	955
27X-3, 0-5	231.62	1,745	216,887	0.8	2.7		0.4	2.7	646
28X-5, 0-5	245.30	4,088	286,378	0.7	4.4		0.4	3.9	929
29X-4, 0-5	253.40	3,515	282,457	1.0	4.9			4.4	717
30X-3, 0-5	261.50	3,321	218,533	0.5	3.9		0.2	2.3	852
31X-2, 0-5	269.70	3,205	154,546	0.5	3.6		0.2	1.0	890
32X-4, 0-5	281.74	5,548	270,856	0.6	5.7		0.2	2.8	973
33X-2, 0-5	288.90	5,246	303,662	0.7	4.6			6.0	1,140
34X-4, 0-5	301.10	3,038	138,190	0.3	3.0			1.6	1,013
35X-4, 0-5	311.01	5,673	209,037	0.5	6.4			3.4	886
36X-3, 0-5	319.21	2,850	155,885	1.1	14.0		2.3	28.5	204
37X-4, 0-5	330.40	5,165	153,465	0.6	6.7			4.3	771
38X-4, 0-5	340.10	4,612	200,821	0.6	4.6			2.9	1,003
39X-4, 0-5	349.70	2,837	143,251	0.2	2.4			1.5	1,182
40X-4, 0-5	359.30	4,581	186,819	0.4	3.3			2.1	1,388
41X-4, 0-5	368.90	5,115	211,704	0.4	4.3			2.6	1,190
42X-4, 0-5	378.60	14,502	322,698	1.4	17.3		0.2	10.9	838
43X-6, 0-5	391.20	3,081	126,581	0.2	3.4			2.1	906
44X-4, 0-5	397.80	2,131	72,718		1.5			0.9	1,421
45X-6, 0-5	410.40	2,730	110,027	0.4	3.1			2.3	881
46X-6, 0-5	419.18	3,563	138,629	0.3	3.4			1.8	1,048
47X-5, 0-5	427.15	3,320	95,049	0.3	2.4			1.6	1,383
48X-6, 0-5	439.07	2,203	78,686		0.7			0.7	3,147
49X-6, 0-5	449.10	850	47,283	0.5	1.4		0.1	1.4	607
50X-5, 0-5	457.20	4,412	127,188	0.4	3.0			1.8	1,471
51X-5, 0-5	466.80	8,057	102,932	0.4	5.9			2.9	1,366
52X-4, 0-5	474.50	1,928	72,465	0.3	2.0			1.5	964
53X-4, 0-5	483.29	7,040	180,890	1.3	14.2		0.3	9.9	496
54X-4, 0-5	493.26	3,747	107,424	1.1	6.4		0.1	4.8	585
55X-3, 0-5	502.10	1,520	50,263	0.8	4.5		0.2	3.7	338
56X-3, 0-5	511.70	5,033	106,451	2.1	15.7		1.3	13.8	321
57X-4, 0-5	522.80	1,828	60,902	1.3	5.7			4.7	321
58X-3, 0-5	531.00	2,080	54,816	1.3	6.7		0.9	6.0	312
59X-3, 0-5	540.70	1,701	47,267	0.8	7.3		0.5	6.0	233
60X-3, 0-5	550.30	7,219	87,005	2.0	12.3		1.3	10.0	587
61X-3, 0-5	560.00	2,632	36,135	0.6	3.8		0.3	3.1	693
62X-5, 0-5	571.40	6,439	102,691	1.3	14.3		0.6	12.2	450
63X-5, 0-5	582.20	6,383	104,360	1.3	9.4		0.6	8.0	679
64X-3, 0-5	588.90	3,485	73,508	1.5	9.5		0.8	9.3	367
65X-4, 0-5	600.00	9,105	69,502	1.1	12.3		0.5	10.2	740

Notes: C_1 = methane; CO_2 = carbon dioxide; C_2= = ethene; C_2 = ethane; H_2S = hydrogen sulfide; C_3= = propene; and C_3 = propane. Dominance of C_1 over C_2 indicates that the gases originate from in situ microbial degradation of organic matter.

Core 175-1084A-2H (6 mbsf) to require perforating the core liner to relieve the pressure and prevent excessive core expansion.

Methane (C_1) concentrations increase rapidly with depth in headspace gas samples from Hole 1084A sediments. Concentrations become significant in sediments below 6 mbsf (Fig. 30). High methane/ethane (C_1/C_2) ratios and the absence of major contributions of higher molecular weight hydrocarbon gases (Table 15) indicate that the gas is biogenic, as opposed to thermogenic, in origin. The origin of the methane is probably from in situ microbial fermentation of the marine organic matter present in the sediments. Similar microbial production of methane from marine organic matter has been inferred from high biogenic gas concentrations in Pliocene–Pleistocene sediments from DSDP Site 532 nearby on the Walvis Ridge (Meyers and Brassell, 1985), Sites 897 and 898 on the Iberian Abyssal Plain (Meyers and Shaw, 1996), and also in middle Miocene sediments from Site 767 in the Celebes Sea (Rangin, Silver, von Breymann, et al., 1990). A biogenic origin of the methane is supported by the disappearance of interstitial sulfate at approximately the same sub-bottom depth where methane concentrations begin to rise (see “Inorganic Geochemistry” section, this chapter), inasmuch as Claypool and Kvenvolden (1983) observe that the presence of interstitial sulfate inhibits microbial methanogenesis in marine sediments.

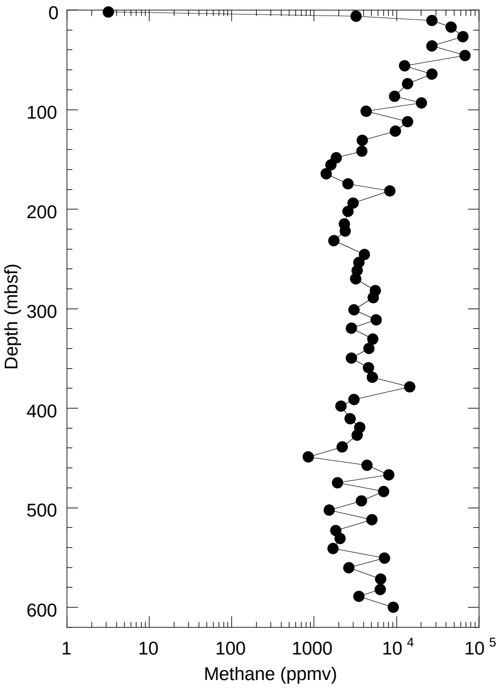

Figure 30. Headspace methane concentrations in sediments from Hole 1084A.

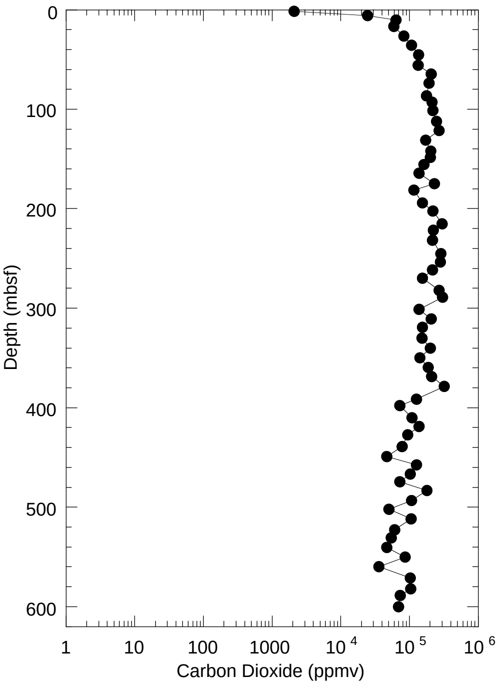

Figure 31. Headspace CO_2 concentrations in sediments from Hole 1084A.

Natural gas analyses determined that the most abundant gas was CO_2 and that headspace concentrations of this gas remained high deep in Hole 1084A (600 mbsf; Fig. 31). Cragg et al. (1992) report the existence of viable microbes to depths of ~500 mbsf in the sediments of the Japan Sea. The abundance of biogenic gases in sediments at Site 1084 suggests the presence of viable microbial communities to similar sub-bottom depths in the Walvis Basin.

PHYSICAL PROPERTIES

Shipboard physical properties measurements conducted at Hole 1084A included nondestructive, high-resolution measurements of GRAPE density, magnetic susceptibility, *P*-wave velocity, and natural gamma radiation on most recovered whole-round core sections.

Index properties data (gravimetric wet bulk density, porosity, and moisture content) were collected at discrete locations on split sections. Method C was used at this site (see “Explanatory Notes” chapter, this volume).

Within all APC sections and where sediment properties permitted, such as intact biscuits from XCB cores, undrained vane shear strength was determined.

Compressional (*P*-wave) velocity measurements were made at a resolution of one or two discrete sampling points per section. For discrete *P*-wave velocity measurements the modified Hamilton Frame was used on split sections of cores from <38 mbsf.

Thermal conductivity was obtained on every second unsplit section in every core by inserting a thermal probe into the sediment (see “Explanatory Notes” chapter, this volume).

Multisensor Track

GRAPE density (Fig. 32), *P*-wave velocity (Fig. 33), and magnetic susceptibility (Figs. 34A, 35A) were determined every 2 cm between 0 and 98 mbsf. MST data are included on CD-ROM (back pocket, this volume). Below 98 mbsf, the resolution was reduced to 4 cm for all MST sensors. Compressional velocities were recorded at an amplitude threshold of 100 incremental units to avoid erroneous determinations of first-arrival times. The MST *P*-wave logger did not record any signals below 18 mbsf (Fig. 33), which confirms the very high gas content in the sediments.

Magnetic susceptibility (Figs. 34A, 35A) and GRAPE density (Fig. 32) show a good correlation over the entire depth range of 600 m. Both profiles correspond well to the identified lithostratigraphic units (see “Lithostratigraphy” section, this chapter).

Index properties wet bulk and GRAPE densities display a high degree of similarity. A majority of discrete wet bulk density values are higher than the GRAPE data. This can be associated with voids and cracks within the recovered sediments, which reduce the effective sediment volume for GRAPE measurements.

All physical properties data sets reveal pronounced cyclicities, which give rise to further detailed analyses after correcting for sediment distortion and combining parallel holes. Intervals of anomalous lithologies will be further studied and compared with results from downhole logging and sediment analyses (see “Lithostratigraphy” and “Downhole Logging” sections, this chapter).

Velocities

Discrete velocities recorded between 0 and 37 mbsf increase from 1540 to 1570 m/s. The *P*-wave logger of the MST recorded systematically lower values between 0 and 18 mbsf (Fig. 33). Density and velocity profiles correspond to each other to a certain degree (Figs. 32A, 33), but because of the high gas content of the sediments (see “Organic Geochemistry” section, this chapter), velocity data are not considered to be very reliable.

Index Properties

Data from discrete measurements of wet bulk density, porosity, and moisture content are displayed in Figures 36A, 36B, and 36C, respectively (also see Table 16 on CD-ROM, back pocket, this volume). The density values vary between 1200 and 1700 kg/m^3, with a

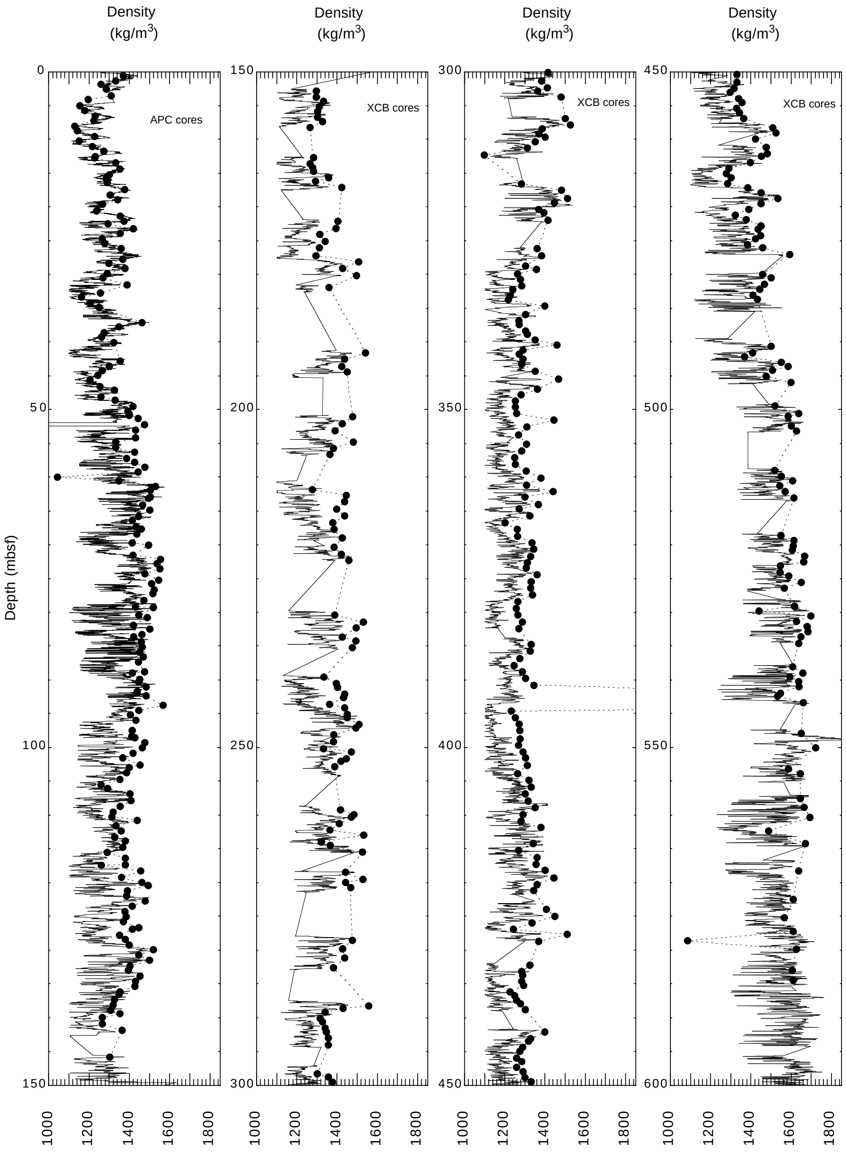

Figure 32. GRAPE density data (solid lines) compared with discrete wet bulk density values (solid circles).

single peak of almost 5000 kg/m³ at 395 mbsf (not displayed in Figs. 32, 36A–C).

The overall trend of the wet bulk density profile shows an increase from 5 to 70 mbsf and a decrease downhole to 140 mbsf. Wet bulk density shows very little variation and few excursions between 160 and 380 mbsf. Below 380 mbsf, the data show a higher level of variation and gradually increase because of compaction down to the end of the sampling depth at 585 mbsf. The most prominent changes in wet bulk density coincide with the lithostratigraphic boundaries (see “Lithostratigraphy” section, this chapter).

In general, porosity and moisture profiles are inversely correlated. Porosities decrease from 90% in the top section to 55% at 585 mbsf, indicating the high clay content of these sediments (Fig. 36B). Moisture content varies between 80% at the top of Hole 1084A and 30% at 585 mbsf (Fig. 36C). The overall variation between higher and lower values corresponds to the observed and identified lithostratigraphic units (see “Lithostratigraphy” section, this chapter).

Thermal Conductivity and Geothermal Gradient

The thermal conductivity profile (Figs. 34B, 35B) at Hole 1084A was measured in every second core section (see “Explanatory Notes” chapter, this volume). Direct contact with the sediments in the core liner of Hole 1084A was sometimes difficult to establish because of the presence of many voids and cracks, which were difficult to identify through the liner. The profile is similar to wet bulk and GRAPE density profiles over some depth intervals at Hole 1084A (Fig. 32).

In Hole 1084A, the Adara tool was deployed to measure formation temperature. A preliminary analysis provided three data points, which were used to estimate a geothermal gradient of 48 °C/km, but further analyses will be required to confirm this result.

Vane Shear Strength

Undrained vane-shear measurements were performed in the bottom part of each core section between 0 and 300 mbsf (Figs. 34D, 35D). The profile for Hole 1084A shows an overall increase in vane shear strength between 0 and 300 mbsf. Below 255 mbsf, vane-shear data show higher scatter, and local maxima generally decrease.

As noticed at other Leg 175 sites, local maxima in shear strength are usually observed in the middle of each core at Site 1084. Lower shear-strength values coincide mostly with the top and the bottom of each core, where gas expansion may have changed the sediment structure significantly.

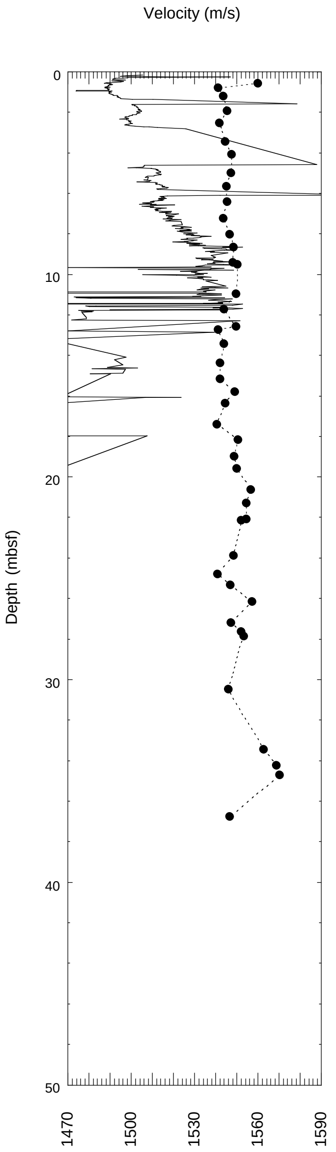

Figure 33. Discrete velocity profile (solid circles) compared with MST velocity data (solid line) measured at Hole 1084A.

DOWNHOLE LOGGING

Hole 1084A was logged with a full suite of sensors to continuously characterize the sedimentary changes and structures, to correlate and compare the lithostratigraphy with that for previous holes, and to provide data for core-log integration.

Logging Operations

Hole 1084A was logged with four different tool strings. The first tool string (seismostratigraphy) included the NGT, DIT, and TLT sondes. The second tool string (lithoporosity) included the NGT, neutron porosity, gamma density, and TLT sondes. The third tool string (FMS, 1 pass) included the NGT, inclinometry, and FMS sondes. The fourth tool string (GHMT) included the NGT, magnetic susceptibility, and vertical component magnetometer sondes. The logs were run uphole from 605 mbsf (total depth) to pipe at 59 mbsf; the two first runs were logged to the seafloor. The natural gamma ray is the only parameter measurable through the pipe, but it should be interpreted only qualitatively in this interval. The pipe was set at 89 mbsf and pulled up to ~59 mbsf during logging for the first three runs and before logging for the fourth run (GHMT). The wireline logging heave compensator was started immediately upon entering the hole.

Data Quality and General Results

Hole 1084A is characterized by a regular hole size (~9- to 11-in diameter) with numerous small enlargements from the bottom to 170 mbsf (see caliper measurements; Fig. 37). Above this interval, the hole conditions are degraded and show a regular increase in the borehole size, with critical washout zones at the top of the logged interval (above 130 mbsf). The downhole measurements are affected by extreme enlargements at the top of the hole, and thus only the logging data in the 600- to 130-mbsf interval are of good quality.

The lithologic succession recovered from Hole 1084A is controlled mainly by changes in the nature and intensity of biogenic production vs. the type and amount of detrital input and is characterized by large changes in sediment composition and compaction, which should be reflected in the log physical properties measurements. The lithostratigraphic boundaries defined from core observation and smear-slide studies (see “Lithostratigraphy” section, this chapter) compare well with the main features observed in the downhole measurements.

Lithologic Unit IV is characterized by increasing magnetic susceptibility and decreasing uranium (U) content, with very steady density and acoustic velocity, which might be explained by changes of the ratio between lithic and organic components in the detrital input. The top of Unit IV is marked by an overall increase in resistivity, acoustic velocity, and density. The boundary between lithologic Units III and II at 498 mbsf is identified in the log data as a shift in all of the physical measurements (Fig. 37), which reflects the change in the nature and intensity of the biogenic production.

The top of lithologic Unit III is marked by a higher U content and small peaks of gamma-ray, resistivity, density, and magnetic susceptibility measurements. The top of the unit marks the FO of the organic-rich levels that were identified as black layers in the cores (see “Lithostratigraphy” section, this chapter). Above this depth, similar “black” layers with high gamma-ray, resistivity, acoustic velocity, and magnetic susceptibility dominate the downhole measurements signals, particularly between 270 and 170 mbsf. The distribution of the “black” layers is restricted to 410–150 mbsf, as shown by the detailed analysis of the FMS images (Fig. 38). The U content is highest between 270 and 170 mbsf (Fig. 37). Because of the presence of “black” layers, the lower part of lithologic Subunit IB is marked by a regular increase in gamma-ray, resistivity, and magnetic susceptibility, and the middle part shows higher amplitudes of the resistivity and the acoustic velocity (Fig. 37). The upper part of lithologic Subunit IB (between 150 and 130 mbsf) shows high resistivity, acoustic velocity, and density, but low U content. This pattern permits the identification of several “dolomitic” layers at this depth, confirmed by the mapping of the FMS images (Fig. 38). The velocity exhibits a regular decrease uphole, with a sharp change at 450 mbsf caused by compaction of the sediment.

Nineteen dolomitic layers and 114 “black” layers (or “organic-rich” layers) were tentatively identified in the logged interval (Fig. 37), both characterized by very high velocity, resistivity, and density, and by low gamma-ray intensity for the dolomites and high gamma-ray intensity for the “black” layers. Because of their high resistivity, the position and thickness of these layers can be identified on the FMS images (Fig. 38). Only one dolomitic layer was visually verified in cores recovered with the extended core barrel, and only 17 black layers were explicitly described in the cores (see “Lithostratigraphy” section, this chapter). These black layers were defined by being dark (e.g., 5y 2.5/1). They had a total reflectance between 20% and 25%. Numerous dark layers were not included in the visual core description, but are identified in Figure 38 based on the resistivity contrast of the FMS images.

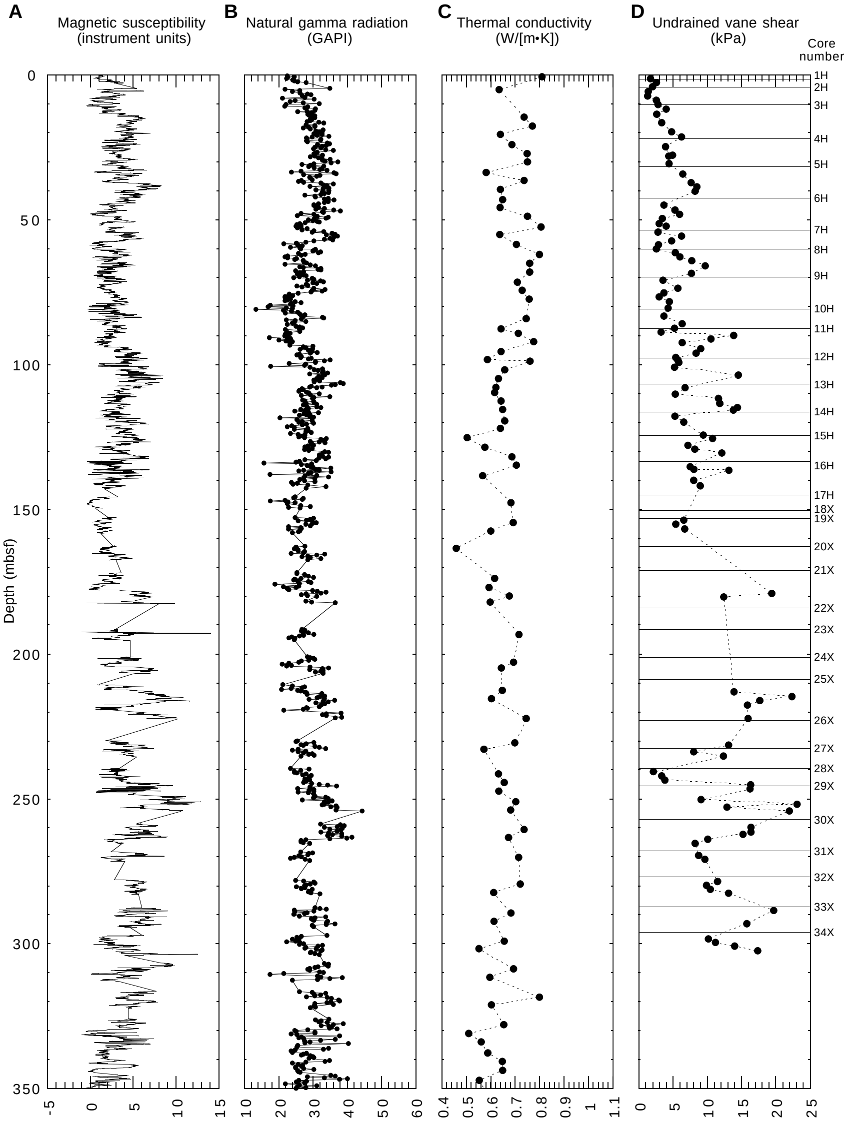

Figure 34. Plots of (**A**) magnetic susceptibility and (**B**) natural gamma radiation from MST measurements compared with discrete values of (**C**) thermal conductivity and (**D**) undrained vane shear strength between 0 and 350 mbsf for Hole 1084A.

The temperature tool measures borehole fluid temperature. The results suggest a downhole thermal gradient of 28.5°C/km, an estimate which is low because of the cooling effect of circulation during drilling.

Correlation Between Holes 1084A (Northern Cape Basin) and 1082A (Walvis Basin)

The downhole measurements of the two neighboring holes are very similar, despite the higher sedimentation rate observed at Site 1084 in the NCB. Both general trends and details can be correlated and allow the establishment of a reliable depth-to-depth correlation, as shown by the gamma-ray intensity (Fig. 39). All the downhole physical properties parameters show the same range of variation at the two holes, despite the different sedimentation rates. The “black” layers are absent at Hole 1082A in the Walvis Basin.

Log-Core Correlations

The core MST and log measurements of natural gamma-ray intensity are very similar. Core data are recorded in counts per second (cps), whereas log data are presented in API (Oil Industry Standard) units. Detailed correlations between the core and log data sets (Fig. 40) promise to be reliable because of the high sedimentation rate at this site and the limited coring disturbance, except in the organic-rich interval (270–170 mbsf). The main trend observed in the gamma-ray log is not exhibited as clearly by the gamma-ray intensity measured on the cores, which is noisier. In Hole 1084A, log depth is close to core depth.

REFERENCES

Austin, J.A., Jr., and Uchupi, E., 1982. Continental-oceanic crustal transition off Southwest Africa. *AAPG Bull.,* 66:1328–1347.

Berggren, W.A., Kent, D.V., Swisher, C.C., III, and Aubry, M.-P., 1995. A revised Cenozoic geochronology and chronostratigraphy. *In* Berggren, W.A., Kent, D.V., Aubry, M.-P., and Hardenbol, J. (Eds.), *Geochronology, Time Scales and Global Stratigraphic Correlation.* Spec. Publ.—Soc. Econ. Paleontol. Mineral. (Soc. Sediment. Geol.), 54:129–212.

Bleil, U., and Shipboard Scientific Party, 1994. Report and preliminary results of SONNE Cruise SO 86, Buenos Aires–Capetown, 22.4.1993–31.5.1993. *Ber. Fachber. Geowiss., Univ. Bremen,*51.

————, 1996. Report and preliminary results of METEOR cruise M34/1, Capetown-Walvis Bay, 3.1.1996–26.1.1996. *Ber. Fachber. Geowiss., Univ. Bremen,* 77.

Bremner, J.M., 1983. Biogenic sediments on the South West African (Namibian) continental margin. *In* Thiede, J., and Suess, E. (Eds.), Coastal Upwelling: its Sediment Record (Pt. B): *Sedimentary Records of Ancient Coastal Upwelling.* NATO Conf. Ser. IV, Mar. Sci., 73–103.

Brown, P.C., Painting, S.J., and Cochrane, K.L., 1991. Estimates of phytoplankton and bacterial biomass and production in the northern and southern Benguela ecosystem. *S. Afr. J. Mar. Sci.,* 11:537–564.

Calvert, S.E., and Price, N.B., 1983. Geochemistry of Namibian Shelf sediments. *In* Thiede, J., and Suess, E. (Eds.), *Coastal Upwelling: its Sedimentary Record* (Pt. A): *Responses of the Sedimentary Regime to Present Coastal Upwelling:* New York (Plenum), 337–376.

Caulet, J.-P., 1991. Radiolarians from the Kerguelen Plateau, Leg 119. *In* Barron, J., Larsen, B., et al., *Proc. ODP, Sci. Results,* 119: College Station, TX (Ocean Drilling Program), 513–546.

Claypool, G.E., and Kvenvolden, K.A., 1983. Methane and other hydrocarbon gases in marine sediment. *Annu. Rev. Earth Planet. Sci.,* 11:299–327.

Cragg, B.A., Harvey, S.M., Fry, J.C., Herbert, R.A., and Parkes, R.J., 1992. Bacterial biomass and activity in the deep sediment layers of the Japan Sea, Hole 798B. *In* Pisciotto, K.A., Ingle, J.C., Jr., von Breymann, M.T., Barron, J., et al., *Proc. ODP, Sci. Results.,* 127/128 (Pt. 1): College Station, TX (Ocean Drilling Program), 761–776.

Dingle, R.V., 1995. Continental shelf upwelling and benthic ostracoda in the Benguela System, southeastern Atlantic Ocean. *Mar. Geol.,* 122:207–225.

Dingle, R.V., Birch, G.F., Bremner, J.M., de Decker, R.H., du Plessis, A., Engelbrecht, J.C., Fincham, M.J., Fitton, T., Flemming, B.W., Gentle, R.I., Goodlad, S.W., Martin, A.K., Mills, E.G., Moir, G.J., Parker, R.J., Robson, S.H., Rogers, J., Salmon, D.A., Siesser, W.G., Simpson, E.S.W., Summerhayes, C.P., Westall, C.F., and Winter, A., 1987. Deep-sea sedimentary environments around southern Africa, South-East Atlantic and South-West Indian Oceans. *Ann. S. Afr. Mus.,* 98:1–27.

Emerson, S., and Hedges, J.I., 1988. Processes controlling the organic carbon content of open ocean sediments. *Paleoceanography,* 3:621–634.

Giraudeau, J., 1993. Planktonic foraminiferal assemblages in surface sediments from the southwest African continental margin. *Mar. Geol.,* 110:47–62.

Giraudeau, J., and Rogers, J., 1994. Phytoplankton biomass and sea-surface temperature estimates from sea-bed distribution of nannofossils and planktonic foraminifera in the Benguela Upwelling System. *Micropaleontology,* 40:275–285.

Kemp, A.E.S., and Baldauf, J.G., 1993. Vast Neogene laminated diatom mat deposits from the eastern equatorial Pacific Ocean. *Nature,* 362:141–144.

Kemp., A.E.S., Baldauf, J.G., and Pearce, R.B., 1995. Origins and paleoceanographic significance of laminated diatom ooze from the eastern equatorial Pacific Ocean. *In* Pisias, N.G., Mayer, L.A., Janecek, T.R., Palmer-Julson, A., and van Andel, T.H. (Eds.), *Proc. ODP, Sci. Results,* 138: College Station, TX (Ocean Drilling Program), 641–645.

Lazarus, D., 1992. Antarctic Neogene radiolarians from the Kerguelen Plateau, Legs 119 and 120. *In* Wise, S.W., Jr., Schlich, R., et al., *Proc. ODP, Sci. Results,* 120: College Station, TX (Ocean Drilling Program), 785–809.

Little, M.G., Schneider, R.R., Kroon, D., Price, B., Bickert, T., and Wefer, G., 1997. Rapid paleoceanographic changes in the Benguela Upwelling System for the last 160,000 years as indicated by abundances of planktonic foraminifera. *Paleogeogr., Paleoclimatol., Palaeoecol.,* 130:135–161.

Lutjeharms, J.R.E., and Meeuwis, J.M., 1987. The extent and variability of SE Atlantic upwelling. *S. Afr. J. Mar. Sci.,* 5:51–62.

Lutjeharms, J.R.E., and Stockton, P.L., 1987. Kinematics of the upwelling front off southern Africa. *S. Afr. J. Mar. Sci.,* 5:35–49.

Lutjeharms, J.R.E., and Valentine, H.R., 1987. Water types and volumetric considerations of the south-east Atlantic upwelling regime. *S. Af. J. Mar. Sci.,* 5:63–71.

Martini, E., 1971. Standard Tertiary and Quaternary calcareous nannoplankton zonation. *In* Farinacci, A. (Ed.), *Proc. 2nd Int. Conf. Planktonic Microfossils Roma:* Rome (Ed. Tecnosci.), 2:739–785.

Merrill, R.T., and McElhinny, M.W., 1983. *The Earth's Magnetic Field: Its History, Origin, and Planetary Perspective:* London (Acad. Press).

Meyers, P.A., 1994. Preservation of elemental and isotopic source identification of sedimentary organic matter. *Chem. Geol.,* 144:289–302.

————, 1997. Organic geochemical proxies of paleoceanographic, paleolimnologic, and paleoclimatic processes. *Org. Geochem.,* 27:213–250.

Meyers, P.A., and Brassell, S.C., 1985. Biogenic gases in sediments deposited since Miocene times on the Walvis Ridge, South Atlantic Ocean. *In* Caldwell, D.E, Brierley, J.A., and Brierley, C.L. (Eds.), *Planetary Ecology:* New York (Van Nostrand Reinhold), 69–80.

Meyers, P.A., and Shaw, T.J., 1996. Organic matter accumulation, sulfate reduction, and methanogenesis in Pliocene–Pleistocene turbidites on the Iberian Abyssal Plain. *In* Whitmarsh, R.B., Sawyer, D.S., Klaus, A., and Masson, D.G. (Eds.), *Proc. ODP, Sci. Results,* 149: College Station, TX (Ocean Drilling Program), 705–712.

Millero, F.J., and Sohn, M.L., 1992. *Chemical Oceanography:* Boca Raton (CRC Press).

Moore, T.C., Jr., 1995. Radiolarian stratigraphy, Leg 138. *In* Pisias, N.G., Mayer, L.A., Janecek, T.R., Palmer-Julson, A., and van Andel, T.H. (Eds.), *Proc. ODP, Sci. Results,* 138: College Station, TX (Ocean Drilling Program), 191–232.

Motoyama, I., 1996. Late Neogene radiolarian biostratigraphy in the subarctic Northwest Pacific. *Micropaleontology,* 42:221–260.

Okada, H., and Bukry, D., 1980. Supplementary modification and introduction of code numbers to the low-latitude coccolith biostratigraphic zonation (Bukry, 1973; 1975). *Mar. Micropaleontol.,* 5:321–325.

Peters, K.E., 1986. Guidelines for evaluating petroleum source rock using programmed pyrolysis. *AAPG Bull.,* 70:318–329.

Rogers, J., and Bremner, J.M., 1991. The Benguela ecosystem (Pt. 7): marine geological aspects. *Mar. Biol. Annu. Rev.,* 29:1–85.

Shackleton, N.J., Crowhurst, S., Hagelberg, T., Pisias, N.G., and Schneider, D.A., 1995. A new late Neogene time scale: application to Leg 138 sites. *In* Pisias, N.G., Mayer, L.A., Janecek, T.R., Palmer-Julson, A., and van Andel, T.H. (Eds.), *Proc. ODP, Sci. Results,* 138: College Station, TX (Ocean Drilling Program), 73–101.

Shannon, L.V., and Nelson, G., 1996. The Benguela: large scale features and processes and system variability. *In* Wefer, G., Berger, W.H., Siedler, G., Webb, D.J. (Eds.), *The South Atlantic: Present and Past Circulation:* Berlin (Springer-Verlag), 163–210.

Shipboard Scientific Party, 1990. Site 767. *In* Rangin, C., Silver, E.A., von Breymann, M.T., et al., *Proc. ODP, Init. Repts.,* 124: College Station, TX (Ocean Drilling Program), 121–193.

Summerhayes, C.P., Kroon, D., Rosell-Melé, A., Jordan, R.W., Schrader, H.-J., Hearn, R., Villanueva, J., Grimalt, J.O., and Eglinton, G., 1995. Variability in the Benguela Current upwelling system over the past 70,000 years. *Prog. Oceanogr.,* 35:207–251.

Weaver, P.P.E., 1993. High resolution stratigraphy of marine Quaternary sequences. *In* Hailwood, E.A., and Kidd, R.B. (Eds.), *High Resolution Stratigraphy.* Geol. Soc. Spec. Publ. London, 70:137–153.

Wefer, G., Berger, W.H., Bickert, T., Donner, B., Fischer, G., Kemle-von Mücke, S., Meinecke, G., Müller, P.J., Mulitza, S., Niebler, H.-S., Pätzold, J., Schmidt, H., Schneider, R.R., and Segl, M., 1996. Late Quaternary surface circulation of the South Atlantic: the stable isotope record and implications for heat transport and productivity. *In* Wefer, G., Berger, W.H., Siedler, G., and Webb, D.J. (Eds.), *The South Atlantic: Present and Past Circulation:* Berlin (Springer-Verlag), 461–502.

Wei, W., 1994. Age conversion table for different time scales. *J. Nannoplankton Res.,* 16:71–73.

Ms 175IR-112

NOTE: Core-description forms ("barrel sheets") and core photographs can be found in Section 4, beginning on page 581. Forms containing smear-slide data and shore-based log processing data can be found on CD-ROM. See Table of Contents for materials contained on CD-ROM.

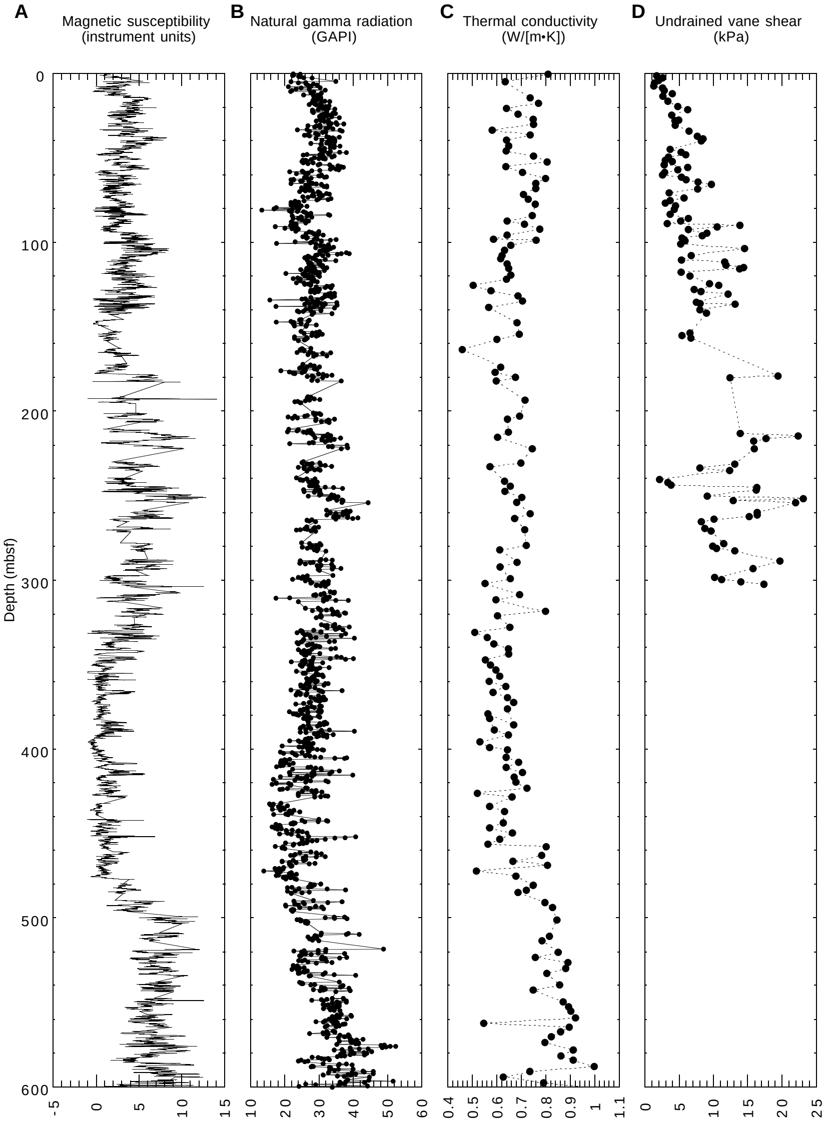

Figure 35. Plots of (**A**) magnetic susceptibility and (**B**) natural gamma radiation from MST measurements compared with discrete values of (**C**) thermal conductivity and (**D**) undrained vane shear strength between 0 and 600 mbsf for Hole 1084A.

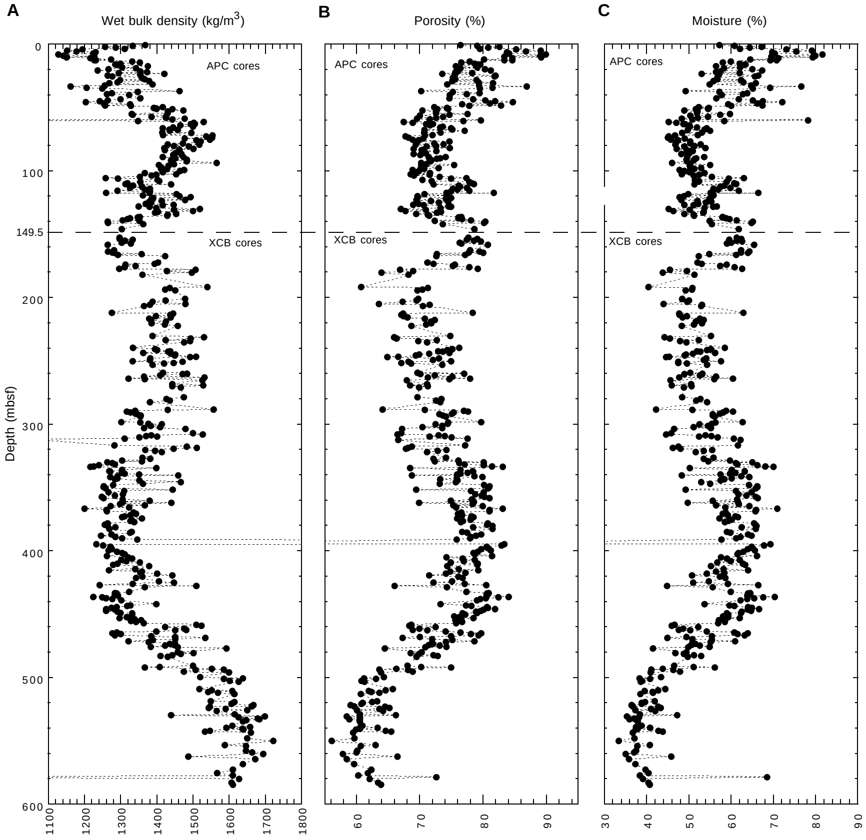

Figure 36. Gravimetric (**A**) wet bulk density, (**B**) porosity, and (**C**) moisture content derived from index properties measurements at Hole 1084A.

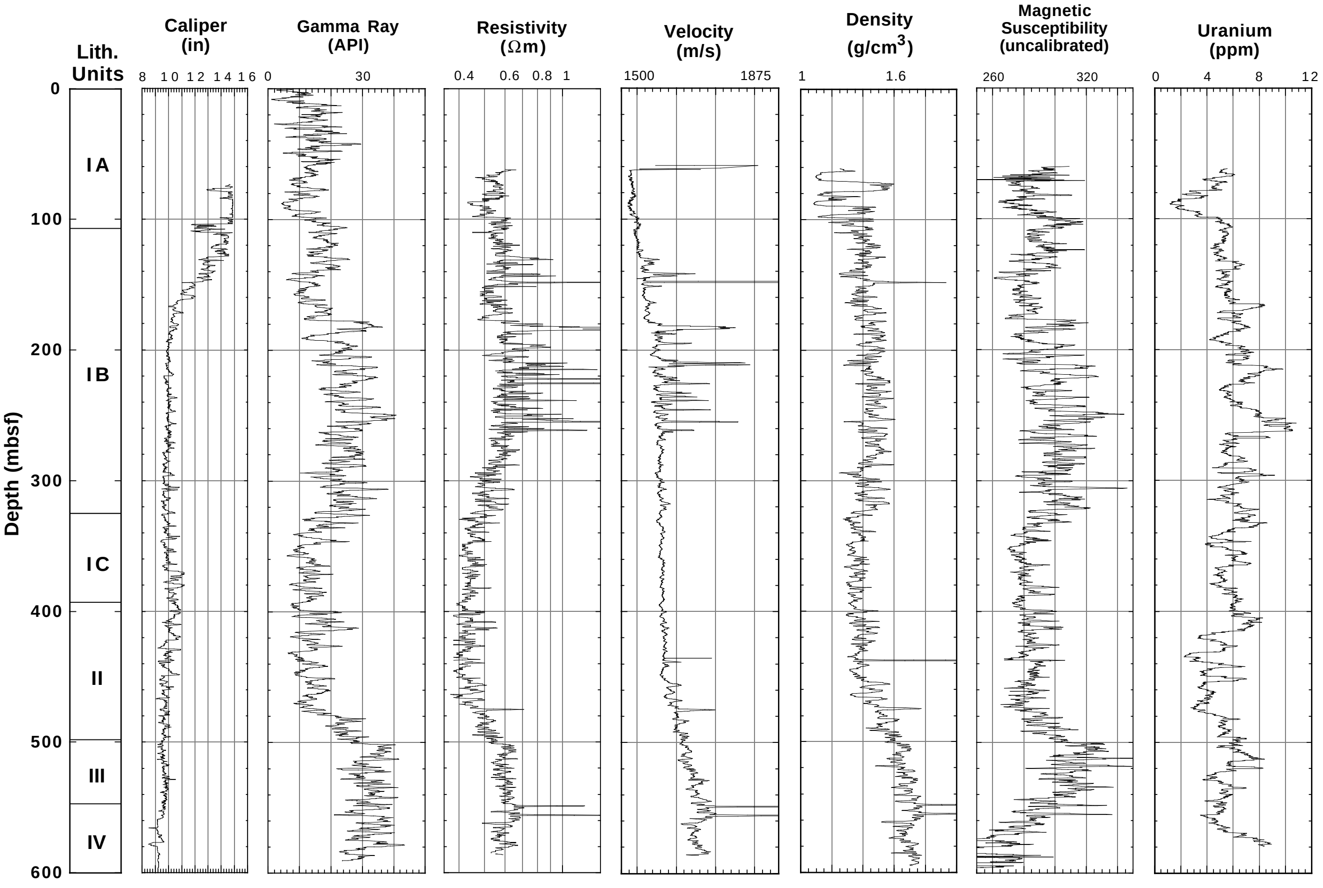

Figure 37. Downhole logs of caliper, natural gamma-ray, resistivity, velocity, density, magnetic susceptibility, and uranium content for Hole 1084A.

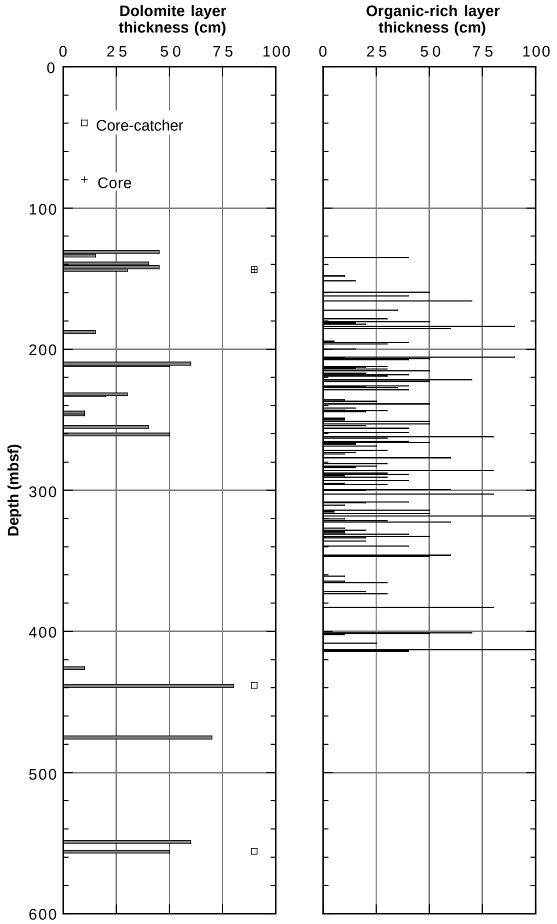

Figure 38. Thickness of the dolomitic and black layers, as identified from logs for Hole 1084A.

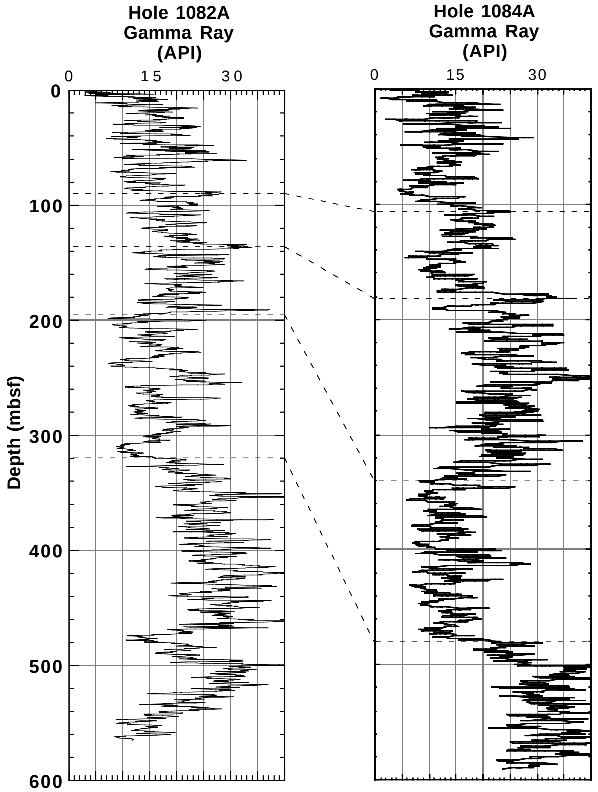

Figure 39. Downhole gamma-ray logs compared between Holes 1084A (Northern Cape Basin) and 1082A (Walvis Basin).

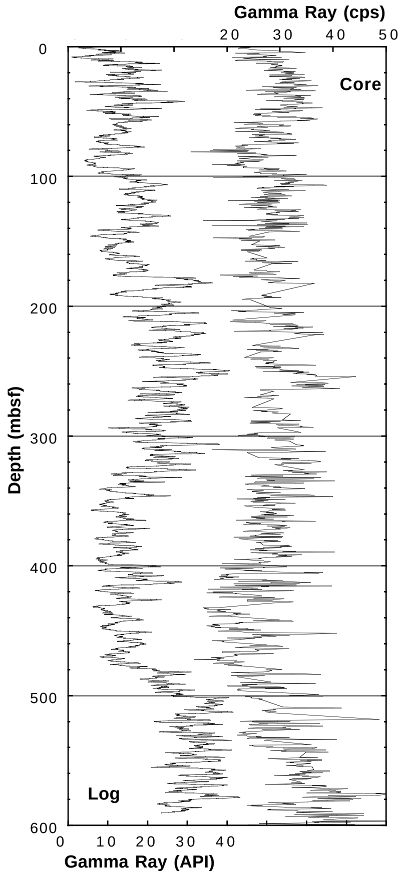

Figure 40. Comparison of core (MST) and log natural gamma-ray data for Hole 1084A.